REPORT DOCUMENTATION PAGE

Form Approved
OMB No. 074-0188

1. AGENCY USE ONLY (Leave blank)	2. REPORT DATE	3. REPORT TYPE AND DATES COVERED
	August 2003	Annual (15 Jul 2002 - 15 Jul 2003)

4. TITLE AND SUBTITLE
Evaluation of Early and Prolonged Effects of Acute Neurotoxicity and Neuroprotection Using Novel Functional Imaging Techniques

5. FUNDING NUMBERS
DAMD17-99-1-9555

6. AUTHOR(S)
Anna-Liisa Brownell, Ph.D.

7. PERFORMING ORGANIZATION NAME(S) AND ADDRESS(ES)
Massachusetts General Hospital
Boston, Massachusetts 02114

E-Mail: abrownell@partners.org

8. PERFORMING ORGANIZATION REPORT NUMBER

9. SPONSORING / MONITORING AGENCY NAME(S) AND ADDRESS(ES)
U.S. Army Medical Research and Materiel Command
Fort Detrick, Maryland 21702-5012

10. SPONSORING / MONITORING AGENCY REPORT NUMBER

11. SUPPLEMENTARY NOTES
Original contains color plates: All DTIC reproductions will be in black and white.

12a. DISTRIBUTION / AVAILABILITY STATEMENT
Approved for Public Release; Distribution Unlimited

12b. DISTRIBUTION CODE

13. ABSTRACT (Maximum 200 Words)
We have explored efficacy of neuroprotection on functional and metabolic pathways in transgenic mouse model and 3-nitropropionic acid induced rat model of huntington's disease. We conducted longitudinal studies of glucose utilization (energy metabolism) in transgenic mice during the treatment with transglutaminase inhibitor cystamine using 4 different doeses; 5/4, 9, 50 and 100 mg/kg ip. In addition, we used CPCCOEt, an antagonist for mGluR 1 receptors with a dose of 5.2 mg/kg. each group of mice had an untreated control group for the parallel imaging studies. In these studies were found that neuroprotection for energy metabolism can be obtained even with a low dose of 5.4 mg/kg. This confirmed also by MRS studies of NAA and the endpoint histological evaluation. However, to protect dopaminergic system a higher dose of cystamine (>50 mg/kg ip.) was required. CPCCOEt with a dose of 5.2 mg/kg ip. Provided neuroprotection for energy metabolism at the same levels as cystamine with 9 mg/kg ip. In 3-NP rat model we found that pretreatment with cystamine (9 mg/kg ip.) before acute administration of 3-NP (25 mg/kg iv.) will significantly enhance 3-NP induced neurotoxicity in rats. This conclusion is based on studies of glucose metabolism, behavior, enhanced mortality and endpoint histological studies.

14. SUBJECT TERMS
Neurotoxin, positron emission tomography, glucose metabolism, dopamine receptors, metabotropic glutamate receptors

15. NUMBER OF PAGES
74

16. PRICE CODE

17. SECURITY CLASSIFICATION OF REPORT	18. SECURITY CLASSIFICATION OF THIS PAGE	19. SECURITY CLASSIFICATION OF ABSTRACT	20. LIMITATION OF ABSTRACT
Unclassified	Unclassified	Unclassified	Unlimited

AD_____

Award Number: DAMD17-99-1-9555

TITLE: Evaluation of Early and Prolonged Effects of Acute Neurotoxicity and Neuroprotection Using Novel Functional Imaging Techniques

PRINCIPAL INVESTIGATOR: Anna-Liisa Brownell, Ph.D.

CONTRACTING ORGANIZATION: Massachusetts General Hospital
Boston, Massachusetts 02114

REPORT DATE: August 2003

TYPE OF REPORT: Annual

PREPARED FOR: U.S. Army Medical Research and Materiel Command
Fort Detrick, Maryland 21702-5012

Table of Contents

FOURTH ANNUAL REPORT "Evaluation of Early and Prolonged Effects of Acute Neurotoxicity and Neuroprotection Using Novel Functional Imaging Techniques"

INTRODUCTION

Exogenous and/or endogenous neurotoxicity has directly or indirectly related to various neurodegenerative diseases including Parkinson's and Huntington's disease (Reiter et al 1998, Gorrell et al 1996, Zayed et al 1996, Checkoway et al 1999, (Mizuno et al 1999, Hattori et al 1998, Schapira et al 1996). Therefore it is a major challenge to develop specific and sensitive in vivo methods to investigate pathophysiological mechanisms of toxins. This information is essential in order to design new methods for neuroprotection and therapy. Our overall research goal is to develop and improve in vivo imaging techniques to examine the neuro-function of glutamatergic and dopaminergic receptors as well as oxidative glucose metabolism and neurochemicals. We focus our efforts in exploring the excitotoxicity induced regional neuronal dysfunction in functional and metabolic pathway. The neuronal toxicity models include 3-nitropropionic acid (3-NP) induced rat model and transgenic mice with gene expression of human Huntington's disease (HD). In the final phase of this project we have tested neuroprotection with novel newly developed ligands effecting on metabotropic glutamate receptor function as well as a ligand, which is a transglutaminase inhibitor. During the past year several publications have proposed neuroprotective characteristics of the transglutaminase inhibitor cystamine (Dedeogly et al 2002, Karpuj et al 2002). We also tested this ligand using different doses in 3-NP induced rat and transgenic mouse models of HD.

BODY

The fourth grant year included especially tasks of testing neuroprotection. Longitudinal imaging studies of energy metabolism, dopamine receptor function by positron emission tomography (PET) and neurochemicals by magnetic resonance spectroscopy (MRS) were conducted in rodent models of HD to investigate neuroprotective response of metabotropic glutamate subgroup 1 antagonist, 7-hydroxyiminocyclo propan [b]chromen-1a-carboxylic acid ethyl ester (CPCCOEt) and transglutaminase inhibitor cystamine using different doses.

In addition, new radiolabeled ligands were developed and tested for imaging of metabotropic glutamate subgroup 5 receptor function. Further development of PET imaging techniques was conducted to enable to produce highly repeatable and efficient imaging studies in longitudinal imaging sessions. This was done with the recently installed commercial microPET system (MicroPET P4, Concord Microsystems), which allows volumetric data acquisition. Progress in the different areas is evaluated in the following.

1. Technical tasks: Further development of imaging techniques was conducted during the fourth grant year. These tasks included development of animal holders with specific head position attachments so that a stack up to 4 rodents could be imaged simultaneously and obtain volumetric data set. Further development was done for data acquisition, implementation of image reconstruction programs to the unix (linux) based computer system and development of image analyses for multimodality data co-registration (Brownell et al 2003a, Appendix).

a) Development for data acquisition: During the earlier grant years we developed a basic model of computer controlled imaging "table" for the small super-high resolution positron emission tomograph. During the fourth grant year we further optimized a stereotactic headholder with earbars and mouth (teeth) bar and developed a stack model, so that up to 4 animals could be positioned for volumetric imaging (data acquisition) simultaneously in a newly installed commercial microPET system. This increase significantly efficacy in data acquisition. However, it increases time in data analyses, but that task can be shared with different computers and overall throughput in the imaging device increases significantly. These animal holders are designed separately for rat and mouse because the size of these two species is significantly different as well as the other experimental maneuvering to prepare animals for imaging studies.

b) Software development: Software developed to combine imaging data of the newly installed PET system with the magnetic resonance imaging and spectroscopy (MRS) data has been and is still a challenge. We are employing a technique, we earlier used based on volume rendering of MR images and fusion of MR and PET images based on the Normalized Mutual Information (NMI) algorithm (Brownell et al 2003a, Appendix) for fusion of the data of the new PET system.

2) Radiopharmaceutical development: Dr. Alan Kozikowski provided us the precursor for labeling of metabotropic glutamate receptor agonist; (methyl-2-(methoxycarbonyl)-2-(methylamino) bicycle[2.1.1] -hexane-5- carbocylate (MMMHC) (Kozikowski et al 1998). We labeled the amine precursor with C-11 methyl triflate and hypothesized that the radiolabeled ligand will be metabolized to (2-aminobicyclo [2.1.1]hexane-2,5-dicarboxylic acid-I (ABHxD-I) in the brain tissue through esterase and aminase (Yu et al 2003, Appendix). Dr. Kozikowski and his team have shown that ABHx-D-I binds both on group I and II metabotropic glutamate receptors. Reported EC50 values are mGluR2 (0.33uM) > mGluR5 (0.72 uM) > mGluR1 (1.6 uM) > mGluR3 (2.2 uM) > mGluR6 (5.3) > mGluR4 (23 uM) (Kozikowski et al 1998, Conti et al 2000). It should be emphasized that according published reports these are the first in vivo imaging studies in the world conducted to visualize mGluR2/3 receptor function.

Because the source to obtain precursor ligand, methyl-2-(methoxycarbonyl)-2-(methylamino) bicycle[2.1.1] -hexane-5- carbocylate, was limited, Dr. Kozikowski was able to provide other precursors, antagonists for metabotropic glutamate subtype 5 receptors. We developed radiolabeling with carbon-11 for these ligands; 2-methyl-6-((3-[^{11}C]methoxyphenyl)ethyl)pyridine ([^{11}C]M-PEP) and 3-[^{11}C]methoxy-5-(pyridine-2-

ylethynyl)pyridine ([^{11}C]M-PEPy) (Figure 2, Appendix) and tested their biodistribution and binding characteristics in normal rats (Figures 3a and 3b, Appendix and Yu et al 2003, Appendix). These preliminary studies have shown that both ligands will cross blood brain barrier and accumulate up to 8 percent into different brain areas including olfactory bulb, cortex and striatum. The imaging studies of mGluR5 receptor function in 3-NP rat as well as in HD mouse model of Huntington's disease are in progress.

3) Biological experiments:

a) Experimental animal studies: During the fourth year, the specific goal was to conduct studies of neuroprotection in a transgenic mouse model of Huntington's disease. Dr. Alan Kozikowski had kindly provided (2-aminobicyclo [2.1.1]hexane-2,5-dicarboxylic acid-I (ABHxD-I) for these experiments. This drug was custom made and he did not have more drug available with the time scale, we needed for the ongoing experiments. Because the last batch of the drug (2-aminobicyclo [2.1.1]hexane-2,5-dicarboxylic acid-I (ABHxD-I) contained impurities, and some of the impurities crossed blood brain barrier, we tested alternative approaches. Mass spectra of the ABHxD-I compound and a sample of microdialysate from the striatum 30 min after iv. injection of ABHxD-I are shown in Figure 1.

After these experiences we selected another drug, 7-hydroxyiminocyclo propan [b]chromen-1a-carboxylic acid ethyl ester, (CPCCOEt), an antagonist for metabotropic glutamate subgroup 1 receptors to investigate neuroprotection. We conducted longitudinal imaging studies of glucose utilization in six transgenic mice treated with CPCCOEt (5.2 mg/kg ip.) and in six untreated transgenic mice as controls to investigate the efficacy of neuroprotection.

In addition we investigated neuroprotection by using cystamine, which is a transglutaminase inhibitor. We conducted studies in 48 transgenic mice using 4 different doses of cystamine (Cystamine dihydrochloride (Sigma, St. Louis, MO) dissolved in PBS). The doses were 100 mg/kg, 50 mg.kg, 9 mg/kg and 5.4 mg/kg injected daily i.p. starting from the age of 8 weeks. The control group was injected similarly with PBS. PET imaging studies were conducted at different time point to investigate changes in glucose metabolism (Figures 5a, 5b) and dopamine D2 receptors. MRI/MRS studies were as well conducted to observe changes in neurochemicals (Figure 6). For the imaging studies mice were anesthetized with halothane (1-1.5% with oxygen flow rate of 3 L/min). Catheters were introduced into the tail vein for administration of radiolabeled ligand. Daily measurements were conducted to register changes in weight progression (Figures 4a, 4b, 4c) and video recording of locomotor activity.

We tested cystamine induced neuroprotection also in 3-nitropropionic acid induced rat model of Huntington's disease. In testing neuroprotection we used an acute model of 3-NP, which includes a single high dose intravenous injection of neurotoxin. Six rats were injected with cystamine using a dose of 9 mg/kg ip. one hour before injection of 3-NP (25 mg/kg iv). Similarly 6 rats were injected only with 3-NP. Progression of neurotoxicity and possible protection were investigated by daily recordings of weight and locomotor activity as well as longitudinal studies of glucose

utilization. For the imaging studies rats were anesthetized with halothane (1-1.5% with oxygen flow rate of 3 L/min). Catheters were introduced into the tail vein for administration of protective ligand, 3-NP and radiolabeled ligands and into the tail artery for collection of blood samples to determine glucose level and blood input function needed for quantification of glucose metabolic rate and/or receptor binding.

Microdialysis was conducted in 3 rats to evaluate transport of ABHxD-I and to determine, if observed impurities of the drug will cross blood brain barrier. Rats were anesthetized with halothane (1.5 % with oxygen flow of 3 L/min) and adjusted into the Kopf surgical stereotactic frame. The dialysis probe was surgically introduced into striatum. Fusion was done with artificial CNS.

b) Results in experimental studies:

Behavior: We followed locomotor activity of the transgenic mice visually by video recording their movement in a square plexiglass box (30 x 40 cm), which bottom was marked with squares of 5 cm x 5 cm. Even these observations were not exactly quantitative, they provide a mean to separate treated from untreated mice. The treated mice were more active, however dose responses could not be indicated between animals with this rough technique.

In analyzing motor score in 3-NP injected rats, we used the method developed by Quary et al 2000 (Guyot et al 1997, Quary et al 2000). Briefly, intermittent dystonia of one hindlimb, score=1; intermittent dystonia of two hind limbs, score=2; permanent dystonia of hind limbs, score=3; gait abnormalities consisting mainly of an uncoordinated and wobbing gait (score=4); recumbence lying on one side but showing uncoordinated movements when stimulated, score=5; near death by almost complete paralysis, score =6; in addition capability to grasp with their forepaws (able=0, unable=1) and capability to stay on small platform for 10s (able=0, unable=1). Using these criteria four of the six cystamine treated rats received a score >5 in 24 hours and died, 2 received a score of 3 after 24 hours and recovered in 2 weeks to score 0 or 1. In untreated group (PBS only before 3-NP toxication) two of the rats received score of 3 in 24 hours and recovered to score 2 and 1 in two weeks. Four of the animals received a score of 1 in 24 hours and three of them stayed in that stage, while one rat progressed to score 6. These experiments were conducted with 3-NP dose of 25 mg/kg iv. At first we used a higher 3-NP dose of 30 mg/kg iv, which we had earlier established as the dose to introduce moderate striatal lesion. However, using this dose of 3-NP and cystamine with a dose of 9 mg/kg ip, all the tested four rats died in 4-6 hours after injections. For that reason we decreased a dose of 3-NP. Based on behavioral response in these rat experiments it appears that administration of cystamine before 3-NP injection enhances 3-NP toxicity.

Imaging studies of glucose metabolism: Longitudinal PET imaging studies of glucose metabolism were conducted using ^{18}F-2-fluorodeoxy-D-glucose as tracer in treated and untreated transgenic mouse and 3-NP induced rat model of HD. Each of five different treated groups of six transgenic mice had own untreated control group of 6 transgenic mice. Imaging studies were conducted in treated and untreated mice in a same day at

different age points to evaluate age dependent rate of progressive degeneration and effect of neuroprotection (Table 1).

Table 1. Rate of percent decrease of glucose utilization between the age of 70 and 85 days investigated by ^{18}F-FDG PET studies. The number of animals in each group was 6.

Treatment	Percent decrease of glucose utilization per day		
	Cortex	Striatum	Cerebellum
Untreated mice	3.873	3.186	3.090
Cystamine 50mg/kg	1.986	1.841	1.739
Cystamine 100mg/kg	1.224	2.385	1.899

Decrease of glucose utilization in the brain of untreated mice has an exponential form starting from the age of 58 days. This might be an indication of fast changes in glucose utilization when the HD-related changes start to progress in the mouse brain. After the age of 70 days changes were stabilized and degenerative process was linear (Figure 5b).

Each six groups were studied for local distribution of ^{18}F-FDG at the age of 85 days. Figure 5b shows that neuroprotection with cystamine can be obtained with small doses, even with a dose of 5.4 mg/kg, when protection is recorded based on glucose utilization. This is an interesting observation, which has been confirmed with histological evaluation (Figure 7).

Neuroprotection in acute toxicity was tested in 6 rats using an ip. injection of cystamine (9mg/kg) one hour before a single high dose administration of 3-NP (25 mg/kg iv.). Table 2 shows results obtained in cystamine treated and untreated rats. These results show that cystamine enhanced the effect of neurotoxicity. The decrease of glucose utilization in the cortex was 17.8%, 23.3% in the striatum and 22.7% in the cerebellum. The observation of the decreased glucose utilization with cystamine treatment is an indication of enhanced neurotoxicity 3-NP combined with cystamine and it is similar than obtained by the behavioral analyses.

Table 2. Glucose utilization in different brain areas 2 hours after administration of 3-NP. In the treated group cystamine (9 mg/kg ip.) was injected one hour before 3-NP. The number of animals in each group was 6.

Treatment	Cortex	Striatum	Cerebellum
3-NP only	5.83+/-1.23	13.93+/-3.46	12.89+/-3.10
Cystamine + 3-NP	4.79+/-0.48	10.68+/-1.88	9.96+/-2.06

Imaging studies of dopamine receptors: The studies of dopamine D2 receptor function in transgenic mouse model of HD showed that dopamine receptor binding was decreased after treatment with 5.4 mg/kg and 9 mg/kg of cystamine as much as in the untreated group. After treatment with higher doses (50 mg/kg or 100 mg/kg ip.) of cystamine, ^{11}C-raclopride binding in striatal dopamine D2 receptors was 13.6% and 17.3% higher than in untreated group, correspondingly (Table 3).

Table 3. ^{11}C-raclopride binding in the striatum of the transgenic mouse model of HD at the age of 74 days. The mice were treated with 4 different doses of cystamine. The number of the studies in each group was 4.

Treatment	Binding potential
Untreated	1.072+/-0.029
Cystamine 5.4 mg/kg	1.064+/-0.071
Cystamine 9 mg/kg	1.076+/-0.065
Cystamine 50 mg/kg	1.218+/-0.058
Cystamine 100mg/kg	1.258+/-0.076

We have earlier conducted imaging studies of dopamine D1 and D2 receptors and dopamine transporters in 3-NP rat model of HD. Dopamine D1 receptors were imaged with ^{11}C-SCH (Schoering 23660) and dopamine D2 receptors with ^{11}C-raclopride. Dopamine transporters were imaged with ^{11}C-CFT (2β-carbomethoxy-3β-(4-fluorophenyl tropane). The interesting observations of transient mechanism of dopamine transporter binding and progressively decreasing dopamine D1 and D2 receptor binding are reported in Brownell et al 2003b (Appendix).

Imaging studies of metabotropic glutamate receptors: Imaging studies of metabotropic glutamate receptors are most exiting imaging approach, what has been for a while. These studies will open a new window for large variety of neurodegenerative diseases. We have done significant progress with the labeling aspects as well as experimental imaging aspects. These binding studies are progressing with collaboration of Dr. Kozikowski, who developed the precursor ligand. He provided us two new precursors; 2-methyl-6-((3-[^{11}C]methoxyphenyl)ethyl)pyridine ([^{11}C]M-PEP) and 3-[^{11}C]methoxy-5-(pyridine-2-ylethynyl)pyridine ([^{11}C]M-PEPy), to investigate metabotropic glutamate subgroup 5 receptors. After developing radiolabeling with carbon-11, we have tested binding characteristics of these compounds in normal rats.

Based on the imaging studies we found that both labeled ligands go fast into the brain and in 2-3 min equilibrium time will be bound in cortical, striatal, and cerebellar areas and highly amount in olfactory bulb. The average binding level in different brain areas varies from 2 to 6 percent. We have also tested specificity of the binding by saturating the receptor sites by administration of the unlabeled 'cold' compound; M-PEP, before injection of the radiolabeled compounds. In these studies were observed high

specificity in different brain areas. Activity distribution, time-activity curves and replacement studies are included in Appendix (Figure 3, Appendix).

Imaging studies of anatomy and neurochemicals (MRI/MRS studies): Imaging studies of neuroanatomy have been used to identify location and size of lesions and for volumetric image rendering. In earlier studies, MRS studies of neurochemicals have shown elevated peaks of lactate and macromolecules as well as succinate immediately after 3-NP toxicity. Using this information, we developed a single dose administration technique, because after administration of 3-NP, the lesion development can be recorded in real time with MRS, as formation of succinate peak (Brownell et al (submitted), Appendix). We used also this injection technique of 3-NP in testing neuroprotection with cystamine.

MRS studies were conducted also in transgenic mice to evaluate effect of neuroprotection. Figure 6a (Appendix) shows MRS spectrum of a mouse treated with cystamine (dose of 9mg/kg) at the age of 85 days; a spectrum of the age matched untreated mouse; and for comparison a spectrum of a normal wild type mouse. In the spectra we can see that NAA (N-acetyl aspartate) is significantly enhanced in the cystamine treated mouse compared to the untreated one and NAA/Cr ratio is almost as high as in the wild type mouse and is significantly higher than in the untreated mouse (Figure 6b, Appendix). NAA is considered to reflect health of the neurons. However, choline peak (Cho) is also enhanced in the cystamine treated mouse compared to the untreated one. Enhanced choline is considered to reflect neurodegenerative processes. We are conducting further studies to investigate sources for enhanced choline.

Evaluation of neuroprotection: In a 3-NP rat model of HD we investigated characteristics of transglutaminase inhibitor cystamine as a neuroprotective agent. These experiments showed based on studies of behavioral analyses, mortality, glucose utilization and endpoint histological evaluation that pretreatment with cystamine will enhance 3-NP neurotoxicity.

Since glucose utilization is a major energy source of the brain, the change in glucose utilization can be a sensitive indicator for the energy dysfunction in the brain. 3-NP, a permanent inhibitor of succinate dehydrogenese (Johnson et al 2000) can disrupt the mitochondrial function, decrease glucose utilization and cause striatal degeneration (Storgaard et al 2000, Guyot et al 1997, Bowyer et al 1996). We are investigating further this enhanced toxicity created by inhibition of succinate dehydrogenase and inhibition of transglutaminase.

In transgenic mouse model of HD we investigated neuroprotective effects of metabotropic glutamate subgroup 1 antagonist, CPCCOEt. Daily ip. administration of CPCCOEt (dose 5.2 mg/kg) from the age of 70 days provided neuroprotection at the same level as ip administration of cystamine with a dose 9 mg/kg. We tested neuroprotection with 4 different doses of cystamine and we found that even a low dose of 5.4 mg/kg could provide neuroprotection for energy metabolism. However, a cystamine dose >50 mg/kg ip was needed to provide neuroprotection for dopaminergic system based on ^{11}C- raclopride binding in dopamine D2 receptors.

Histological confirmation of neural loss: Histological endpoint studies were conducted in 8 rats to confirm the neural loss after 3-NP and possible protection factor in the rats treated with neuroprotective ligand; cystamine. These histological studies of Nissl staining and calbindin immunoreactivity support the observations done with studies of glucose utilization. Pretreatment with cystamine will enhance 3-NP toxicity.

Histological endpoint studies were conducted also in 12 transgenic mice to evaluate effects of cystamine induced neuroprotection. Figure 7 (Appendix) confirms that neuroprotection can be obtained also with low doses, like 5.4 mg/kg ip. of cystamine.

Dr. Francesca Cicchetti has done these histological analyses. She has done both Nissl staining and calbindin immunoreactivity.

KEY RESEARCH ACCOMPLISHMENT

- development of stack system to image up to 4 animals simultaneously and further enhance of the stereotactic headholders for mouse and rat studies

- development of data acquisition and reconstruction for stack imaging with a newly installed microPET system

- further development and testing image algorithms for image reconstruction for multi modality image co-registration

- conclusion of enhanced neurotoxicity in a 3-NP rat model of HD pretreated with cystamine (dose 9 mg/kg ip.) based on observations of decreased glucose utilization in different brain areas, increased deficit in motor score, increased mortality and histological verification of neural damage

- observation that decrease of glucose utilization (energy metabolism) has exponential correlation with age in early ages and correlates with development of HD like degeneration in a transgenic mouse model of HD

- observation that neuroprotection can be provided by cystamine in transgenic mouse model of HD even with a low dose of 5.4 mg/kg ip. based on studies of glucose (energy) metabolism by PET, MRS studies of neurochemicals and endpoint histological verification

- observation that neuroprotection in dopaminergic system of transgenic mouse can be obtained with cystamine, doses higher than 50 mg/kg based on studies of ^{11}C-raclopride of dopamine D2 receptors

REPORTABLE OUTCOME

A-L Brownell, YI Chen, KE Canales, E Livni, RT Powers, A Dedeoglu, FM Beal, BG Jenkins. 3-NP induced neurotoxicity – assessed by ultra high resolution PET with comparison to MRI and MRS. 1st Annual Meeting of the Society for Molecular Imaging. Boston, August 24-26, 2002

Anna-Liisa Brownell, Kelly Canales, Y. Iris Chen, Bruce G. Jenkins, Christopher Owen, Elijahu Livni, Meixiang Yu, Francesca Cicchetti, Rosario Sanchez-Pernaute, Ole Isacson. Mapping of brain function after MPTP induced neurotoxicity in primate Parkinson's disease model. 2nd Annual Meeting of Neuroscience. Orlando, Florida, November 2002.

Anna-Liisa Brownell, Iris Y. Chen, Xukui Wang, Meixiang Yu, Bruce G. Jenkins. Neurotoxicity-Induced Changes in Striatal Dopamine Receptor Function. Parkinson's disease: The Life Cycle of the Dopamine Neuron. Ann. N.Y. Acad. Sci. 991:281-283, 2003.

Meixiang Yu, Kjell Nagren, Y. Iris Chen, Elijahu Livni, David Elmaleh, Alan Kozikowski, Xukui Wang, Kimmo Jokivarsi, Anna-Liisa Brownell. Radiolabeling and biodistribution of methyl 2-(methoxycarbonyl)-2-(methylamino) bicyclo [2.1.1]-hexane-5-carboxylate, a potential neuroprotective drug. Life Sciences 73:1577-1585, 2003.

Anna-Liisa Brownell, Kelly Canales, Y.Iris Chen, Bruce G. Jenkins, Christopher Owen, Elijahu Livni, Meixiang Yu, Francesca Cicchetti, Rosario Sanchez-Pernaute, Ole Isacson. Mapping of brain function after MPTP induced neurotoxicity in a primate Parkinson's disease model. NeuroImage 2003 (in press).

Meixiang Yu, Thomas Klaess, Alan Kozikowski, Anna-liisa Brownell. Synthesis of [11C]methoxymethyl-MPEP and [11C]methoxy-PEPy, potent and selective PET ligands for metabotropic glutamate subtype 5 mGluR5) receptors. 33rd Annual Meeting of Neuroscience. New Orleans. November 2003.

Anna-Liisa Brownell, Y. Iris Chen, Meixiang Yu, Xukui Wang, Kimmo Jokivarsi, Aparajita Sarkar, Alp Dedeoglu, Francesca Cicchetti, M. Flint Beal, Bruce G. Jenkins. 3-Nitropropionic acid induced neurotoxicity – assessed by ultra high resolution PET with comparison to MRI and MRS. Journal of Neuroscience (submitted).

Meixiang Yu and Anna-Liisa Brownell. Synthesis of C-11 CPCCOMe, a Potential PET Ligand for Imaging mGluR1 In Vivo. Molecular Imaging Vol. 1, No. 3, July 2002.

Manuscripts under process:

Meixiang Yu, Thomas Klaess, Xukui Wang, Kimmo Jokivarsi, Aparajita Sarkar, Alan P. Kozikowski, Anna-Liisa Brownell. The synthesis and initial applications of [11C]M-PEP and [11C]methoxyl-PEPy to image mGluR5 receptor function. To be submitted to the Journal of Neurochemistry.

Xukui Wang, Aparajita Sarkar, Meixiang Yu, Kimmo Jokivarsi, Anna-Liisa Brownell. Transglutaminase inhibitor cystamine induced neuroprotection in transgenic mouse model of Huntington's disease – assessed by PET studies of glucose utilization. To be submitted to the Nature Neuroscience.

Meixiang Yu, Francesca Cicchetti, Y. Iris Chen, Xukui Wang, Aprajita Sarkar, Kimmo Jokivarsi, Anna-Liisa Brownell. 3-NP induced neurotoxicity has opposite effect on mGluR2/3 and dopamine receptor function. To be submitted to the Journal of Neurochemistry.

CONCLUSIONS

The fourth grant year has been very successful and significant amount of biological information has been obtained regarding neuroprotection in transgenic mouse model of HD as well as in 3-NP rat model of HD and a rigorous detailed data analyses is still in process. In 3-NP rat model we found that pretreatment with cystamine will enhance 3-NP induced neurotoxicity. In transgenic mouse model of HD we demonstrated neuroprotection even with low doses of cystamine (5.4 mg/kg ip.). In the recently published paper (Dedeoglu et al 2002) significantly higher doses; 112-400 mg/kg ip. has been used. We observed that neuroprotection of dopaminergic system can be obtained with cystamine doses >50 mg/kg ip. and there was no significant difference in neuroprotection with doses of 50 or 100 mg/kg ip.in different brain areas based on studies of glucose utilization. Neuroprotection with CPCCOEt, an antagonist for metabotropic glutamate subtype 1 receptors provided neuroprotection with a dose of 5.2 mg/kg ip. in transgenic mice at the same lavel as cystamine with a dose of 9 mg/kg.

Metabotropic glutamate receptors provide a new interesting insight to investigate degenerative processes and neuroprotective characteristics as well as their usability as drugs. Metabotropic glutamate receptor functions will be investigated world wide in the coming years, and we are proud to express that our effort supported by this research grant has pioneered the first in vivo imaging studies of mGluR2/3 receptor function and now we are expanding our effort to investigate mGluR5 receptor function.

During the fourth grant year, a number of technical tasks have also been accomplished including a development of stack system to image up to 4 animals simultaneously. Algorithm development for data analyses and especially for fusion of the data sets of different imaging modalities have been very successful.

REFERENCES

Borlongan CV, Koutouzis TK, Freeman TB, Hauser RA, Cahill DW, Sanberg PR. Hyperactivity and hypoactivity in a rat model of Huntington's disease: the systemic 3-nitropropionic acid model. Brain Res Brain Res Protoc 1997;1(3):253-7.

Bowyer JF, Clausing P, Schmued L, Davies DL, Binienda Z, Newport GD, Scallet AC, Slikker W Jr. Parenterally administered 3-nitropropionic acid and amphetamine can combine to produce damage to terminals and cell bodies in the striatum. Brain Res 1996; 712(2):221-9.

Brownell A-L, Chen YI, Wang X, Yu M, Jenkins BG. Neurotoxicity-induced changes in striatal dopamine receptor function. Ann N Y Acad Sci 2003; 991:281-283.

Checkoway H, Nelson LM. Epidemiologic approaches to the study of Parkinson's disease etiology. Epidemiology 1999;10(3): 327-36.

Conti P, Kozikowski AP. New synthesis of 2-aminobicyclo[2.1.1]hexane-2,5-dicarboxylic acid-I (ABHxD-I), a potent metabotropic receptor agonist. Tetrahedron Letters 0 (2000) 1-4.

Dedeoglu A, Kubilus JK, Jeitner TM, Matson S, Bogdanov M, Kowall NW, Matson WR, Cooper AJL, Ratan RR, Beal FM, Hersch SW, Ferrante RJ. Therapeutic effects of cystamine in a murine model of Huntington's disease. J Neurosci 2002; 22(20):8942-8950.

Eradiri OL, Starr MS. Striatal dopamine depletion and behavioural sensitization induced by methamphetamine and 3-nitropropionic acid. Eur J Pharmacol 1999; 386(2-3):217-26.

Gorrell JM, DiMonte D, Graham D. The role of the environment in Parkinson's disease. Environmental Health Perspective1996; 104: 652-4.

Guyot MC, Hantraye P, Dolan R, Palfi S, Maziere M, Brouillet E. Quantifiable bradykinesia, gait abnormalities and Huntington's disease-like striatal lesions in rats chronically treated with 3-nitropropionic acid. Neuroscience 1997; 79(1):45-56.

Johnson JR, Robinson BL, Ali SF, Binienda Z. Dopamine toxicity following long term exposure to low doses of 3-nitropropionic acid (3-NPA) in rats. Toxicol Lett 2000; 116(1-2):113-8.

Karpuj MV, Becher MW, Springer JE, Chabas D, Youssef S, Pedotti R, Mitchell D, Steinman L. Prolonged survival and decreased abnormal movements in transgenic model of Huntington's disease, with administration of the transglutaminase inhibitor cystamine. Nature Medicine 2002; 8:143-149.

Kozikowski AP, Steensma D, Araldi GL, Tuckmantel W, Wang S, Pshenichkin S, Surina E, Wroblewski JT. Synthesis and biology of the conformationally restricted ACPD analogue, 2-aminobicyclo[2.1.1]hexane-2,5-dicarboxylic acid-I, a potent mGluR agonist. J Med Chem 1998; 41,1641-1650.

Lee W-T, Lee C-S, Pan Y-L, Chang C. Temporal changes of cerebral metabolites and striatal lesions in acute 3-nitropropionic acid intoxication in the rat. Magnetic Resonance in Medicine 2000; 44: 29-34.

Mizuno Y, Hattori N, Matsumine H. Neurochemical and neurodegenerative correlates of Parkinson's disease. Journal of Neurochemistry 1998;71(3): 893-

Quary S, Bizat N, Altairac S, Menetrat H, Mittoux V, Conde F, Hantraye P, Brouillet E. (2000). Major strain differences in response to chronic systemic administration of the mitochondrial toxin 3-nitropropionic acid in rats: implications for neuroprotection studies. Neuroscience 2000; 97: 521-530

Reiter LM, DeRosa C, Kavlock RJ, Lucier G, Mac MJ, Melillo J, Melnick RL, Sinks T, Walton BT, The U.S. Federal framework for research on endocrine disruptors and an analysis of research programs supported during fiscal year 1996. Environmental Health Prespect 1998; 106: 105-113.

Schapira A H V. Neurotoxicity and the mechanisms of cell death in Parkinson's disease. Advances in Neurology. L. Battistin, G. Scarlato, T. Carceni and S. Ruggieri. Philadelphia, Lippincott-Raven. 1996;69: 161-165.

Storgaard J, Kornblit BT, Zimmer J, Bert J, Gramsbergen P. 3-Nitropropionic acid in organotypic striatal and corticostriatal slice cultures is dependent on glucose and glutamate. Exp Neurol 2000; 164(1):227-35.

Yu M, Nagren K, Chen YI, Livni E, Elmaleh D, Kozikowski A, Wang W, Jokivarsi K, Brownell A-L. Radiolabeling and biodistribution of methyl 2-(methoxycarbonyl)-2-(methylamino) bicyclo [2.1.1]-hexane-5-carboxylate, a potential neuroprotective drug. Life Sciences 2003; 73:1577-1585.

Zayed J, Mikhail M, Loranger S, Kennedy G, L'Esperance G. Exposure of taxi drivers and office workers to total and respirable manganese in an urban environment. American Industrial Hygiene Association Journal 1996; 57: 376-80.

APPENDICES

Figures 1-7.

Abstracts and reports:

A-L Brownell, YI Chen, KE Canales, E Livni, RT Powers, A Dedeoglu, FM Beal, BG Jenkins. 3-NP induced neurotoxicity – assessed by ultra high resolution PET with comparison to MRI and MRS. 1st Annual Meeting of the Society for Molecular Imaging. Boston, August 24-26, 2002

Anna-Liisa Brownell, Kelly Canales, Y. Iris Chen, Bruce G. Jenkins, Christopher Owen, Elijahu Livni, Meixiang Yu, Francesca Cicchetti, Rosario Sanchez-Pernaute, Ole Isacson. Mapping of brain function after MPTP induced neurotoxicity in primate Parkinson's disease model. 2nd Annual Meeting of Neuroscience. Orlando, Florida, November 2002.

Anna-Liisa Brownell, Iris Y. Chen, Xukui Wang, Meixiang Yu, Bruce G. Jenkins. Neurotoxicity-Induced Changes in Striatal Dopamine Receptor Function. Parkinson's disease: The Life Cycle of the Dopamine Neuron. Ann. N.Y. Acad. Sci. 991:281-283, 2003.

Meixiang Yu, Kjell Nagren, Y. Iris Chen, Elijahu Livni, David Elmaleh, Alan Kozikowski, Xukui Wang, Kimmo Jokivarsi, Anna-Liisa Brownell. Radiolabeling and biodistribution of methyl 2-(methoxycarbonyl)-2-(methylamino) bicyclo [2.1.1]-hexane-5-carboxylate, a potential neuroprotective drug. Life Sciences 73:1577-1585, 2003.

Anna-Liisa Brownell, Kelly Canales, Y.Iris Chen, Bruce G. Jenkins, Christopher Owen, Elijahu Livni, Meixiang Yu, Francesca Cicchetti, Rosario Sanchez-Pernaute, Ole Isacson. Mapping of brain function after MPTP induced neurotoxicity in a primate Parkinson's disease model. NeuroImage 2003 (in press).

Meixiang Yu, Thomas Klaess, Alan Kozikowski, Anna-liisa Brownell. Synthesis of [11C]methoxymethyl-MPEP and [11C]methoxy-PEPy, potent and selective PET ligands for metabotropic glutamate subtype 5 mGluR5) receptors. 33rd Annual Meeting of Neuroscience. New Orleans. November 2003.

Anna-Liisa Brownell, Y. Iris Chen, Meixiang Yu, Xukui Wang, Kimmo Jokivarsi, Aparajita Sarkar, Alp Dedeoglu, Francesca Cicchetti, M. Flint Beal, Bruce G. Jenkins. 3-Nitropropionic acid induced neurotoxicity – assessed by ultra high resolution PET with comparison to MRI and MRS. Journal of Neuroscience (submitted).

Meixiang Yu and Anna-Liisa Brownell. Synthesis of C-11 CPCCOMe, a Potential PET Ligand for Imaging mGluR1 In Vivo. Molecular Imaging, Vol. 1, No. 3, July 2002.

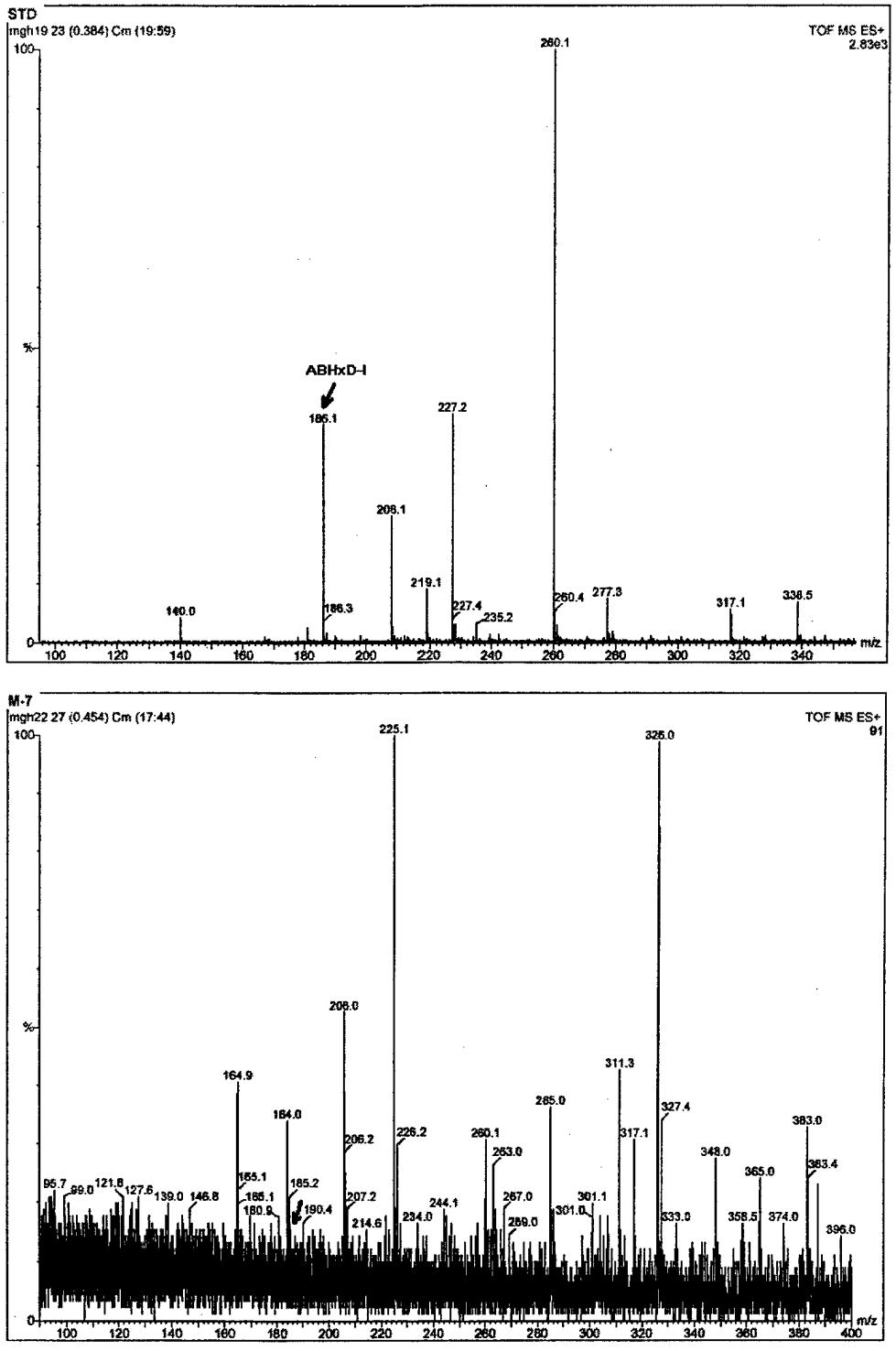

Figure 1: (above) Mass spectrometry of the compound ABHxD-I shows many impurities (real peak is 186.1). (below) Mass spectrometry of the dialysate showed tiny penetration of the ABHxD-I and higher peaks were measured of observed impurities.

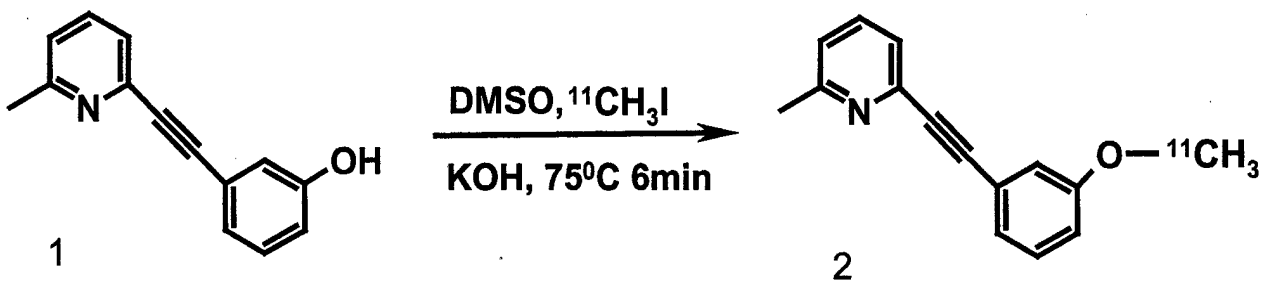

1

2

3-[(6-methylpyridin-2-yl) ethynyl]phenol, **Precursor**

2-[(3-methoxyphenyl)ethynyl] -6-methylpyridine, **M-MPEP**

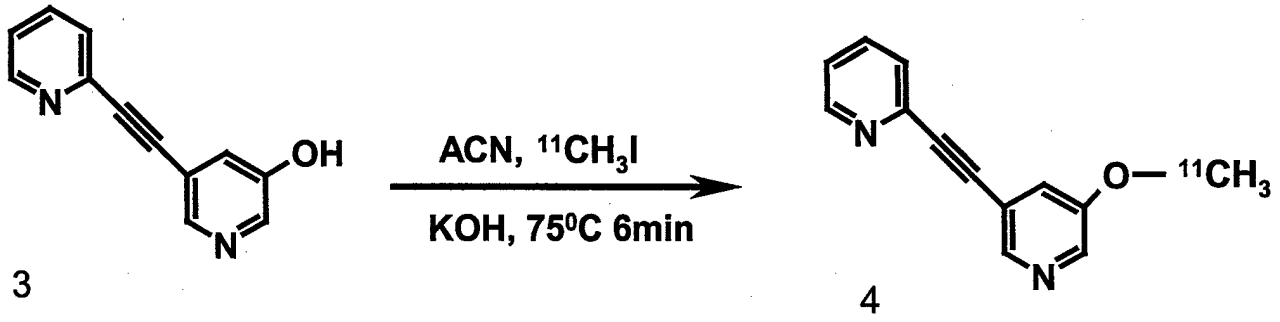

3

4

5-(pyridin-2-ylethynyl) pyridin-3-ol, **Precursor**

3-methoxy-5-(pyridin-2-ylethynyl)pyridine, **M-PEPy**

Figure 2. Schematic diagram of radiolabeling of [^{11}C]M-MPEP (2) and [^{11}C]M-PEPy (4)

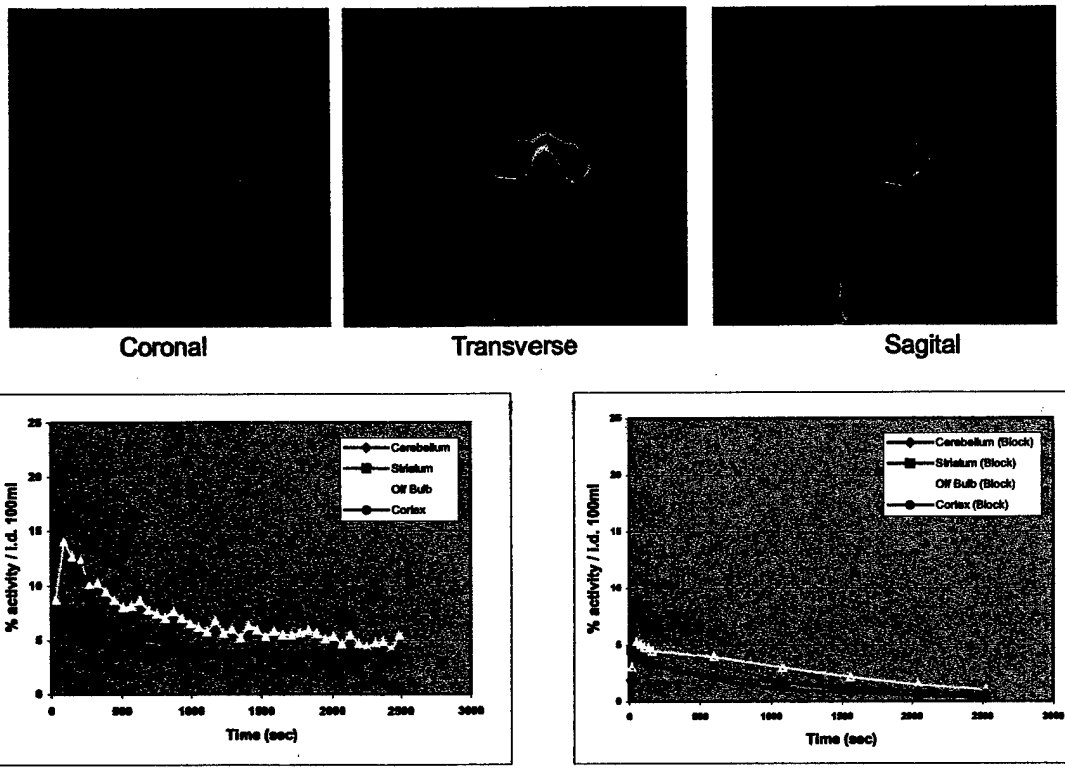

Figure 3a: [^{11}C]M-MPEP distribution 20 min. after injection (upper panel). Time dependent distribution in different brain areas (left) and corresponding distribution 10 min. after pretreatment with 3.5mg/kg M-PEP (right).

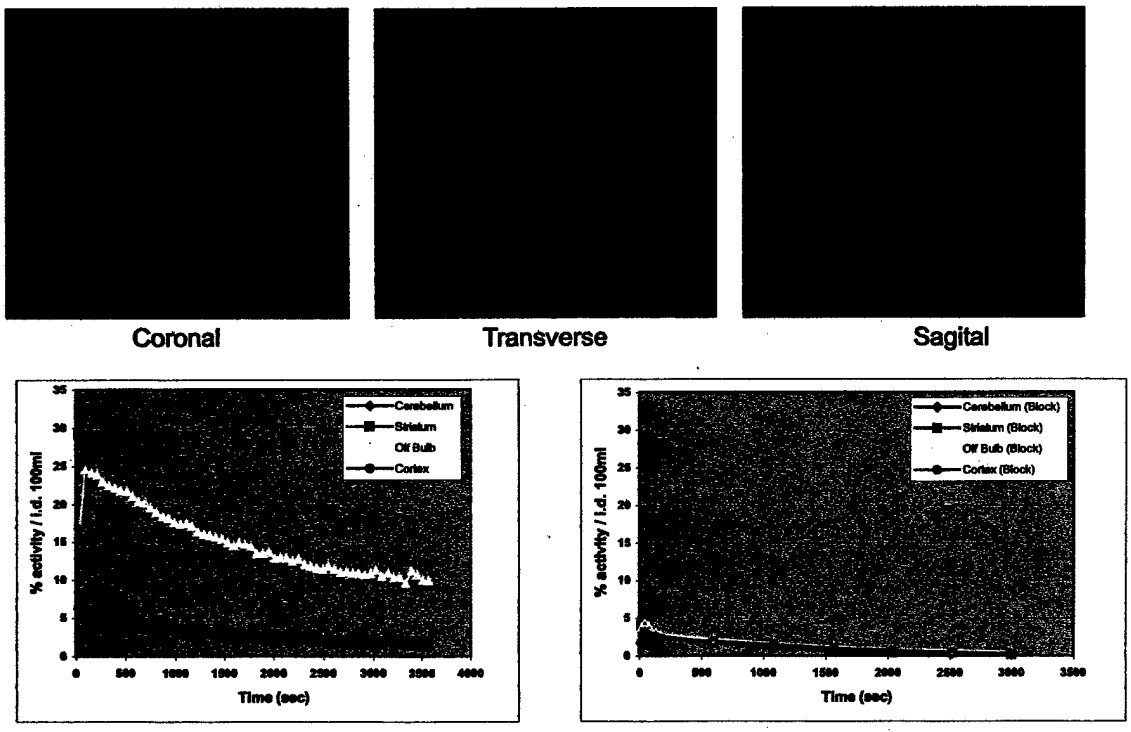

Figure 3b: [^{11}C]M-PEPy distribution 20 min. after injection (upper panel). Time dependent distribution in different brain areas (left) and corresponding distribution 10 min. after pretreatment with 3.5mg/kg M-PEPy (right).

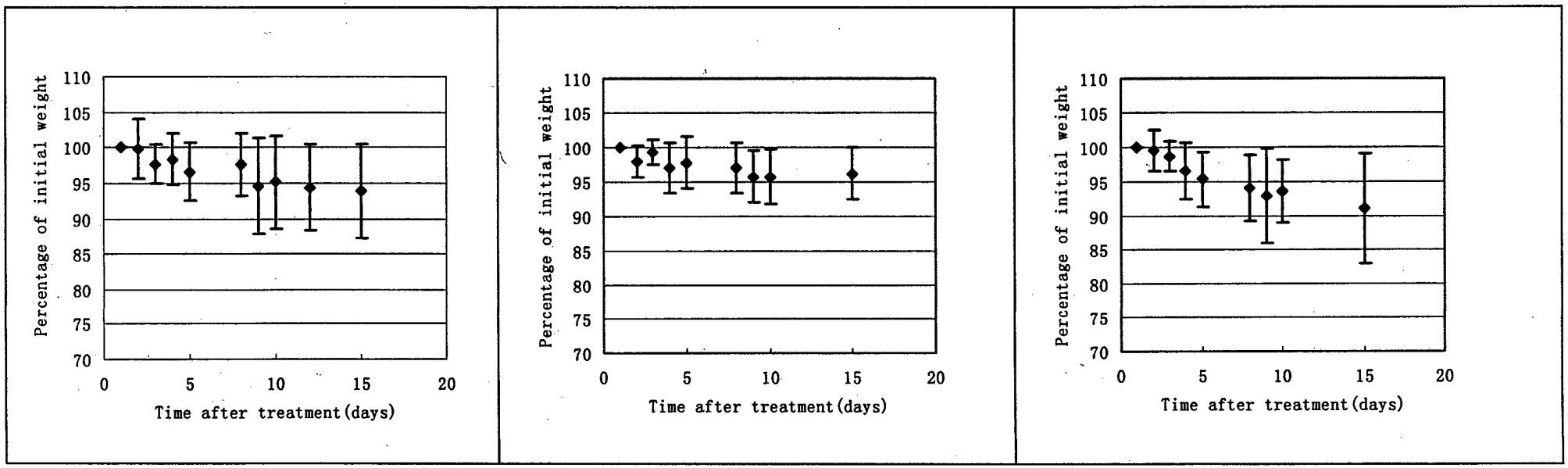

Figure 4A. Weight progression (a) in untreated; (b) in cystamine treated with a dose of 100 mg/kg/day and (c) in cystamine treated with a dose of 50 mg/kg/day.

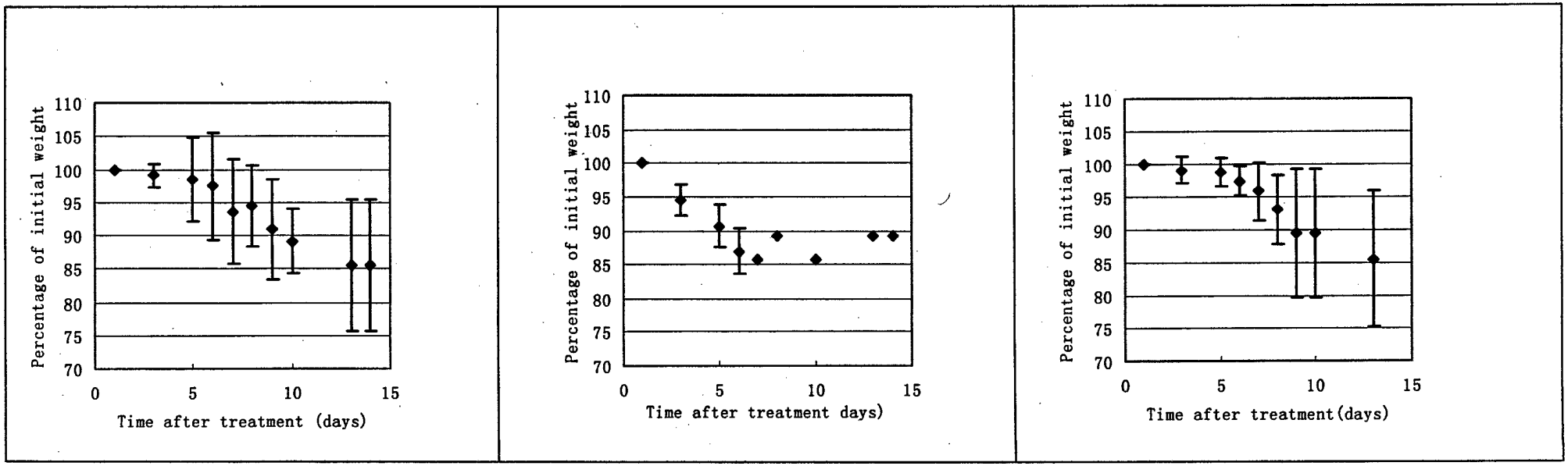

(a) (b) (c)

Figure 4B. Weight progression (a) in untreated; (b) in CPCCOEt treated with a dose of 5.2 mg/kg/day and (c) in cystamine treated with a dose of 9 mg/kg/day.

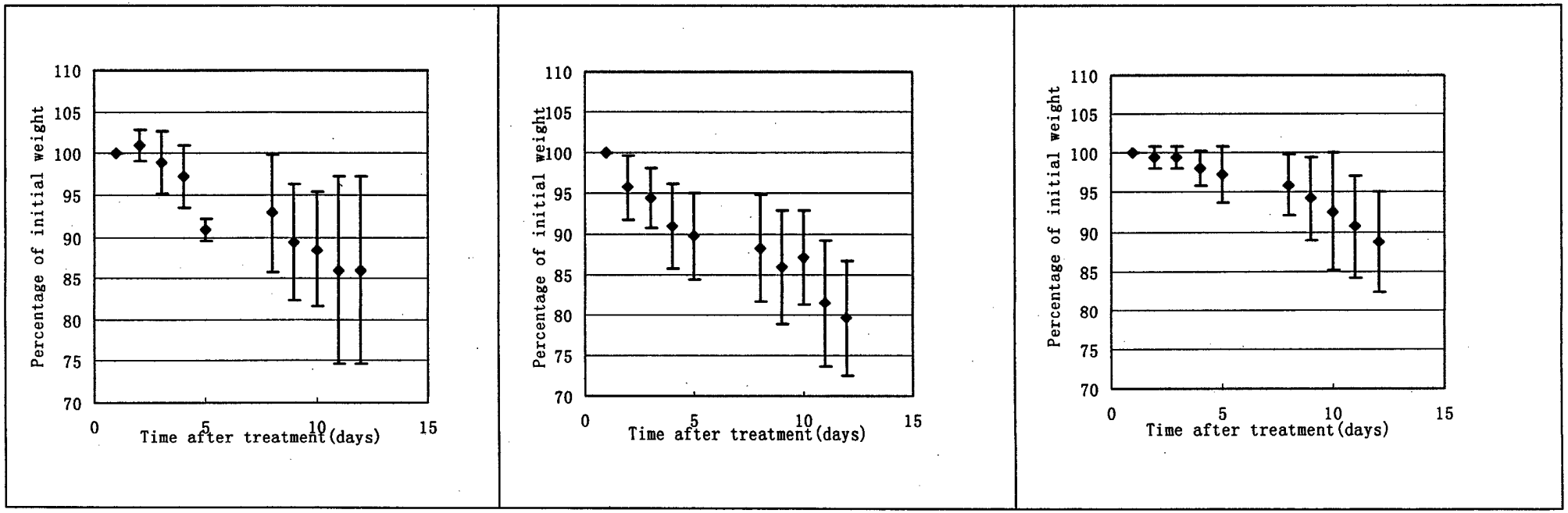

Figure 4C. Weight progression (a) in untreated; (b) in cystamine treated with a dose of 9 mg/kg/day and (c) in cystamine treated with a dose of 5.4 mg/kg/day.

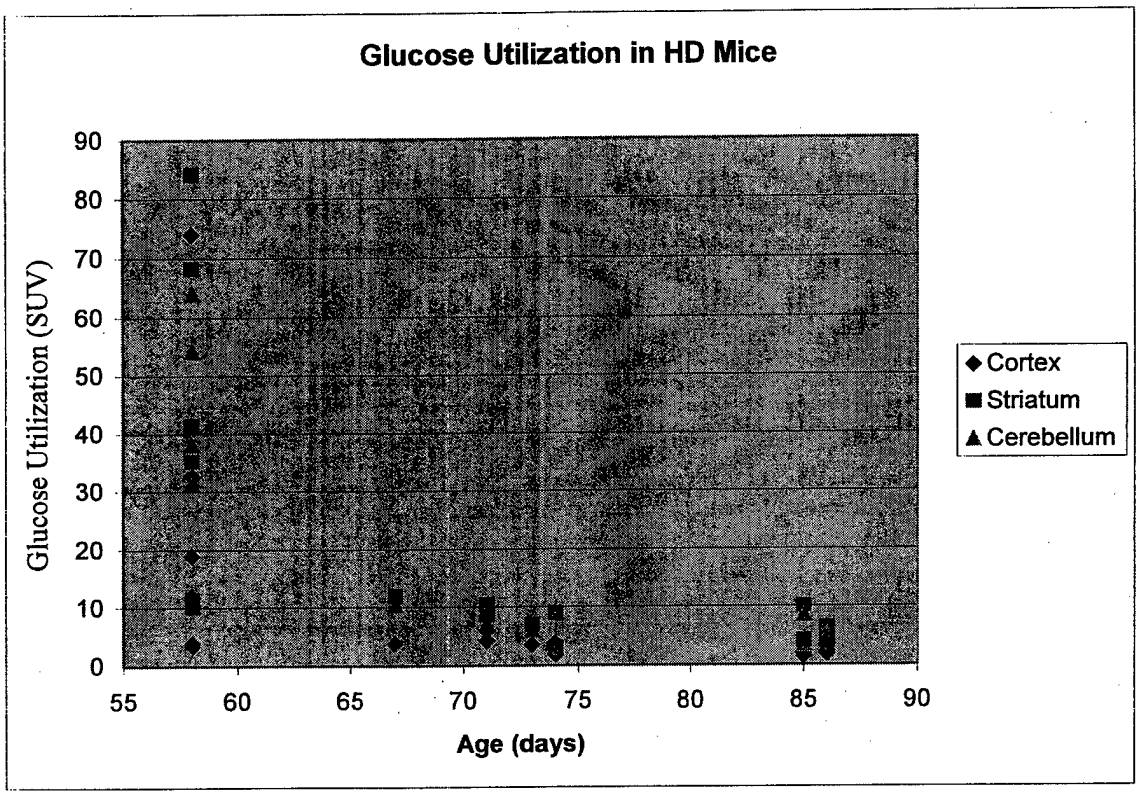

Figure 5a. Decrease of glucose utilization as a function of age in HD mice. Note the early exponential decrease when the HD symptoms start to develop.

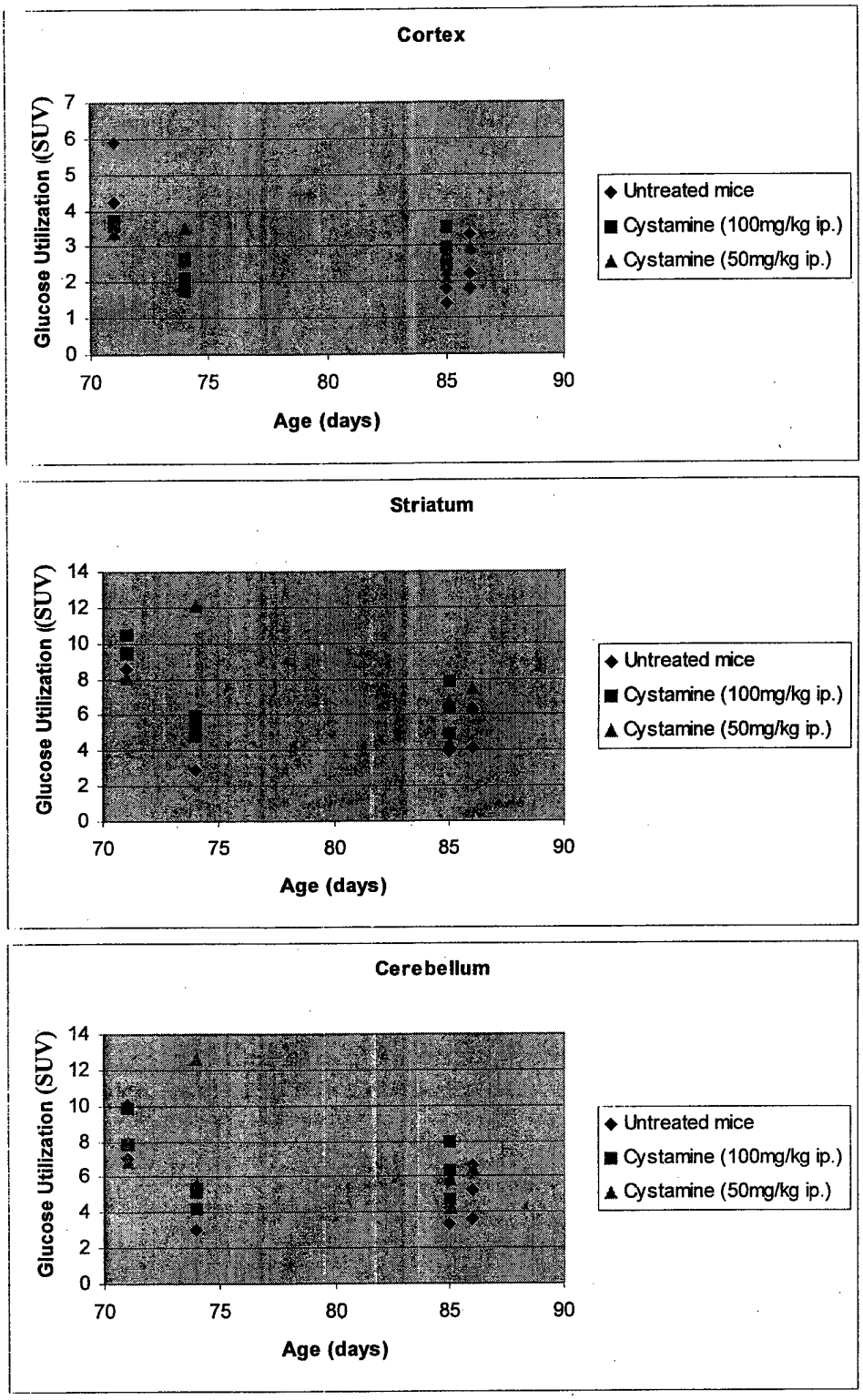

Figure 5b. Effect of neuroprotection with cystamine using doses of 100 mg/kg and 50mg/kg on glucose utilization in cortex, striatum and cerebellum as a function of age in HD mouse model.

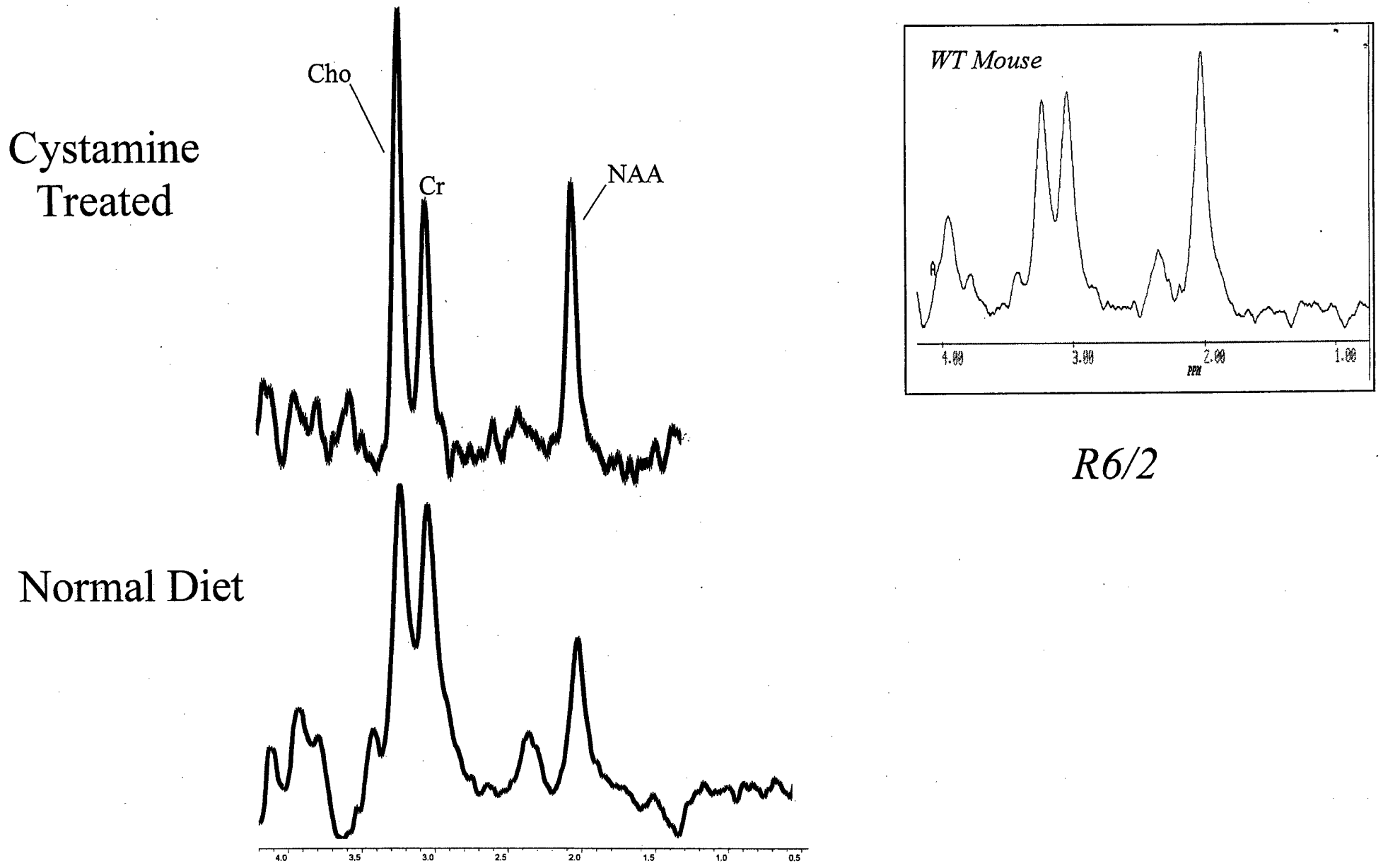

Figure 6: Striatal MR Spectra of Cystamine treated and Untreated HD Mice. Cystamine spectrum was averaged from 3 different mice. Note that both choline and NAA are significantly enhanced in Cystamine treated HD mice as compared to the Normal Diet HD Mice or the Wild Type Mice.

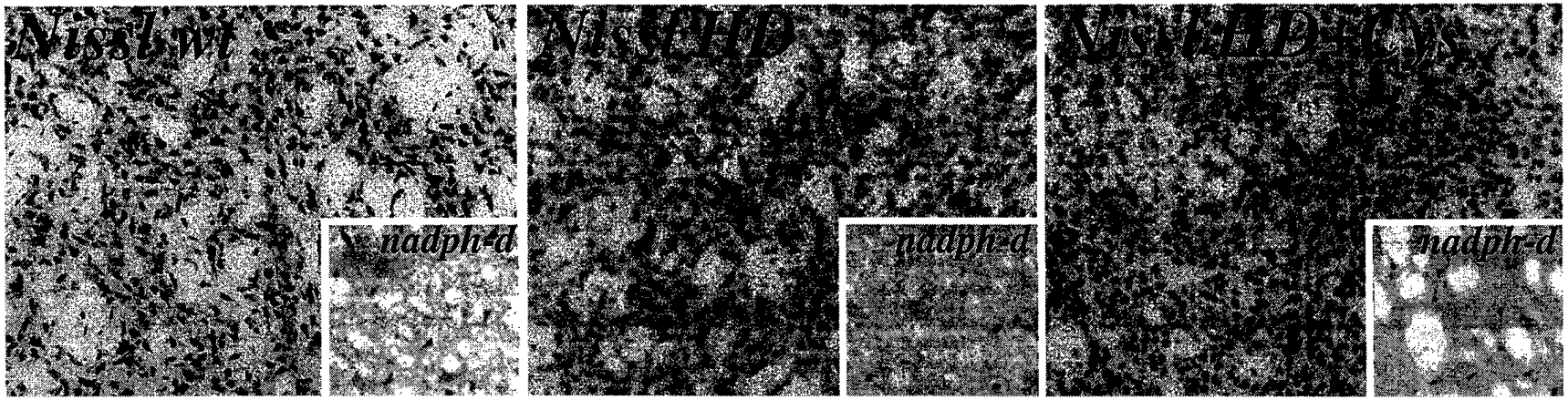

Figure 7a: Post-mortem histological evaluation of HD R6/2 transgenic mice treated with the transglutaminase inhibitor cystamine (dose 9 mg/kg). Photomicrographs illustrate frontal sections through the striatum at the level of the anterior commissure in wild-type, untreated R6/2 HD mice and cystamine treated HD mice. Nissl staining reveals less numerous and unhealthy striatal cells as compared to wild-type. Following low dose cystamine treatment, striatal cells are more numerous and depict a healthier appearance. The presence and intensity of the enzyme B-nicotinamide adenine dinucleotide phosphatase (nadph-d), associated to a subpopulation of interneurons not targeted in HD, shows no significant difference in wt, HD and HD treated animals.

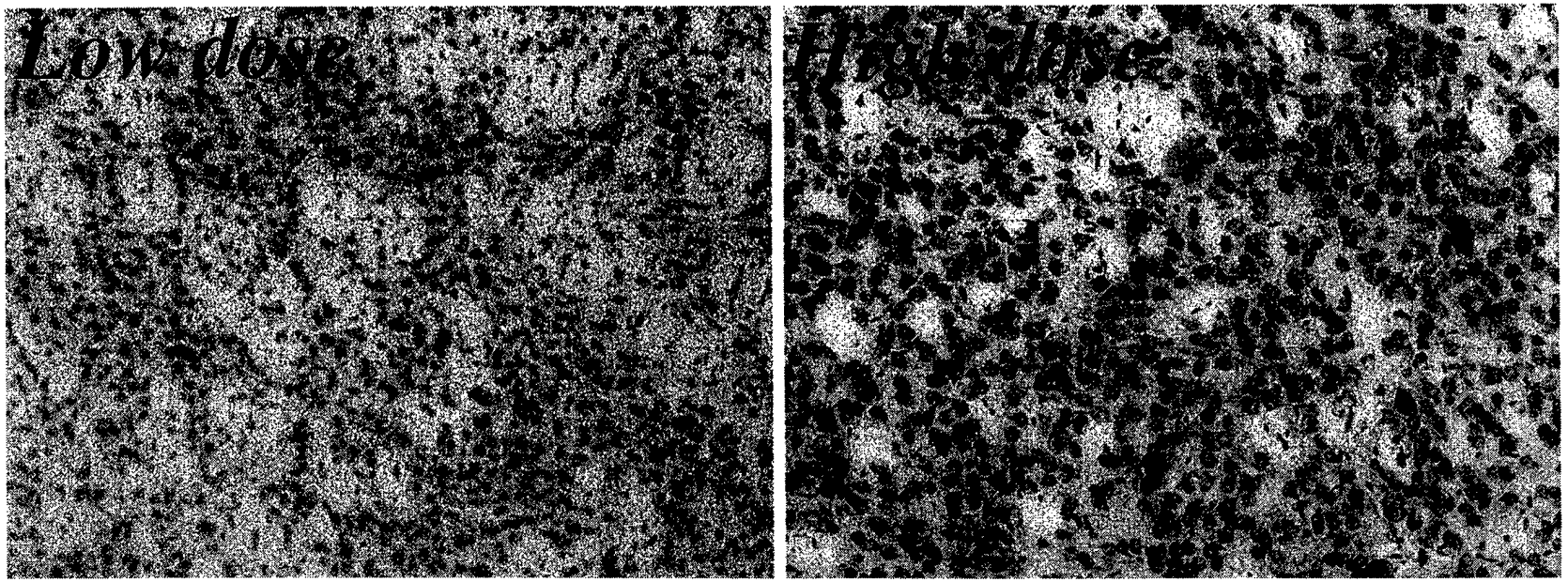

Figure 7b: Neuroprotective effects of cystamine are dose dependent. High dose treatment (100mg/kg) shows more neuroprotection (number of cells and overall health appearance) than lower doses (50mg/kg), which also demonstrate neuroprotective potential, as revealed by Nissl staining.

Abstract ID: 286

3-NP-Induced Neurotoxicity—Assessed by PET and MRI/MRS

A.-L. Brownell, Y. I. Chen, M. Yu, and B. G. Jenkins
Radiology, Massachusetts General Hospital
Neurobiology

3-Nitropropionic acid (3-NP), a succinate dehydrogenase inhibitor, is widely used as an experimental model to study Huntington's disease (HD), energy metabolism, and cell death. We used a rat model to investigate 3-NP-induced acute and prolonged neurotoxicity using in vivo imaging of cerebral glucose utilization (CGU) and dopamine receptor function by PET, neuroanatomy by MRI and neurochemicals by MRS. 3-NP was administered (male Sprague–Dawley) twice a day (10 mg/kg ip) until symptomatic or max of 5 days. PET studies of CGU were conducted daily using a super high resolution ($1.3 \times 1.3 \times 1.8$ mm^3) in-house built PET device. MRI and MRS studies were conducted with a GE Omega 4.7-T imager. Studies of CGU showed significant interanimal variation in the acute response of toxin, similar to motor activity. The average decrease of CGU in the lesions a day after cessation of 3-NP was 31 ± 12%. Four weeks later, CGU was recovered to −13 ± 5% and then in 3 months decreased again to 48 ± 10%. After 3-NP, dopamine D1 and D2 receptors showed progressively decreasing binding using ^{11}C-SCH and ^{11}C-raclopride, respectively. However, the binding of dopamine transporter imaged by ^{11}C-CFT showed an early increase (1 week after 3-NP) followed by a progressive decrease. MRS showed elevated peaks of lactate and macromolecules as well as succinate immediately after 3-NP toxicity, which diminished in 4 months, indicating a reversible process. Choline peak increased and NAA peak decreased in 4 months indicating loss and damage of neurons. Postmortem histological studies confirmed the neural loss indicated by in vivo imaging.

Program Number: 125.12 **Day / Time:** Sunday, Nov. 3, 3:45 PM - 4:00 PM

MAPPING OF BRAIN FUNCTION AFTER MPTP INDUCED NEUROTOXICITY IN A PRIMATE PARKINSON'S DISEASE MODEL

A.Brownell [1*]; K.Canales [1]; Y.I.Chen [1]; B.G.Jenkins [1]; C.Owen [2]; E.Livni [1]; M.Yu [1]; F.Cicchetti [3]; R.Sanchez-Pernaute [3]; O.Isacson [3]

1. Radiology, Massachusetts General Hospital, Boston, MA, USA; 2. Neurology, Massachusetts General Hospital, Boston, MA, USA; 3. Neuroregeneration laboratory, McLean Hospital, Belmont, MA, USA

Neurophysiological studies of the brain in normal and Parkinson's disease (PD) patients have indicated intricate connections for basal ganglia induced control of signaling into the motor cortex. To investigate if similar mechanisms are controlling function in the primate brain (Macaca fascicularis) after MPTP induced neurotoxicity, we conducted PET studies of blood flow, oxygen and glucose metabolism, dopamine transporter and D2 receptor function. After MPTP, blood flow was increased (15%) in the globus pallidus (GP), decreased 40% in the primary motor cortex (PMC) and moderately decreased (15-25%) in the other brain areas. Oxygen extraction fraction was moderately increased (10-20%) in all brain areas. Oxygen metabolism was increased in the GP and supplementary motor area by a range of 20-40% and moderately decreased in the putamen, caudate and in the PMC. Glucose metabolism was enhanced in the GP by 15% and decreased in the caudate, putamen, thalamus and PMC (range 35-50%). 11C-CFT (2β -carbomethoxy-3 β -(4-fluorophenyl- tropane) dopamine transporter binding was significantly decreased in the putamen and caudate (range 60-65%). 11C-raclopride binding of dopamine D2 receptors did not show significant changes.These results conceive observations made in PD patients. We conclude that elevated blood flow, oxygen consumption and glucose utilization detected in the GP and SMA are part of a compensatory functional mechanism obtained by neurophysiological changes in the neural motor circuitry.
Supported by: NINDS NS-P50-39793

Citation: A.Brownell, K.Canales, Y.I.Chen, B.G.Jenkins, C.Owen, E.Livni, M.Yu, F.Cicchetti, R.Sanchez-Pernaute, O.Isacson. MAPPING OF BRAIN FUNCTION AFTER MPTP INDUCED NEUROTOXICITY IN A PRIMATE PARKINSON'S DISEASE MODEL. Program No. 125.12. *2002 Abstract Viewer/Itinerary Planner.* Washington, DC: Society for Neuroscience, 2002. CD-ROM.

Available online at www.sciencedirect.com
SCIENCE DIRECT®
ELSEVIER
Life Sciences 73 (2003) 1577–1585
Life Sciences
www.elsevier.com/locate/lifescie

Radiolabeling and biodistribution of methyl 2-(methoxycarbonyl)-2-(methylamino) bicyclo [2.1.1] - hexane -5-carboxylate, a potential neuroprotective drug

Meixiang Yu[a,*], Kjell Någren[b], Y. Iris Chen[a], Elijahu Livni[a], David Elmaleh[a], Alan Kozikowski[c], Xukui Wang[a], Kimmo Jokivarsi[a], Anna-Liisa Brownell[a]

[a] *Department of Radiology, Massachusetts General Hospital and Harvard Medical School, Bartlett Hall 511R, Boston, MA 02114, USA*
[b] *Turku PET Center, Turku, Finland*
[c] *Georgetown University Medical Center, Washington DC, USA*

Received 29 October 2002; accepted 18 March 2003

Abstract

Methyl 2-(methoxycarbonyl) -2-(methylamino) bicyclo[2.1.1] -hexane -5-carboxylate (MMMHC) is developed as a potential neuroprotective drug. It was labeled with C-11 from the desmethyl precursor methyl 2-(methoxycarbonyl)-2-amino bicyclo[2.1.1]-hexane-5-carboxylate with [^{11}C]methyl triflate in acetone solution at 60 °C with labeling yield of 69% and with radiochemical purity of >99%. Positron Emission Tomography (PET) studies in a normal rat showed that Methyl 2-(methoxycarbonyl)-2-([^{11}C]methylamino)bicyclo[2.1.1]-hexane-5-carboxylate ([^{11}C] MMMHC) accumulated mainly in the cortical brain areas after iv administration. Frontal cortex/cerebellum ratios in a rat brain were 8.0/6.0, 6.8/4.2, 6.3/4.3, 5.5/4.2 and 5.2/4.5 percent of the injected dose in 100 ml at 2 min, 5 min, 10 min, 20 min and 40 min respectively after i.v. injection. During 20–40 min, 2.9 ± 0.4% of the total activity stayed in the brain. These results showed that MMMHC could be labeled with C-11 with high yield, and it passed the brain-blood barrier and accumulated in several brain regions.

Keywords: Metabotropic glutamate receptors; Neuroprotection; Positron emission tomography; Carbon-11

* Corresponding author. Tel.: +1-617-726-6756; fax: +1-617-726-5123.
E-mail address: ymeixiang@partners.org (M. Yu).

0024-3205/03/$ - see front matter © 2003 Elsevier Science Inc. All rights reserved.
doi:10.1016/S0024-3205(03)00482-X

Introduction

L-Glutamate is the major excitatory neurotransmitter in the mammalian central neural system, acting through both ligand gated ion channels (ionotropic receptors) and G-protein coupled (metabotropic) receptors (Dhami et al., 2002; Bonvento et al., 2002; McFeeters and Oswald, 2002). Glutamate has a role in a variety of physiological processes including development of synaptic plasticity, motor control, respiration and cardiovascular regulation (Sigrist et al., 2002; Fendt and Schmid, 2002; Gordon and Sved, 2002). An excessive or inappropriate stimulation of glutamate receptors leads to neural cell damage or loss, by a mechanism known as excitotoxicity (Blondeau et al., 2002). Neurotoxicity and chronic neurodegenerative diseases (e.g. Parkinson's and Huntington's disease) are also associated with abnormal activation of metabotropic glutamate receptors (mGluRs) (Rouse et al., 2000; Difazio et al., 1992). Investigation of metabotropic receptor function has been hampered because of lack of specific receptor ligands. So far, no functional in vivo imaging studies were published using mGluR labeled ligands. However, several drug discovery projects targeting metabotropic receptors were published recently (Fundytus, 2001; Ossowska et al., 2000; Knopfel et al., 1995). Kozikowski et al (Kozikowski et al., 1998) developed a mGluR agonist, 2-aminobicyclo[2.1.1]hexane-2,5-dicarboxylic acid-I (ABHx D-I, compound A in Fig. 1). In preliminary in vitro studies ABHx D-I was found to protect against neural death in several neurotoxic models including neurotoxicity induced by NMDA, by oxygen and glucose deprivation in mouse cortical neuronal-glial cultures. The ABHx D-I has two carboxylic acid functions, it is unlikely that the compound ABHx D-I can pass the brain-blood barrier (BBB) because of its high polarity (Platts et al., 2001). To overcome the polarity issue and allow potential BBB penetration, we designed a new compound, methyl 2-(methoxycarbonyl) -2-(methylamino) bicyclo[2.1.1] -hexane -5-carboxylate (MMMHC, Compound B in Fig. 1). We postulated that this methyl ester analogue might act as a pro-drug if it is metabolized into ABHx D-I in the brain by enzymatic degradation. To study the in vivo behavior of this compound (MMMHC), we labeled it with C-11 and conducted positron emission tomography (PET) imaging studies of its dynamic biodistribution in a rat model. The vivo pharmacokinetic behavior of the compound is essential to determine if it will be used as a drug for therapeutic purposes (Torchilin, 2000).

Materials and Methods

Materials

The reference compound MMMHC and the precursor for labeling were provided by Dr. Kozikowski (Kozikowski et al., 1998). Silver triflate was purchased from Aldrich and Graphpac

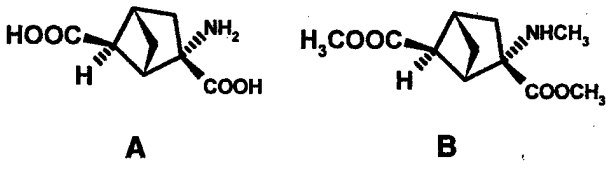

Fig. 1. Chemical structure of ABHx-D-I (A), MMMHC (B).

GC (80–100 mesh) from Alltech. Other chemicals were obtained from commercial sources and were of analytical grade.

Radiochemistry

Production of [^{11}C]carbon dioxide

[^{11}C]carbon dioxide was produced with the cyclotron using 16 MeV protons by the $^{14}N(p, \alpha)^{11}C$ nuclear reaction on nitrogen. The [^{11}C]carbon dioxide was trapped in a stainless-steel coil cooled with liquid nitrogen before being transferred to the [^{11}C]methyl iodide/[^{11}C]methyl triflate system.

Preparation of [^{11}C]methyl triflate

[^{11}C]methyl iodide was prepared from cyclotron produced [^{11}C]carbon dioxide by standard methods (Någren and Halldin, 1998) and passed through a heated soda glass column (oven temperature 200 °C) containing silver triflate impregnated graphitized carbon (Jewett, 1992).

Preparation of methyl 2-(methoxycarbonyl) -2-([^{11}C]methylamino) bicyclo[2.1.1] -hexane -5-carboxylate ([^{11}C]MMMHC) from methyl 2-(methoxycarbonyl) -2-amino bicyclo[2.1.1] -hexane -5-carboxylate

0.3 mg precursor (Compound C in Fig. 2) in 300 μL acetone was used to trap [^{11}C]methyl triflate at 0 °C. After trapping, the reaction mixture was heated at 60 °C for 1 min. After addition of 200 μL HPLC solvent (0.01 M H_3PO_4/acetonitrile 9/1), the reaction mixture was purified by HPLC. The radioactive peak with a retention time (5 min) similar to a reference standard was collected. After evaporation, the residue was dissolved in saline buffer and sterilized by filtration through a 0.2-μm filter (Millex®-GV).

Preparative HPLC system

The radiotracer methyl 2-(methoxycarbonyl)-2-([^{11}C]methylamino) bicyclo[2.1.1] -hexane -5-carboxylate ([^{11}C]MMMHC) was purified by a HPLC system comprising a mobile phase, pump (Merck), an automatic sample injector (Merck, with 5 ml loop) and radioactivity detector (in-house construction). Separation was performed on a μ-Bondapak® C-18 column (7.8 × 300 mm, Waters) using acetonitrile and 0.01 M phosphoric acid (90/10) as the mobile phase with a flow of 6 ml/min.

Analytical HPLC system

The radioligand [^{11}C]MMMHC was analyzed by reversed-phase HPLC on a μ-Bondapak® C-18 column (3.9 × 300 mm, Waters) using a PC-controlled system with Merck HITACHI pump (type L-

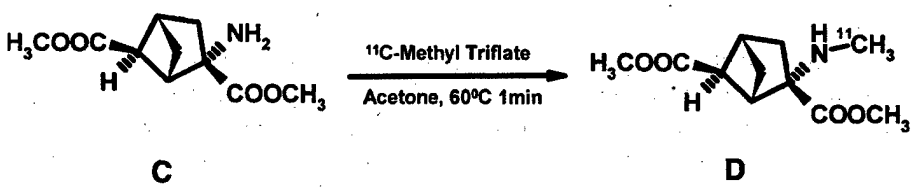

Fig. 2. The reactions of [^{11}C]Methyl triflate with desmethyl precursor C.

7100) and a UV absorbance detector (type L-7400) in series with radioactivity detector (model) (Yu et al., 1998). After injection of the purified product [^{11}C]MMMHC together with the unlabelled reference, the column was eluted with a gradient system starting from 90% of 0.01M H_3PO_4 and 10% of CH_3CN to 20% of 0.01M H_3PO_4 and 80% of CH_3CN at 8 min, then back to 90% of 0.01M H_3PO_4 and 10% of CH_3CN at 10 min with a flow rate of 2 ml/min, and UV absorbance was measured at 220 nm (the retention time R_t of the compound was 3.2 min).

Positron emission tomography studies

Positron emission tomography studies were carried out with in-house-built PET scanners PCR-I (Brownell et al., 1989) and super high-resolution rodent PET scanner (Correia et al., 1999). Both scanners are one-ring systems. The PCR-I (built 1983) has resolution of 4.5 mm and super high-resolution rodent PET scanner of 1.16 mm. However, the sensitivity in PCR-I is higher, which enables us to acquire whole body images of rats using "step and shoot" mode and a short acquisition time for each slice.

For PET imaging studies, animals were anaesthetized with halothane (1-1.5%) mixed to oxygen (3 L/min). Tail vein and artery were catheterized for infusion of the labeled ligand and drawing of blood samples needed for quantification at 2, 5, 10, 20 30 and 60 min after administration. The animal was placed in the imaging cradle and the head was adjusted into an in-house-built stereotactic head-holder. 0.5-1.0 mL volume was injected. For high resolution brain imaging with super high-resolution rodent PET scanner, sequential dynamic imaging data was acquired at one coronal midbrain level. For whole body imaging with PCR-I, data was acquired over the whole animal with 5 mm steps using a slice thickness of 5 mm. Calibration of the positron tomographs were performed in each study session using cylindrical plastic phantoms (diameters 2 or 6 cm) and ^{18}F solution. Imaging data was corrected for uniformity, sensitivity, attenuation, decay and acquisition time. PET images were reconstructed using Hanning-weighted convolution back projection with a cut-off value of 1.0. The coronal images of the whole body distribution were packed into a volume and reprocessed to transverse slices (Fig. 4). To determine the total accumulation in the brain, region of interest was drawn on all coronal slices, which cover the organ. Accumulation of radioactivity and number of pixels were determined of each slice to obtain the whole organ's specific values, which were related to the corresponding values of the whole animal. In addition, in the high resolution PET images (Fig. 5A), regions of interest, including the striatum, midbrain and cerebellum on both sides of the brain, were drawn and radioactivity per unit volume, percentage activity of injected dose and the ligand concentration were calculated (Fig. 5B).

Results

The desmethyl precursor reacted with [^{11}C]methyl triflate leading to the desired product [^{11}C]MMMHC (Fig. 2). The radiochemical yield of the labeling method was 69% (decay-corrected) within 40 min from EOB (end of bombardment), and the radiochemical purity of [^{11}C]MMMHC was higher than 99% as shown in Fig. 3. Using this method, the final product [^{11}C]MMMHC was prepared in batches containing more than 100 mCi, with high specific activity 800–1200 mCi/μmol. In the preparative HPLC purification system, the precursor was washed out earlier than the

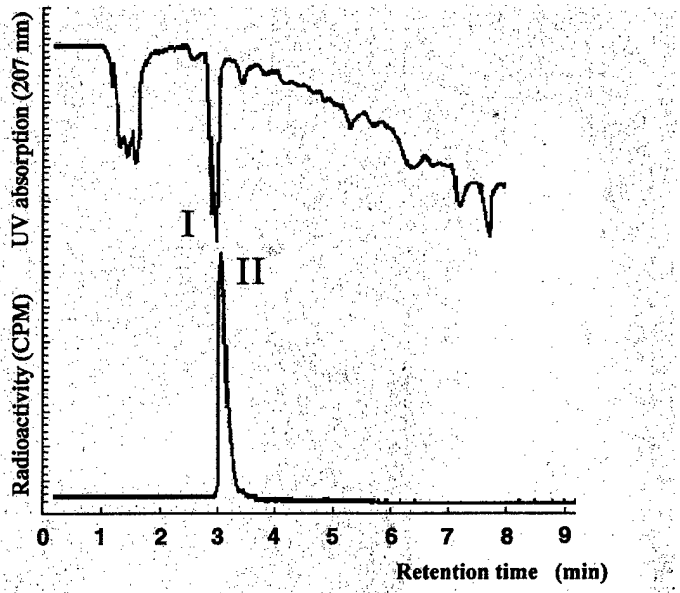

Fig. 3. Radiochemical purity analysis of the labeled compound [^{11}C]MMMHC by the HPLC chromatography (U.V. and radioactivity resus time). I (UV peak) and II (radioactivity peak) are product.

labeled compound, and the precursor cannot be detected by analytical HPLC system in the final product.

The whole body distribution of [^{11}C]MMMHC in a rat (Fig. 4) showed that after i.v. administration the radioactivity enters the brain, liver, kidneys and bladder. During 20–40 min, 2.9 ± 0.4% of the total activity stayed in the brain. The dynamic distribution of [^{11}C]MMMHC reached the peak around 2 minutes after i.v. injection as shown in Fig. 5B. After that, the radioactivity was partly washed out and the equilibrium was reached in several brain regions after 20 minutes. In the rat brain accumulation ratios of frontal cortex/cerebellum were 8.0/6.0, 6.8/4.2, 6.3/4.3, 5.5/4.2 and 5.2/4.5 percent of the injected dose in 100 ml (%ID/100mL) at 2 min, 5 min, 10 min, 20 min and 40 min respectively after i.v. injection. Furthermore, the high resolution imaging in the rat brain (Fig. 5A) showed that the [^{11}C]MMMHC accumulated especially in cortical areas.

Discussion

Three positions of the compound MMMHC (Compound B in Fig. 1) can be labeled with [^{11}C]methyl groups (two methyl ester positions, one methyl amine position). If a methyl ester position is chosen to label with [^{11}C]methyl triflate from the corresponding acid precursor, then the amine group in the precursor must be protected because of its high reactivity. After labeling, this protective group has to be selectively removed, which makes the labeling process more difficult. Alternatively, a better way to label the N-methyl function is to use [^{11}C]methyl triflate as we have done. C-11 methyl iodide is converted to C-11 methyl triflate before it is trapped in the reaction mixtures, because the C-11 methyl triflate was more reactive and the labeling yield was higher (Någren and Halldin, 1998).

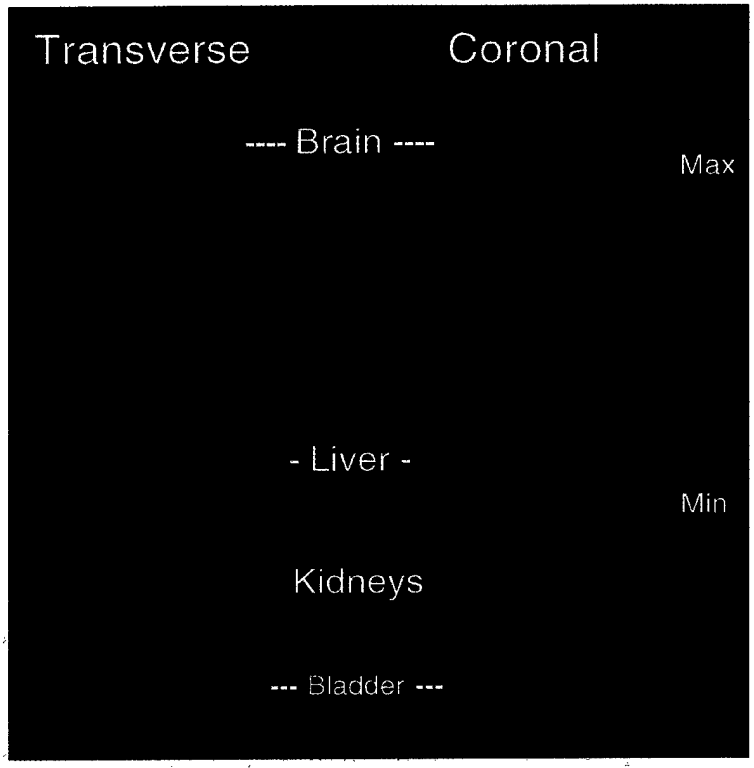

Fig. 4. Distribution of [^{11}C]MMMHC binding in a normal rat 20–40 min after administration of the labeled ligand.

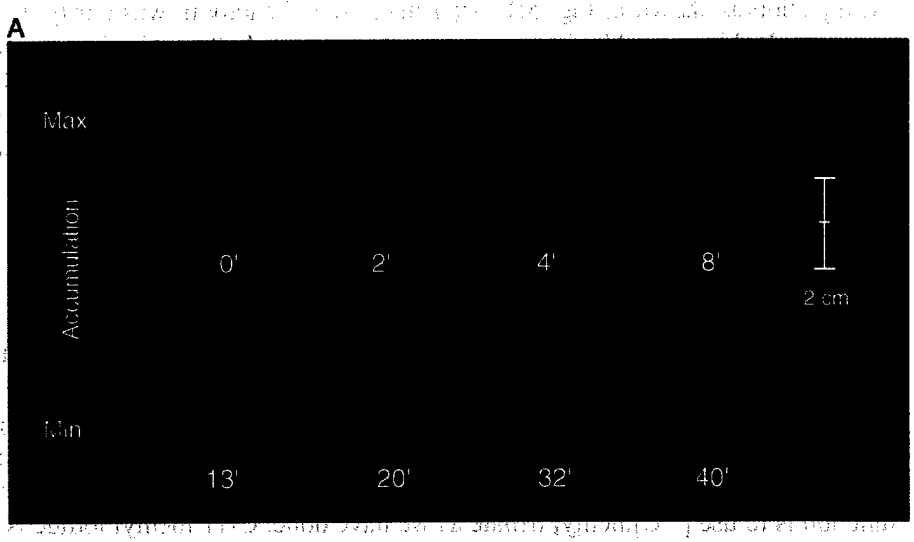

Fig. 5. A. Dynamic distribution of [^{11}C]MMMHC in a rat at the coronal midbrain level after iv injection. B. Time activity curves of [^{11}C]MMMHC binding in cerebellum and frontal cortex of a rat.

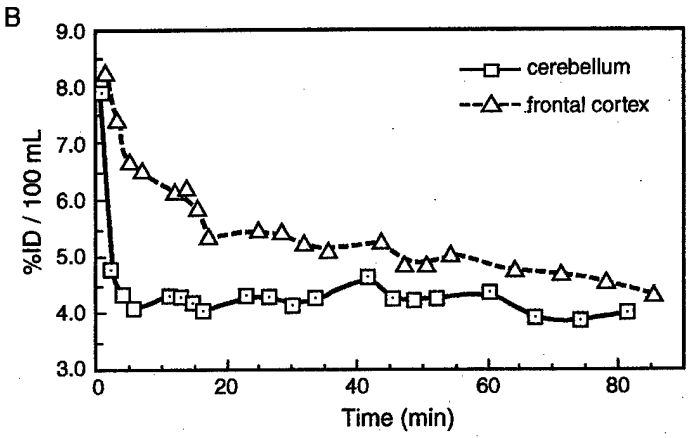

Fig. 5 (*continued*).

By using the N-desmethyl precursor, we got the C-11 labelled MMMHC in a good yield (69%) and high radiochemical purity (higher than 99%) as shown in Fig. 3. The byproduct with two [^{11}C]methyl groups on the amine nitrogen was not observed. The possible reason was that the amount of precursor was in high excess to [^{11}C]methyl triflate which had a high specific radioactivity (800–1200 mCi/μmol). It is useful to label one molecule in different positions in order to study its metabolites (Yu et al., 1999), however the selection of the position has to be done so that there will be no unwanted radiolabeled metabolites, which may interfere the imaging quality (Yu et al., 1997).

The distribution of [^{11}C]MMMHC in a normal rat showed that the radioactivity went into the brain (Fig. 5A and B) and the total brain accumulation between 20–40 min after i.v. administration was 2.9 ± 0.4% injected dose (ID). [^{11}C]MMMHC accumulates in the liver, and will be excluded through the kidneys into the bladder (Fig. 4). Most importantly, the [^{11}C]MMMHC kinetic distribution indicated reversible binding (Fig. 5B). The uptake reached the peak value in the brain (8–10% of the injected activity) at around 2 minutes after injection as shown in Fig. 5B, which was followed by a wash out that was a blood flow effect, and it reached equilibrium after 20 minutes. The high-resolution PET images show that the accumulation concentrated mainly in cortical structures (Fig. 5A).

The ABHx D-I (compound A in Fig. 1) is a physiologically active mGluR agonist (Kozikowski et al., 1998), it has two acid functions which make it quite polar and then difficult to pass the BBB. Schoepp et al have demonstrated that (2S)-2-Amino-2-(1S, 2S)-2-carboxycycloprop-1-yl)-3-(9-xanthyl)propanoic acid, a mGlu II receptor antagonist also with two acid functions, has very low potential to pass the BBB. By using 10 mg/kg dose, they verified that the peak values of the compound in the brain were 243.4 ng/g (iv), 245.5ng/g (ip) at 30 min after administration (Ornstein et al., 1998). It is valuable to design a new lipophilic pro-drug (as compound B, MMMHC in Fig. 1) to pass the BBB which will be metabolized there to get an active metabolite. There are two ester and one N-methyl groups in the compound MMMHC, which make the MMMHC lipophilic and easy to pass the BBB as demonstrated in this experiment. Ester hydrolysis happens in the liver, meanwhile the ester hydrolase in the brain (in both myelin and microsomes) is also active for the ester metabolism (Shand and West, 1995; Ghosh and Grogan, 1990; Arnaud et al., 1981), and ester hydrolysis is a mechanism to carry

some drug into the brain (Walovitch et al., 1994). Meanwhile, N-demethylation happens in the liver and also in the brain. N-desmethyl metabolite is a degradation product for the drugs with N-methyl amine structure by N-demethylase in the brain microsomes (Ravindranath et al., 1989; Hahn and Fishman, 1980; Kawashima et al., 1996). The pro-drug MMMHC can go to the brain and might be metabolized there to active ABHx D-I. We will continue this project to study the MMMHC metabolism in future experiments.

Conclusion

The compound methyl 2-(methoxycarbonyl)-2-(methylamino) bicyclo[2.1.1] hexane-5-carboxylate could be labeled with carbon-11 from its free base desmethyl precursor in high yield and high radiochemical purity. In vivo studies showed that the [^{11}C]MMMHC passed the brain-blood barrier and illustrated reversible binding properties in the brain.

Acknowledgements

This work was supported by the DOD grant DAMD17-99-1-9555 to A-LB.

References

Arnaud, J., Nobili, O., Boyer, J., 1981. Effect of adrenocorticotrophic hormone on the activity of sterol ester hydrolase from rat brain. Biochemical and Biophysical Research Communications 100 (3), 1167–1172.

Bonvento, G., Sibson, N., Pellerin, L., 2002. Does glutamate image your thoughts? Trends in Neurosciences 25 (7), 359–364.

Blondeau, N., Lauritzen, I., Widmann, C., Lazdunski, M., Heurteaux, C., 2002. A potent protective role of lysophospholipids against global cerebral ischemia and glutamate excitotoxicity in neuronal cultures. Journal of Cerebral Blood Flow and Metabolism 22 (7), 821–834.

Brownell, G.L., Burnham, C.A., Stearns, C.W., Chesler, D.A., Brownell, A.-L., Palmer, M., 1989. Development in high-resolution positron emission tomography at MGH. Int. J Img Systems and Technol 1, 207–217.

Correia, J., Burnham, C., Kaufman, D., Fischman, A., 1999. Development of a small animal PET imaging device with resolution approaching 1 mm. IEEE Trans Nucl Sci 46 (3), 631–635.

Dhami, G.K., Anborgh, P.H., Dale, L.B., Sterne-Marr, R., Ferguson, S.S., 2002. Phosphorylation-independent regulation of metabotropic glutamate receptor signaling by G protein-coupled receptor kinase 2. Journal of Biological Chemistry 277 (28), 25266–25272.

Difazio, M.C., Hollingsworth, Z., Young, A.B., Penney Jr., J.B., 1992. Glutamate receptors in the substantia nigra of Parkinson's disease brains. Neurology 42 (2), 402–406.

Fendt, M., Schmid, S., 2002. Metabotropic glutamate receptors are involved in amygdaloid plasticity. European Journal of Neuroscience 15 (9), 1535–1541.

Fundytus, M.E., 2001. Glutamate receptors and nociception: implications for the drug treatment of pain. CNS Drugs 15 (1), 29–58.

Gordon, F.J., Sved, A.F., 2002. Neurotransmitters in central cardiovascular regulation: glutamate and GABA. Clinical and Experimental Pharmacology and Physiology 29 (5–6), 522–524.

Ghosh, S., Grogan, W.M., 1990. Activation of myelin-associated cholesteryl ester hydrolase in developing rat brain. Brain Research. Developmental Brain Research 54 (1), 147–149.

Hahn, E.F., Fishman, J., 1980. Changes in brain N-demethylation and opiate receptor content correlate with analgesic effectiveness of morphine. Research Communications in Chemical Pathology and Pharmacology 29 (1), 197–200.

Jewett, D.M., 1992. A simple synthesis of [^{11}C] methyl Triflate. Appl Radiat Isot 43, 1383–1385.

Kozikowski, A.P., Steensma, D., Araldi, G.L., Tuckmantel, W., Wang, S., Pshenichkin, S., Surina, E., Wroblewski, J.T., 1998. Synthesis and biology of the conformationally restricted ACPD analogue, 2-aminobicyclo[2.1.1]hexane-2,5-dicarboxylic acid-I, a potent mGluR agonist. Journal of Medicinal Chemistry 41 (10), 1641–1650.

Kawashima, H., Sequeira, D.J., Nelson, D.R., Strobel, H.W., 1996. Genomic cloning and protein expression of a novel rat brain cytochrome P-450 CYP2D18* catalyzing imipramine N-demethylation. Journal of Biological Chemistry 271 (45), 28176–28180.

Knopfel, T., Kuhn, R., Allgeier, H., 1995. Metabotropic glutamate receptors: novel targets for drug development. Journal of Medicinal Chemistry 38 (9), 1417–1426.

McFeeters, R.L., Oswald, R.E., 2002. Structural mobility of the extracellular ligand-binding core of an ionotropic glutamate receptor. Analysis of NMR relaxation dynamics. Biochemistry 41 (33), 10472–10481.

Någren, K., Halldin, C., 1998. Methylation of amide and thiol functions with [^{11}C]methyl triflate, as exemplified by [^{11}C]NMSP, [^{11}C]flumazenil and [^{11}C]Methionine. Journal of Labelled Compounds and Radiopharmaceuticals 41 (9), 831–841.

Ossowska, K., Pietraszek, M., Wardas, J., Nowak, G., Zajaczkowski, W., Wolfarth, S., Pilc, A., 2000. The role of glutamate receptors in antipsychotic drug action. Amino Acids 19 (1), 87–94.

Ornstein, P.L., Bleisch, T.J., Arnold, M.B., Kennedy, J.H., Wright, R.A., Johnson, B.G., Tizzano, J.P., Helton, D.R., Kallman, M.J., Schoepp, D.D., Herin, M., 1998. 2-substituted (2SR)-2-amino-2-((1SR,2SR)-2-carboxycycloprop-1-yl)glycines as potent and selective antagonists of group II metabotropic glutamate receptors. 2. Effects of aromatic substitution, pharmacological characterization, and bioavailability. Journal of Medicinal Chemistry 41 (3), 358–378.

Platts, J.A., Abraham, M.H., Zhao, Y.H., Hersey, A., Ijaz, L., Butina, D., 2001. Correlation and prediction of a large blood-brain distribution data set-an LFER study. European Journal of Medicinal Chemistry 36 (9), 719–730.

Rouse, S.T., Marino, M.J., Bradley, S.R., Awad, H., Wittmann, M., Conn, P.J., 2000. Distribution and roles of metabotropic glutamate receptors in the basal ganglia motor circuit: implications for treatment of Parkinson's disease and related disorders. Pharmacology and Therapeutics 88 (3), 427–435.

Ravindranath, V., Ananda Theertha Varada, H.K., 1989. High activity of cytochrome P-450-linked aminopyrine N-demethylase in mouse brain microsomes, and associated sex-related difference. Biochemical Journal 261 (3), 769–773.

Sigrist, S.J., Thiel, P.R., Reiff, D.F., Schuster, C.M., 2002. The postsynaptic glutamate receptor subunit DGluR-IIA mediates long-term plasticity in Drosophila. Journal of Neuroscience 22 (17), 7362–7372.

Shand, J.H., West, D.W., 1995. Inhibition of neutral cholesteryl ester hydrolase by the glycolytic enzyme enolase. Is this a secondary function of enolase? Lipids 30 (8), 763–770.

Torchilin, V.P., 2000. Drug targeting. European Journal of Pharmaceutical Sciences 11 (Suppl. 2), S81–S91.

Walovitch, R.C., Cheesman, E.H., Maheu, L.J., Hall, K.M., 1994. Studies of the retention mechanism of the brain perfusion imaging agent 99mTc-bicisate (99mTc-ECD). Journal of Cerebral Blood Flow and Metabolism 14 (Suppl. 1), S4–S11.

Yu, M., Någren, K., Halldin, C., Swahn, C.-G., Helfenbein, J., Guilloteau, D., 1999. Synthesis of [p-methyl-^{11}C]RTI-32: A New Tool for the In Vivo Evaluation of the metabolism of phenyltropane dopamine reuptake compounds. Labelled Compounds and Radiopharmaceuticals 42 (Suppl. 1), S469–S471.

Yu, M., Bergstrom, K.A., Kuikka, J.T., Yang, J., Vanninen, E., 1998. Comparison of HPLC, TLC and Minicolumn for measuring the radiochemical purity of [^{99}Tc^{m}]Q12. Nuclear Medicine Communication 19, 483–487.

Yu, M., Bergström, K.A., Halldin, C., Kuikka, J.T., Swahn, C.G., Åkerman, K., Hiltunen, J., Tiihonen, J., Lassen, N., Widebeck, C., Farde, L., 1997. Does The Lipophilic Labeled Metabolite of [^{123}I]Epidepride Obstruct Dopamine D2 Brain Imaging? European Journal of Nuclear Medicine 24, 880.

Neurotoxicity-Induced Changes in Striatal Dopamine Receptor Function

ANNA-LIISA BROWNELL, IRIS Y. CHEN, XUKUI WANG, MEIXIANG YU, AND BRUCE G. JENKINS

Department of Radiology, Massachusetts General Hospital, Boston, Massachusetts 02114, USA

KEYWORDS: dopamine receptor; dopamine transporter; striatum

Impairment of dopaminergic neurotransmission can be primary, as in Parkinson's disease or secondary, as in Huntington's disease (HD). The secondary dopamine dysfunction is related to the progressive loss of the striatal neurons bearing the postsynaptic dopamine D1 and D2 receptors. PET studies have shown a significant decrease, at an annual rate of 2–6.5%[2], in striatal glucose metabolism[1] and in dopamine D1 and D2 receptor binding in both asymptomatic and symptomatic HD patients.

Huntington's disease can be modeled by 3-nitropropionic acid (3-NP), which is an inhibitor of succinate dehydrogenase.[3] It causes mitochondrial inhibition and striatal degeneration. We used *in vivo* PET studies to investigate 3-NP–induced acute and prolonged neurotoxic effects on striatal dopamine receptors and transporters in a rat model. 3-NP was administered twice a day at a dose of 10 mg/kg i.p. to eight rats (male Spraque-Dawley rats from Charles River Laboratories, average weight 300 g) until symptomatic gait was observed or for a maximum of 5 days. Imaging studies of dopamine D1 and D2 receptors and transporters were conducted before 3-NP administration and 2 and 7 days and 4 and 16 weeks after 3-NP administration. To validate the striatal deficit, an additional PET study of glucose metabolism was done two days after the cessation of 3-NP using ^{18}F-2-fluorodeoxy-D-glucose (^{18}F-FDG). Studies of dopamine D1 receptors were done using ^{11}C-SCH (Schoering 23660) as a tracer. Dopamine D2 receptors were imaged by ^{11}C-raclopride, and dopamine transporters using 2β-carbomethoxy-3β-4-fluorophenyl tropane (^{11}C-CFT). All the PET imaging studies were conducted using an in-house built tomographic instrument.[4]

FIGURE 1 shows PET studies conducted 2 days after 3-NP administration. The glucose study revealed large striatal lesions. At that time a moderate decrease of dopamine D1 and D2 receptor binding and an increase in dopamine transporter binding were observed. After that, progressive decrease was observed in pre and postsynaptic dopamine receptor function (TABLE 1, FIG. 1).

Address for correspondence: Anna-Liisa Brownell, Department of Radiology, Massachusetts General Hospital, 55 Fruit St., Boston, MA 02114.
abrownell@partners.org

Ann. N.Y. Acad. Sci. 991: 281–283 (2003).

TABLE 1. 3-NP–Induced degeneration of the binding of striatal dopamine D1 and D2 receptors and transporters

Time after 3-NP	Percent change in the binding of dopamine		
	D1 receptors	D2 receptors	Transporters
2 days	−4 ± 2	−5 ± 2	+6 ± 3
4 weeks	−24 ± 8	−23 ± 7	−10 ± 3
4 months	−36 ± 9	−33 ± 8	−12 ± 4

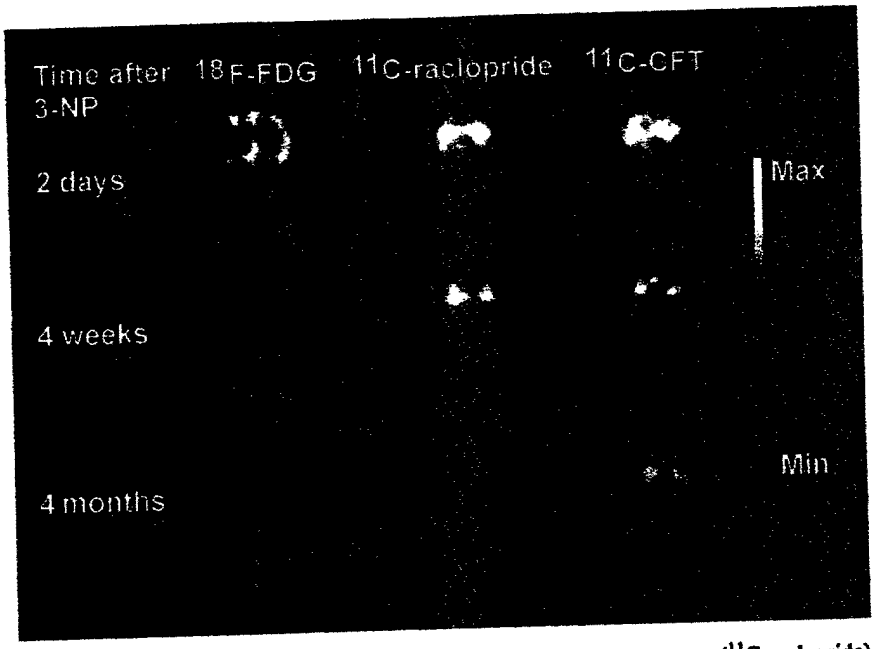

FIGURE 1. Longitudinal follow-up studies of dopamine D2 receptors (^{11}C-raclopride) and dopamine transporters (^{11}C-CFT) after 3-NP toxicity. Coronal slices show the binding distribution at the midstriatal level. Study of glucose utilization with ^{18}F-FDG shows large striatal lesions 2 days after 3-NP.

Even though HD is associated mainly with the impairment of postsynaptic dopamine receptors as a result of neural loss,[1,2] dopamine transporter binding might have a significant role in predicting the time course of dopaminergic degeneration. We found temporal variation in dopamine transporter binding in the 3-NP rat model. A similar observation has been published in a quinolinic acid rat model.[5] The reports of dopamine transporter function in HD patients include increased, unchanged, or decreased dopamine transporter binding.[6,7] Altogether, these observations might present degeneration at different time points and might well support our observation of the transient mechanism.

ACKNOWLEDGMENT

This work was supported by the DOD Grant DAMD17-99-1-9555.

REFERENCES

1. ANDREWS, T.C., *et al.* 1998. Advances in the understanding of early Huntington's disease using the functional imaging techniques of PET and SPECT. Mol. Med. Today 4(12): 532–539.
2. ANDREWS, T.C., *et al.* 1999. Huntington's disease progression, PET and clinical observations. Brain **122**(Pt. 12): 2353–2363.
3. ALSTON, T.A., *et al.* 1977. 3-Nitropropionate, the toxic substance of Indigofera, is a suicide inactivator of succinate dehydrogenase. Proc. Natl. Acad. Sci. USA **74:** 3767–3771.
4. BROWNELL, G.L., *et al.* 1985. High resolution tomograph using analog coding. *In* The Metabolism of the Human Brain. Studies with Positron Emssion Tomography. T. Greitz *et al.*, Eds.: 13–19. Raven Press. New York.
5. ARAUJO, M.D. *et al.* 2000. Deficits in striatal dopamine D2 receptors and energy metabolism detected by in vivo mirco PET imaging in a rat model of Huntington's disease. Exp. Neurol. **166**: 287–297.
6. SUZUKI, M. *et al.* 2001. Vesicular neurotransmitter transporters in Huntington's disease: initial observations and comparison with traditional synaptic markers. Synapse 41(4): 329–336.
7. GINOVART, N. *et al.* 1997. PET study of pre- and post-synaptic dopaminergic markers for neurodegenerative process in Huntington's disease. Brain **120:** 503–514.

ACADEMIC PRESS

Available online at www.sciencedirect.com
SCIENCE DIRECT®

NeuroImage

NeuroImage 0 (2003) 000–000

www.elsevier.com/locate/ynimg

Mapping of brain function after MPTP-induced neurotoxicity in a primate Parkinson's disease model

Anna-Liisa Brownell,[a,*] Kelly Canales,[a] Y. Iris Chen,[a] Bruce G. Jenkins,[a] Christopher Owen,[b] Elijahu Livni,[a] Meixiang Yu,[a] Francesca Cicchetti,[d] Rosario Sanchez-Pernaute,[c] and Ole Isacson[c,d]

[a] *Department of Radiology, Massachusetts General Hospital, Boston, MA 02114, USA*
[b] *Department of Neurosurgery, Massachusetts General Hospital, Boston, MA 02114, USA*
[c] *Department of Neurology, Massachusetts General Hospital, Boston, MA 02114, USA*
[d] *Udall Parkinson's Disease Research Center of Excellence, Neuroregeneration Laboratory, McLean Hospital, Belmont, MA 02478, USA*

Received 30 October 2002; revised 1 June 2003; accepted 3 June 2003

Abstract

Neurophysiological studies of the brain in normal and Parkinson's disease (PD) patients have indicated intricate connections for basal ganglia-induced control of signaling into the motor cortex. To investigate if similar mechanisms are controlling function in the primate brain (*Macaca fascicularis*) after MPTP-induced neurotoxicity, we conducted PET studies of cerebral blood flow, oxygen and glucose metabolism, dopamine transporter, and D2 receptor function. Our observations after MPTP-induced dopamine terminal degeneration of the caudate and putamen revealed increased blood flow (15%) in the globus pallidus (GP), while blood flow was moderately decreased (15–25%) in the caudate, putamen, and thalamus and 40 % in the primary motor cortex (PMC). Oxygen extraction fraction was moderately increased (10–20%) in other brain areas but the thalamus, where no change was observable. Oxygen metabolism was increased in the GP and SMA (supplementary motor area including premotor cortex) by a range of 20–40% and decreased in the putamen and caudate and in the PMC. Glucose metabolism was decreased in the caudate, putamen, thalamus, and PMC (range 35–50%) and enhanced in the GP by 15%. No change was observed in the SMA. In the parkinsonian primate, [^{11}C]CFT (2β-carbomethoxy-3β-(4-fluorophenyltropane) dopamine transporter binding was significantly decreased in the putamen and caudate (range 60–65%). [^{11}C]Raclopride binding of dopamine D_2 receptors did not show any significant changes. These experimental results obtained in primate studies of striato-thalamo-cortico circuitry show a similar trend as hypothetized in Parkinson's disease-type degeneration.

Keywords: Positron emission tomography; Volume rendering; MPTP; Parkinson's disease

Introduction

Parkinson's disease (PD) is characterized neuropathologically by a severe depletion of DA neurons and an associated loss of axons and terminals in the basal ganglia (Kish et al., 1988). Diagnosis is based on clinical signs of tremor, rigidity, bradykinesia, and postural instability (Marsden, 1992).

Hypotheses of the etiology of PD focus on the potential contribution of environmental toxins (exogenous and/or endogenous) and their interactions with genetic components (Checkoway and Nelson, 1999; Gorrell et al., 1996; Mizuno et al., 1999; Schapira, 1996). Cell death introduced by toxins may trigger a cascade of biological processes with an endpoint of continuous degeneration (Brownell et al., 1998, 1999; Schmidt and Ferger, 2001). These biological processes affect primarily the dopaminergic system in the basal ganglia and the neural network of the motor system (Alex-

* Corresponding author. Department of Radiology, Massachusetts General Hospital, Bartlett Hall 504R, Boston, MA 02114. Fax: +1-617-726-5123.
E-mail address: abrownell@partners.org (A.L. Brownell).

1053-8119/$ – see front matter © 2003 Elsevier Inc. All rights reserved.
doi:10.1016/S1053-8119(03)00348-3

ander et al., 1986, 1990; Wichman and DeLong, 1996; DeLong and Wichman, 2001).

MPTP (1-methyl-4-phenyl-1,2,5,6-tetrahydropyridine) neurotoxicity has long been used as a model for Parkinson's disease because it induces dopaminergic cell death in the substantia nigra pars compacta and striatal dopaminergic degeneration (Palombo et al., 1991; Schmidt and Ferger, 2001). MPTP-induced dopaminergic degeneration causes decreases in the binding of presynaptic dopamine transporters and reduces locomotor activity (Hantraye et al., 1992; Wullner et al., 1994).

A number of in vivo imaging studies in PD patients have shown regional differences in glucose metabolism and blood flow (Brooks, 2001; Eidelberg et al., 1995b; Fukuda et al., 2001; Markus et al., 1995). These studies show that glucose utilization and cerebral blood flow reductions in the brain correlate with the severity of the disease (Berding et al., 2001; Eberling et al., 1994; Eidelberg et al., 1995a; Moeller and Eidelberg, 1997; Imon et al., 1999). Antonini et al. (1998) have even proposed that studies of glucose metabolism can be used for differential diagnosis of PD.

There is, however, great variability in the reports of absolute values of local metabolic functions (Antonini et al., 1995; Bohnen et al., 1999; Eberling et al., 1994). This may originate from methodological differences during imaging studies, variability in the resolution of the imaging devices and, finally, differences in the selection of regions of interest, as well as level of degenerative process. Eidelberg et al. (1996) and Brooks (2001) have used a statistical parametric mapping technique with normalized values to evaluate metabolic changes in different brain areas in PD patients before and after therapeutic regimen. Autoradiographic studies in awake primates (Palombo et al., 1990; Porrino et al., 1987) have shown significant local changes in glucose utilization in basal ganglia, cerebral cortex, and cerebellum after an unilateral intracarotid administration of MPTP.

Based on neurophysiological experiments five different loops have been characterized to control signaling between the basal ganglia and the cortex (Alexander et al., 1990). In PD, the most sensitive loop is between the putamen, globus pallidus, thalamus, and cortex. The motor loop links the supplementary motor area (SMA) to the primary motor cortex, dorsal putamen, pallidum and ventrolateral thalamus, while the dorsolateral prefrontal cortex loop links dorsal caudate and ventroanterior thalamus (Isacson et al., 2001). Studies in PD patients have postulated that the nigrostriatal DA deficiency leads to decreased inhibition of the internal segment of the globus pallidus by both direct and indirect pathways (Alexander et al., 1990). The resulting excessive inhibitory output from the globus pallidus suppresses the ventral thalamus, reducing activation of the supplementary motor area and prefrontal cortex, and creates the motor impairments characteristic of PD (Alexander, 1987; Crutcher and DeLong, 1984; Wichman and DeLong, 1996).

To investigate if similar neural circuitry-linked mechanisms are operating in primate models of parkinsonism induced by MPTP, we conducted experimental imaging studies before and after MPTP of cerebral blood flow, oxygen extraction fraction, oxygen and glucose metabolism, dopamine transporters, and dopamine D_2 receptors using positron emission tomography (PET).

For data analyses, a volumetric technique was developed to select regions of interest based both on a primate brain atlas (Paxinos et al., 2000) and on actual MRI data. PET data were coregistered with the complete brain volume of MR data, and the resulting volumetric-PET data were used for quantitative data analyses.

Methods

Procedures in primates

Five male aged monkeys (*Macaca fascicularis*) (age: 11–16 years) were injected with MPTP (0.3 or 0.5 mg/kg iv weekly) until PD symptoms appeared including hypokinesia, tremor, rigidity, and bradykinesia (Wullner et al., 1994). The total dose of the injected MPTP varied between 25 and 42 mg and the total administration time between 6 and 21 months. PET imaging studies were conducted before MPTP administrations and 2–3 months after cessation of MPTP, when the PD symptoms were stabilized. For the imaging studies, primates were anesthetized using halothane (1.5% with oxygen flow rate of 3 L/min). Arterial and venous catheterization was done for drawing blood samples and injecting of labeled ligands. Animals were adjusted into a stereotactic head holder with ear bars at the origin. Interior orbital supports ensure that images are acquired on a pseudocoronal plane perpendicular to the orbito-meatal line. This allows superposition of the data from MRI studies. Level of anesthesia, blood gases, heartbeat, and vital signs were monitored throughout the imaging procedures (Propaq, Vital Signs Monitor, Protocol Systems. Inc., Beaverton, OR).

Imaging studies of blood flow and oxygen and glucose metabolism were conducted in one imaging session, and studies of dopamine transporters and D_2 receptors were conducted in another session within the time span of a week. The MRI studies, needed for anatomical data, were conducted within a month. This short time span is necessary to eliminate possible errors in volumetric data fusion, raised by neurotoxicity-induced morphologic volumetric changes. MPTP-induced changes in blood flow, oxygen, and glucose metabolism were conducted in four primates and changes in dopamine transporter and receptor function in five primates, correspondingly.

Animals used in this study were maintained according to the guidelines of the Committee on Animals of the Harvard Medical School and Massachusetts General Hospital and of the *Guide for Care and Use of Laboratory Animals* of the Institute of the Laboratory Animal Resources, National Re-

search Council, Department of Health, Education and Welfare, Publication No. (NIH)85-23.

Detection of locomotor activity

Spontaneous locomotor activity was monitored by an Actiwatch system (Mini Mitter Company, Inc., Sunriver, OR) mounted in a shirt pocket in the back of the animal (Puyau et al., 2002). The Actiwatch reader was connected to a computer, and data were transferred from the Actiwatch to a computer through a wireless link. The Actiwatch allows analyses of circadian rhythms, average activity during light and dark, mean activity score, movement, and movement-type index. Prior to MPTP injections, there was a significant difference between day and night time locomotor activities, while after MPTP no activity difference was observable (Fig. 1). Even though the Actiwatch data cannot be used to measure clinical score of PD, it provides a useful follow-up method to visualize daily changes in spontaneous locomotor activity.

MR imaging

MR imaging was conducted in anesthetized primates using the same stereotactic head frame as in the PET studies. T2-weighted images (TR = 4500, TE = 100/10 ms) were acquired with a GE Signa 3.0 T imager in coronal planes using continuous acquisition of 3-mm slices to obtain anatomical information to be used in fusion with PET data to obtain volume of interest for quantitative analyses.

PET imaging

PET imaging studies were conducted with an in-house-built single ring PET device, PCR-I (Brownell et al., 1989). The resolution of PCR-I for a point source at the center is 4.5 mm, and the sensitivity is 46 kHz/μCi for a source of 20 cm in diameter with a concentration of 1 μCi/ml. The overall efficiency is 64% of the theoretical maximum for a 1-cm-plane thickness corresponding to the 2-cm-high detectors. The plane thickness of 5 mm used in this study is obtained by the use of cylindrical collimators, which limit the effective height of the detectors. The resolving time of PCR-I is 6 ns (FWHM). Data acquisition over the whole brain volume with this single ring device was done with 5-mm steps starting from the cerebellar level. Imaging data were corrected for uniformity, sensitivity, attenuation, decay, and acquisition time. PET images were reconstructed using a Hanning filtered convolution backprojection with a cutoff value of 1.0 (Chesler, 1973). Calibration of the positron tomograph was performed prior to each study using a cylindrical plastic phantom (diameter 6 cm) containing water solution of ^{18}F. The corrected reconstructed data set was repacked on the Linux workstation and converted into ANALYZE/AVW image format. The voxel size in coronal PET images is 5 mm in the axial Z direction and 1.19 mm $\times$ 1.19 mm in x-y plane.

After that T2-weighted MRI data from the same subject were loaded and converted into ANALYZE/AVW image format. A segmentation routine in ANALYZE was used to separate the brain from the surrounding tissue in the MRI data. PET data were then thresholded and coregistered to its respective MRI data using the NMI (Normalized Mutual Information) voxel match algorithm of the ANALYZE software package and cubic spline interpolation. A resulting transformation matrix maps the PET images onto its respective MR images, and the multimodality image registration routine returns fused PET-MRI images. The fused PET-MR images were then volume rendered for display (Fig. 2).

Selection of the volume of interest

Three-dimensional regions of interest were outlined on coronal MR slices based on anatomical borderlines observed from the primate brain atlas and MR images (Fig. 3). These regions were also computationally compared and verified with the corresponding slices in the primate brain atlas (Paxinos et al., 2000). The transformation matrix for fusing the PET data to the MRI data was then reapplied to the PET images to generate the data for three- dimensional VOI (volume of interest) analysis. Volumetric radioactivity concentration was calculated for each VOI, and these data were then used for further data analyses to calculate values for blood flow, oxygen extraction fraction and metabolism, glucose metabolism, and binding potential for dopamine transporters and dopamine D_2 receptors.

Validation of the volumetric data analyses

To validate the three-dimensional data analyses we conducted studies with a phantom consisting of two concentric spheres (Data Spectrum Corporation, Chapel Hill, NC). The volume of the inner sphere was 20 ml, and the volume of the outer sphere was 79 ml. In the first experiment the outer sphere was filled with ^{18}F-labeled water, and the inner sphere was filled with water without radioactivity. The phantom was scanned stepwise with 5-mm steps (Fig. 4). In the second experiment the inner sphere was filled with higher radioactivity concentration than in the outer sphere, which had the same radioactivity concentration as in the first experiment. Additionally, T2-weighted MR images were done with both concentric spheres filled with water. The data analyses were conducted in the same way as above by drawing ROIs on MR images and then fusing PET data with MRI data. Finally, radioactivity concentration was determined and compared with actual measured radioactivity. For comparison, radioactivity concentration was also calculated based on conventional 2-dimensional pixel analyses (Table 1).

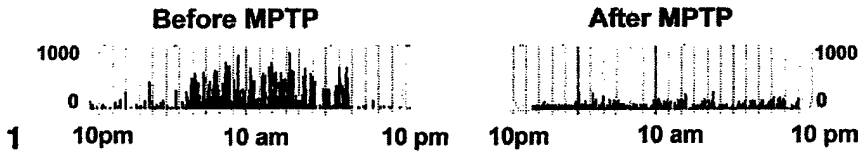

1

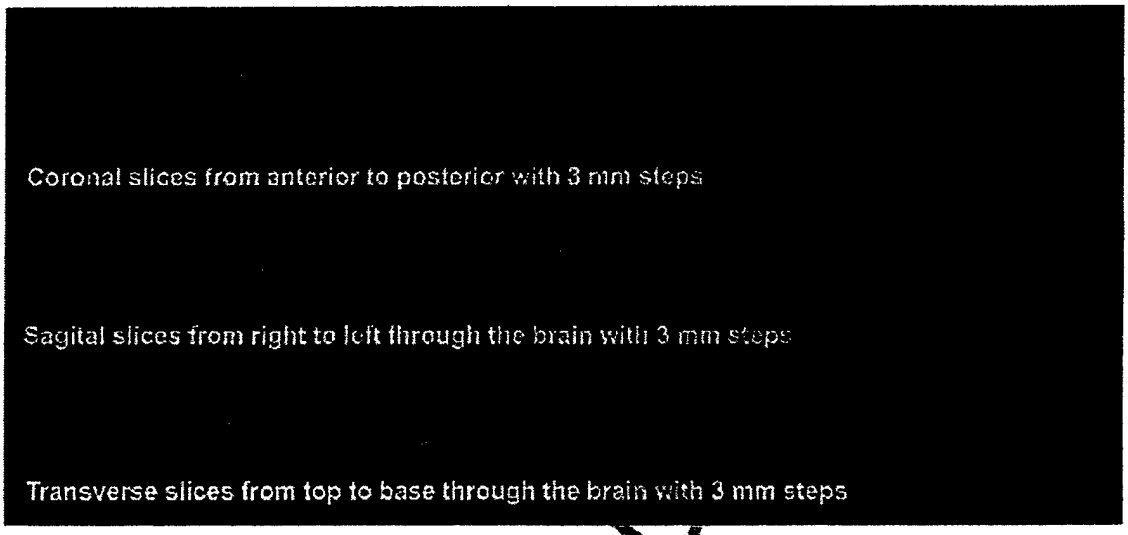

COLOR

2

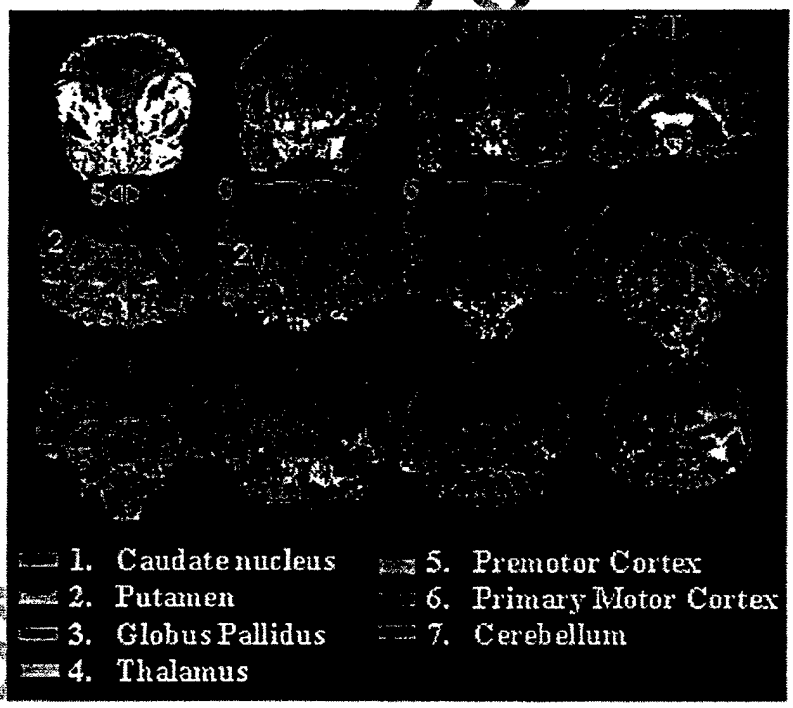

COLOR

3

Fig. 1. Effect of MPTP-induced neurotoxicity on spontaneous locomotor activity detected by an Actiwatch before and after MPTP. Before MPTP there was a significant difference between day and nighttime locomotor activity, while after MPTP no activity difference was observable.

Fig. 2. A PET study of the distribution of [^{11}C]raclopride binding in dopamine D_2 receptors after MPTP toxicity in a primate brain. PET data were fused with volume-rendered MR images. The upper row shows coronal slices from anterior to posterior direction. Binding to D_2 receptors are localized mainly in the putamen and caudate. The middle row shows sagital slices from right to left. Slices 1–7 represent right hemisphere and slices 8–13 left hemisphere. At the bottom row transverse slices are shown from top to base. Volumetric distribution of radioactivity is used in selecting region (volumes) for interest used in quantitative data analyses of receptor function.

Fig. 3. Anatomical borderlines observed from MR images were used to define the regions of interest for volumetric data analysis on the fused PET-MRI data set. Segmented brain areas are numbered and color-coded as shown in the image. The data from the left and right hemispheres were analyzed separately.

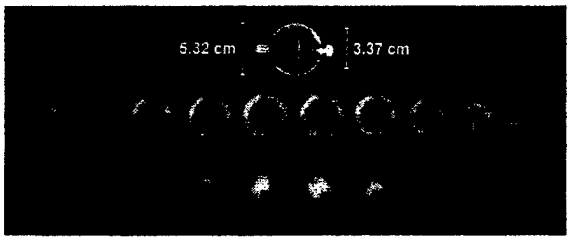

Fig. 4. To evaluate the accuracy of the volumetric data reconstruction a phantom consisting of two concentric spheres was imaged by PET. Coronal PET images were acquired with 5-mm steps and slice thickness of 5 mm over the phantom. The middle row shows images, when the outer sphere was filled with ^{18}F-labeled water and the inner sphere with water without radioactivity. The lower row shows images, when the inner sphere was filled with the same radioactivity concentration as above and activity concentration in the outer shell was about 44% of it. For data analysis PET images were fused with T2-weighted MR images and radioactivity concentrations in the inner and outer shell were determined (Table 1) using the same volumetric data analysis as in the experimental primate studies.

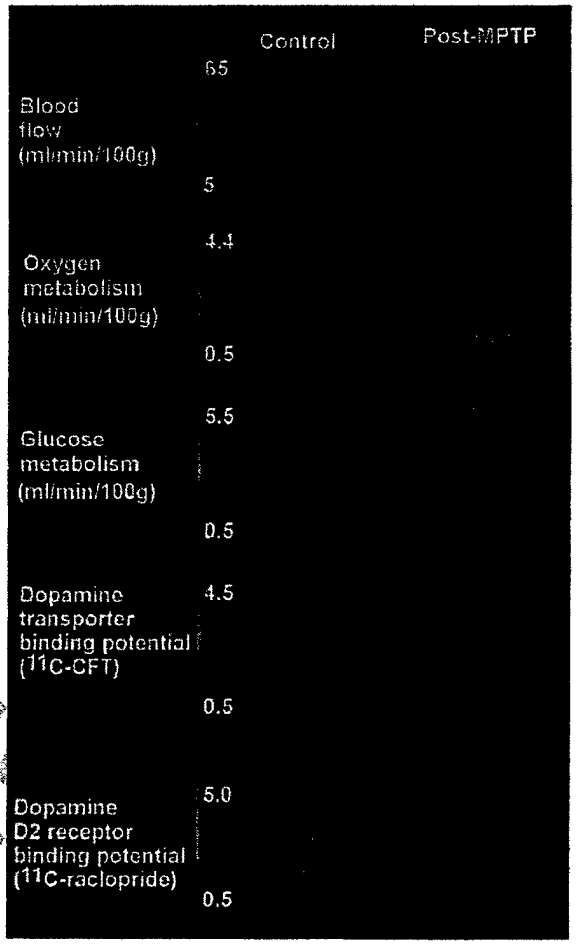

Fig. 5. Coronal midbrain slices of a monkey brain illustrate the quantitative distribution of hemodynamic, metabolic, and dopamine receptor function before and after MPTP neurotoxicity. Studies of blood flow were conducted with a steady-state inhalation technique using a $C^{15}O_2$ gas mixture (Jones, 1976). Studies of oxygen metabolism were conducted with a steady-state inhalation technique using a $^{15}O_2$ gas mixture (Jones, 1976; Subramanyam, 1978). Studies of glucose metabolism were conducted with [^{18}F]FDG (2-^{18}F-fluoro-2-deoxy-D-glucose). Studies of dopamine transporters were conducted with [^{11}C]CFT (2β-carbomethoxy-3β-(4-fluorophenyltropane). Studies of dopamine D_2 receptors were conducted with [^{11}C]raclopride.

COLOR

Blood flow studies

Blood flow studies were conducted using a steady-state technique based on the inhalation of $C^{15}O_2$ (Frackowiak et al., 1980; Jones et al., 1976; Subramanyam et al., 1978). ^{15}O-labeled CO_2 gas mixture was delivered at a constant concentration and flow rate (2 L/min) into the inhalation tube. After 6–8 min of inhalation of $C^{15}O_2$ gas mixture, a steady-state activity level was obtained in the brain, and sequential imaging over the brain was performed starting from the cerebellar level using 5-mm steps and an acquisition time of 60 s. During imaging, a series of arterial blood samples were drawn to determine blood gases and radioactivity in the plasma and whole blood. These data are needed for calculation of the oxygen extraction level (Subramanyam et al., 1978). Radioactivity was measured in a gammacounter (Packard Cobra Auto-gamma, Downers, IL), which was cross-calibrated with the tomograph. Arterial blood and plasma radioactivity concentrations were then computed after corrections for dead time and decay.

Table 1
Radioactivity based on the volumetric data analyses compared to the measured radioactivity and the conventional 2-dimensional pixel analyses in two concentric spheres

	Inner sphere (μCi/100 ml)	Outer sphere (μCi/100 ml)
First experiment		
Radioactivity determined on the volumetric data analyses	86 +/− 7	893 +/− 62
Measured radioactivity	0	869 +/− 11
Conventional 2D ROI analyses	110 +/− 12	1012 +/− 94
Second experiment		
Radioactivity determined on the volumetric data analyses	527 +/− 20	239 +/− 7
Measured radioactivity	516 +/− 5	225 +/− 4
Conventional 2D ROI analyses	572 +/− 72	275 +/− 55

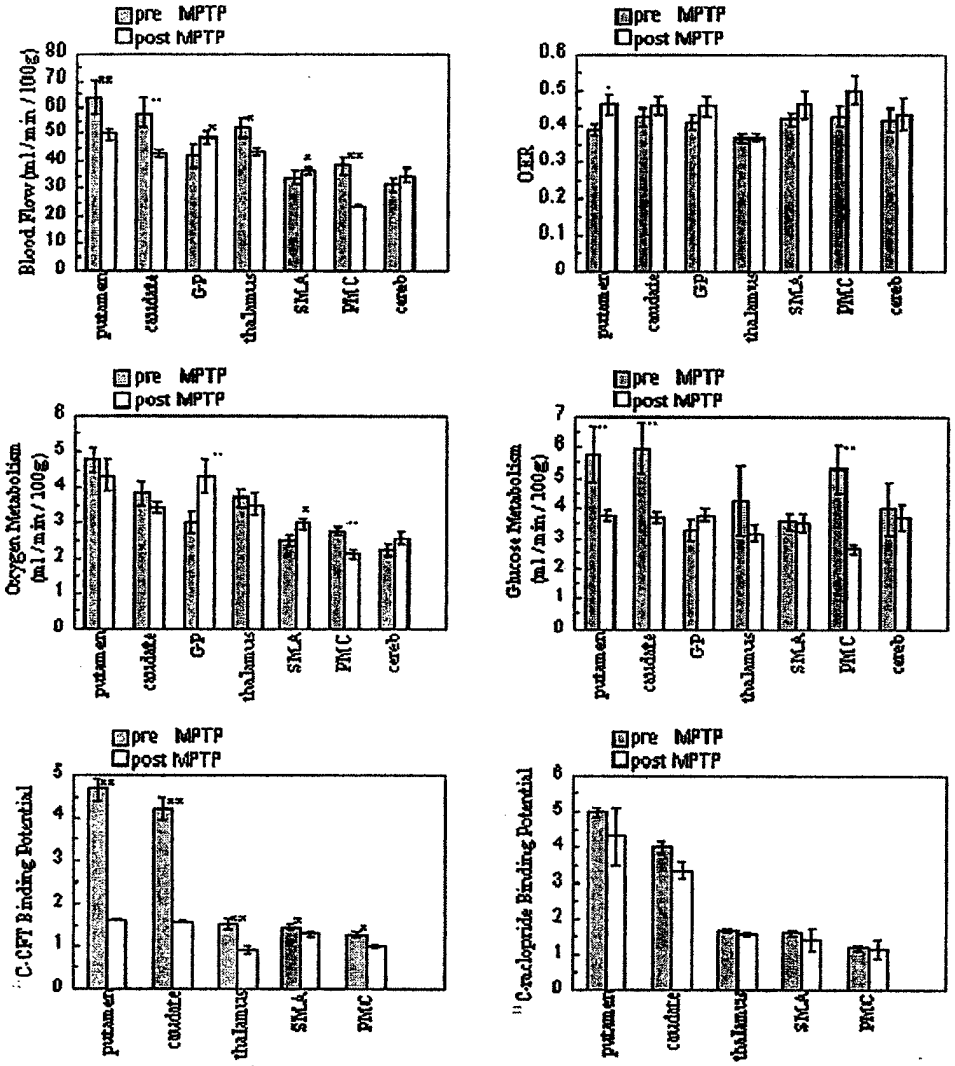

Fig. 6. Quantitative topographic distribution (mean +/− SEM) of hemodynamic, metabolic, and dopamine receptor function before and after MPTP-induced neurotoxicity in the different brain areas. All the data analyses are based on volumetric data analyses using fused PET and MR images. Significant difference was calculated as compared to the pre-MPTP values by using Dunnett's *t* test. Blood flow studies show a significant decrease in putamen, caudate, and PMC ($P < 0.01$) and thalamus ($P < 0.05$) and an increase in GP and SMA ($P < 0.05$). Oxygen extraction fraction (OER) shows an overall increase with significant change in putamen ($P < 0.05$). Oxygen metabolism shows a significant increase in the GP ($P < 0.01$) and SMA ($P < 0.05$) and a significant decrease in PMC ($P < 0.01$) and an overall decrease in the other brain areas. Glucose metabolism shows a significant decrease in putamen, caudate, and PMC ($P < 0.01$) and an overall decrease in the other brain areas but GP and SMA. Dopamine transporter binding investigated by [^{11}C]CFT shows significant decrease in putamen, caudate, and thalamus ($P < 0.01$) and SMA and PMC ($P < 0.05$). Dopamine D_2 receptor binding investigated by [^{11}C]raclopride does not show any significant changes.

Studies of oxygen extraction fraction and metabolism

After the blood flow study, the inhalation gas mixture was switched to $^{15}O_2$. In 10–12 min a steady-state activity level was obtained in the brain based on stabilized oxygen metabolism and blood flow (Jones et al., 1976; Subramanyam et al., 1978). A similar sequential imaging over the whole brain was performed as above. During imaging arterial blood was drawn to determine blood gases, hematocrite, hemoglobin, and radioactivity levels in the plasma and whole blood. These data are necessary to calculate the oxygen extraction fraction (Jones, 1976; Subramanyam et al., 1978). Regional cerebral oxygen metabolism can be calculated when blood flow, oxygen extraction fraction, blood gases, and hemoglobin are known (Subramanyam et al., 1978). Finally, values of oxygen metabolic rate were converted to molar units for stoichiometric comparisons with glucose utilization.

Studies of glucose metabolism

Studies of glucose metabolism were done using [^{18}F]FDG (2-^{18}F-fluoro-2-deoxy-D-glucose) as a tracer. FDG distributes in tissue like glucose but remains unme-

Table 2
Stoichiometry of glucose utilization and O_2 consumption in different brain areas before and after MPTP

	Before MPTP	After MPTP
Putamen	6.68 +/− 1.06	8.71 +/− 0.86
Caudate	5.13 +/− 0.69	6.92 +/− 0.34
GP	7.39 +/− 0.78	8.23 +/− 0.92
Thalamus	6.98 +/− 1.91	7.71 +/− 0.71
SMA	5.63 +/− 0.89	5.84 +/− 0.32
PMC	4.19 +/− 0.53	6.00 +/− 0.54
Cerebellum	4.42 +/− 0.98	5.04 +/− 0.38

tabolized in the form of 6-phosphate making quantitative imaging studies possible. The kinetic model of Sokoloff et al. (1977) extended by Phelps et al. (1979) was used in data analysis. Following a rapid intravenous injection of 5 mCi of ^{18}F-FDG, dynamic PET images were acquired at a level 15 mm anterior from the earbar for 30 min using an acquisition time of 15 s. After this, when activity had reached a steady-state level, coronal slices were acquired over the brain at 5-mm steps starting from the cerebellar level and an acquisition time of 60 s. Arterial blood samples were drawn for determination of plasma radioactivity. The plasma data were fitted to a 2-exponential function and used as an input function in calculating glucose metabolic rate. In addition, arterial glucose values were determined before and after the experiment. Values for the transport parameters k_1–k_4 were calculated from the dynamic tissue data using plasma input function (Phelps et al., 1979). Values for regional cerebral glucose metabolism were calculated using transport parameters and blood data information, regional tissue data from the areas of interest and a value of 0.5 for the lumped constant (Reivich et al., 1985). Finally, the values of glucose metabolic rate were converted to molar units for stoichiometric comparison with O_2 consumption.

Studies of dopamine D_2 receptors and transporters

Each study included two experiments. The first experiment was carried out with [^{11}C]raclopride to investigate dopamine D_2 receptors, and the second experiment was conducted 2–3 h later with [^{11}C]CFT (2β-carbomethoxy-3β-(4-fluorophenyltropane) in order to investigate dopamine transporters. Radiolabeled ligand, [^{11}C]raclopride (Ehrin et al., 1985) or [^{11}C]CFT (Brownell et al., 1996) (6–8 mCi, specific activity 600–1000 mCi/μmol) was injected into the femoral vein; and imaging data were acquired stepwise on seven coronal brain levels, initially using 15 s per image. The acquisition time was subsequently increased to 60 s, the total imaging time being 90 min in both experiments. Eighteen arterial blood samples of 0.1 ml were drawn at different time points starting from 10 s frequency and ending with 15 min frequency in order to monitor the decrease in radioactivity. In addition, three arterial blood samples were drawn for HPLC analyses of metabolites of the labeled ligands.

Kinetic behavior of [^{11}C]CFT was studied with a four-parameter estimation of the three-compartmental model approach. In the three-compartmental model, the first compartment is the plasma pool, the second is the exchangeable tracer pool including free and nonspecifically bound ligand in the brain, and the third compartment is a trapped tracer pool including bound ligand in the brain. The exchangeable tracer pool contains ligand but no receptors; and the third compartment includes all the receptors, partly or totally occupied by ligands. The kinetic parameters k_3 and k_4 describe the binding to and dissociation from the receptors.

The transfer coefficients k_1–k_4 were mathematically resolved using a least-square fit, Levenburg-Marquardt method. All numerical analyses were done with the optimization tool SAAM II (Foster et al., 1994). For stabilization of the k values the fitting procedure was performed using two steps. Since the cerebellum does not have specific receptor binding or is negligible, fitting was done with the cerebellar data, letting all the k values float. The ratio k_1/k_2 was then calculated. In further iterations this fixed ratio was used as a constraint and applied with a sequential quadratic programming method combined with a cost function to reach parameter optimization. Regional binding potential was calculated as a ratio of k_3/k_4 (the ratio of the transport from the exchangeable tracer pool into the bound tracer pool to the transport from the bound tracer pool back into the exchangeable tracer pool). Regional binding potentials were

Table 3
MPTP-induced changes in dopamine receptor function, hemodynamics, and metabolism in different brain areas

	Dopamine transporter	Dopamine D_2 receptor	Blood flow	Oxygen extraction	Oxygen metabolism	Glucose metabolism
Putamen	↓**	↓	↓**	↑*	↓	↓**
Caudate	↓**	↓	↓**	↑	↓	↓**
GP	—	—	↑*	↑	↑**	↑
Thalamus	↓**	↕	↓*	↕	↓	↓
SMA	↓*	↓	↑*	↑	↑*	↕
PMC	↓*	↕	↓**	↑	↓**	↓**
Cerebellum	—	—	↑	↑	↑	↓

↑ indicates an increase, ↓ indicates a decrease and ↕ indicates no change compared to the pre-MPTP value.
* signs $P < 0.05$ and ** $P < 0.01$.

calculated separately for left and right caudate, putamen, SN, thalamus, SMA, and PMC.

Results

Accuracy of the volumetric data analyses

Development of image fusion and volumetric data analysis has been an essential part of this work. This approach is absolutely necessary to obtain reliable data from small brain regions. Fig. 2 shows coronal, transverse, and sagittal segmentation with 3-mm steps (slice thickness) of a volume-rendered MR images fused with PET images of dopamine D_2 receptor distribution after MPTP. The original PET images were acquired with 5-mm steps and a slice thickness of 5 mm. Fig. 3 demonstrates selection of the regions of interest on a single slice level.

The validation of the volumetric data analyses was done with a phantom of concentric spheres (Fig. 4). Table 1 shows the accuracy of the obtained results based on the volumetric data analyses and actual measurement of radioactivity, with comparison to the conventional 2-dimensional pixel analyses. In the first experiment radioactivity was only in the outer sphere and the calculated radioactivity using volumetric data analyses was 3% and with conventional 2D pixel analyses 16% higher that the measured radioactivity. There was only water in the inner sphere, but because of the scatter and spillover of the radioactivity in the outer sphere it was possible to record an activity, which corresponded 9.7% of the activity in the outer sphere using volumetric data analyses and 10.9% using 2D analyses.

In the second experiment radioactivity was in both spheres with the inner sphere more active. The values calculated using volumetric data analyses were 2–6 % higher than measured radioactivity while conventional 2D pixel analyses gave 11–22% higher values. The activity concentration in the inner sphere was in the same range as the striatal activity concentration in blood flow and receptor studies before MPTP toxication. These phantom studies were not corrected for the partial volume effects, because in each slice the smallest thickness of the sphere in the image was equal or bigger than two times the resolution element of the tomograph (Hoffman et al., 1979).

These basic tools have been used to analyze data for blood flow, oxygen extraction fraction, and metabolism as well as glucose metabolism and binding parameters for dopamine transporters and dopamine D_2 receptors in different brain regions.

Hemodynamics and cerebral energy metabolism

Fig. 5 (see Table 3) shows the quantitative distribution and calculated values of blood flow, oxygen metabolism, glucose metabolism, dopamine transporters, and dopamine D_2 receptors at one midbrain level before and after MPTP. From these images it can be observed, that the most striking change after MPTP is the decrease in striatal dopamine transporter binding. Fig. 6 shows the calculated values obtained by volumetric data analyses in different brain areas of hemodynamic, metabolic, and dopamine receptor function both before and after MPTP induced neurotoxicity.

The largest decrease in blood flow after MPTP was observed in the primary motor cortex (39+/−4%). Blood flow was decreased in the striatal area (caudate and putamen) by 22–26%, and in the thalamus by 17+/−3%. In the globus pallidus, blood flow was increased by 15+/−3% and in the SMA by 4+/−1%.

After MPTP, oxygen extraction fraction was moderately enhanced in other brain areas but the thalamus (Fig. 6). Values for oxygen metabolism in the GP and SMA were significantly elevated, partly being a reflection of elevated oxygen extraction fraction. Oxygen metabolism was decreased in the putamen and caudate by 10+/−2% and significantly in the PMC (23+/−2%).

Glucose metabolism was decreased in all other brain areas but the GP (Fig. 6). In the striatal area glucose utilization was decreased by 35+−/17% in the caudate, 38+/−8% in the putamen, 25+/−7% in the thalamus, and (50+/−12%) in the PMC. Glucose utilization was enhanced in the GP by 15+/−3% (see Table 3).

Stoichiometry of glucose utilization and O_2 consumption

Table 2 shows the calculated values for stoichiometric balance in different brain areas before and after MPTP. The stoichiometric balance increased in all brain areas after MPTP, indicating that, in addition to glucose, other substrates were also metabolized after MPTP.

Dopamine transporters and receptors

The binding of [^{11}C]CFT was significantly decreased in the putamen (65+/−4%), caudate (62+/−5%), thalamus (39+/−4%), SMA (25+/−2%), and PMC (25+/−2%) (Figs. 5 and 6), indicating degeneration of the dopamine transporter sites in the presynaptic terminals. [^{11}C] Raclopride binding in dopamine D_2 receptors showed overall decreases (Figs. 5 and 6, Table 3). However, because of a large variation in the results there was no significant change in raclopride binding after MPTP.

Studies of receptor function and metabolism in relation to neural circuitry

To compare the obtained experimental results of dopamine receptor function, hemodynamics, and metabolism with the known neural circuitry, we analyzed MPTP neurotoxicity-induced changes in different brain areas, conventionally included in neurophysiological studies of the neural networks. Table 3 shows the direction of MPTP-induced significant changes in different brain areas.

Discussion

Parkinson's disease is characterized neuropathologically by a severe depletion of dopamine neurons in the basal ganglia. Our experiments, conducted in primates after MPTP-induced neurotoxicity, showed significantly decreased binding of [^{11}C] CFT in striatum, indicating depletion of presynaptic dopamine terminals. We have published this observation in 1992 (Hantraye et al., 1992), and in 1994 we further demonstrated the correlation to locomotor activity (Wullner et al., 1994). In these experiments we also found that the total dose or injection period of MPTP does not correlate with locomotor activity or clinical scores (Wullner et al., 1994). Since then, about 200 papers have been published, with a unanimous observation of declining dopamine transporter binding (van Dyck et al., 2002; Antonini et al., 2001; Chouker et al., 2001; Huang et al., 2001; Marck et al., 2001; Sakakibara et al., 2001). Even though there is an unequivocal decline in presynaptic dopamine transporter binding in PD, there is inconsistency in reported results of [^{11}C]raclopride binding in dopamine D_2 receptors in PD (Doudet et al., 2000; Hwang et al., 2002; Kaasinen et al., 2000). In our present experiments, we have found a tendency for a decrease but with a large variation in dopamine D_2 receptor binding after MPTP toxication. During MPTP administration (acute MPTP-induced neurotoxicity) and after 6-hydroxydopamine toxicity (van Nguyen et al., 2000) we have observed a moderately increased [^{11}C]raclopride binding in D_2 receptors. Altogether, our observations of dopamine D_2 receptor binding are consistent with a number of publications that propose a biphasic behavior of D_2 receptor binding; indicating that in the early phase of Parkinson's disease, D_2 receptor binding is enhanced because of supersensitivity and it will decline later with progression of the disease (Stoessl and de la Fuentes-Fernandez, 2003; Hwang et al., 2002; Kaasinen et al., 2000). In addition, there are some other aspects, which might effect on [^{11}C]raclopride binding. First, it has low binding affinity, and it is impossible to determine whether the changes in binding reflect alterations in the number of available dopamine receptors or whether they are due to changes in synaptic dopamine concentration (Stoessl and de la Fuente-Fernandez, 2003). In addition, it may be possible that these effects could cancel each other out.

By using the volume of interest determined from the fusion with MR images we were able to investigate also binding characteristics of [^{11}C]CFT and [^{11}C]raclopride in the thalamus, SMA, and PMC. Using conventional PET image analysis it is impossible to localize these sites because the accumulation of radioactivity is so low compared to striatal accumulation. The binding values obtained (Figs. 5 and 6) correlate well with the values obtained using autoradiographic techniques (Kaufman and Madras, 1992).

In addition to studies of dopamine transporters and dopamine D_2 receptors, we conducted hemodynamic and metabolic studies in this preclinical model of PD with the ultimate aim of finding parallels to human PD in adaptive changes including metabolic neural networks and dopaminergic function.

Brooks (1997, 1999) has shown that slowness in free performed motion in PD patients corresponds with changes in blood flow in the supplementary motor area and dorsal prefrontal cortex, areas which get subcortical input from the basal ganglia. Notably, blood flow changes consistent with a compensatory overactivation in premotor area were observed. In PD, there appears to be a synchronization of GPe and GPi output signals as a result of the loss of DA tonic input to the putamen; that together with a reduced thalamic input to the SMA and PM cortices may explain the motor signs of PD (Brooks, 1999; Eidelberg et al., 1995b; Schmidt and Ferger, 2001). Moreover, the recruitment of more cortical regions and the increased and widespread activation of PM and SMA-associated cortices suggest that these structures are compensating for the abnormal input, to be able to activate the motor cortex for initiation of the movement (Brooks, 1997; Eidelberg et al., 1996).

We observed enhanced blood flow in the supplementary motor area as well as in the globus pallidus, while blood flow was decreased in the putamen, caudate, and primary motor cortex of the parkinsonian primate. Oxygen metabolism was marginally enhanced in the globus pallidus and supplementary motor area and decreased in the putamen, caudate, and primary motor cortex. Glucose metabolism was decreased in all brain areas after MPTP but the GP and SMA. In short, we found (1) a decreased striatal dopamine transporter binding, indicating degeneration of presynaptic terminals; (2) an increased blood flow in the globus pallidus, indicating activation in that brain area; (3) a decreased glucose metabolism in the thalamus, indicating decreased energy metabolism; and (4) decreased blood flow and glucose metabolism in the PMC, indicating decreased motor activity. However, at the same time, blood flow in the SMA was increased while no change in glucose metabolism was observed indicating a compensatory mechanism in motor function. These observations (see Table 3) support a neural circuitry-based reasoning for changes seen in functional interactions of the motor system in human parkinsonism (Wichman and DeLong, 2003; Carbon et al., 2003; DeLong and Wichman, 2001; Isacson et al., 2001).

As a comparison of the values obtained for the regional changes of glucose utilization in this "chronic" MPTP model it can be emphasized that Palombo et al. (1991) obtained 40% enhanced glucose utilization in a globus pallidus by autoradiographic studies of [^{14}C]deoxyglucose in a hemiparkinsonian model induced by a unilateral intracarotid administration of MPTP into the striatum. As well Porrino et al. (1987) found a significantly reduced glucose utilization in substantia nigra, thalamus, and ventral tegmental area and increased values in globus pallidus by autoradiographic studies of [^{14}C]deoxyglucose in MPTP-treated awake primates. Eidelberg et al. (1994) found in human Parkinson's disease patients a 20–30% average decrease in

glucose utilization depending on the level of disease. It is obvious that there is a difference in absolute values between animal models and species. However, interestingly the trend of the changes is similar.

We have considered the globus pallidus as one brain region in these experiments. However, it has two parts interna and externa, which have different functions. The observed increase in hemodynamic functions, blood flow and oxygen and glucose metabolism, in the GP area could reflect (1) an increased firing of GPi neurons (which project to the thalamus), (2) an increased metabolism at synaptic terminals from GPe and putamen, projecting to GPi, or (3) a metabolic activity of interneurons of GP. Differentiation of these mechanisms is not possible with the conducted PET techniques, but requires additional electrophysiological measurements.

In the normal in vivo state, glucose is the only substrate for energy metabolism in the brain. Under normal circumstances, no other potential energy yielding substrate has been found to be extracted from the blood in more than trivial amounts. For complete oxidation of glucose, the theoretical ratio of O_2 to glucose utilization is 6.0. A value of 5.2 has been obtained in human studies conducted with $^{15}O_2$ gas and [^{18}F]FDG (Frey, 1999). In the present experiments, an average value for the stoichiometry of the glucose utilization and oxygen consumption is 5.8+/− 0.6 before MPTP regimen and 7.0+/−0.9 after MPTP calculated as a mean of 8 investigated brain areas (see Table 2). An average 20% increase in oxygen consumption compared to glucose utilization after MPTP may be explained by a reduced mitochondrial function or combined effect of decreased metabolism and anesthesia. Halothane anesthesia might have an enhancing effect on the absolute values of blood flow and metabolism depending on the level of halothane concentration. The effect is, however, smaller in the spontaneous inhalation used in these experiments (Amory et al., 1971). In addition, the same anesthesia protocol was used before and after MPTP so the possible anesthesia-induced changes were minimized in the evaluation of MPTP-induced changes on blood flow, metabolism, and dopaminergic function.

To obtain quantitative information from small brain areas in imaging studies, we have developed a volumetric technique for data analyses and used fused PET and MRI data. In addition, the primate brain atlas was utilized to outline the regions of interest on MR images. Even when the selection of the volume of interest is accurate on a technical level, there is a potential error in the absolute values because of effects of partial volume (Hoffman et al., 1979). In addition, outlining tiny brain areas there is a personal factor. When these data were analyzed by two scientists independently, there was an average of 20% difference between the absolute values, they obtained. However, when they analyzed the data together, the values were equal to the lower values in the first time. Moreover, in the absolute values internal scatter radiation is a factor in nearby low activity tissue if the neighboring tissue has a high activity concentration. In biological studies this shows up especially in the [^{11}C]CFT studies of dopamine transporters, where the putamen has a high activity accumulation compared to the nearby tissues (Fig. 5). To validate volumetric data analyses, imaging studies in concentric sphere phantoms were conducted. The absolute values calculated for radioactivity concentration were higher than measured radioactivity mainly because of the internal scatter. This is clearly demonstrated in the first phantom study when the inner sphere did not have any radioactivity but based on data acquisition and analyses it had about 10% of the activity of the outer sphere (Table 1).

These experiments provide in-depth information on changes in metabolic and dopaminergic function in neural networks after MPTP-induced parkinsonism in primates. This information is valuable for investigations of a compensatory mechanism during degeneration and structural repair. In addition, these experiments enhance the use of MPTP neurotoxicity as a model to investigate human Parkinson's disease.

Acknowledgments

We thank cyclotron operators William Bucklewicz and David Lee for preparing radiopharmaceuticals for these experiments as well as Jack McDowell for taking good care of the primates. This work was supported by DOD Grant DAMD17-98-1-8618 and NINDS Grant NS P50-39793 to O.I. at McLean Hospital and DOD Grant DAMD17-99-1-9555 to A.-L.B. at Massachusetts General Hospital. F.C. was supported by the Medical Research Council of Canada.

References

Alexander, G., 1987. Selective neuronal discharge in monkey putamen reflects intended direction of planned limb movement. Exp. Brain Res. 67, 623–634.

Alexander, G., DeLong, M.R., Strick, P.L., 1986. Parallel organization of functionally segregated circuits linking basal ganglia and cortex. Annu. Rev. Neurosci. 9, 357–381.

Alexander, G.E., Crutcher, M.D., Delong, M.R., 1990. Basal ganglia thalamo-cortical circuits: parallel substrates for motor, oculomotor, "prefrontal" and "limbic" functions. Prog. Brain Res. 85, 119–146.

Amory, D.W., Steffenson, J.L., Forsyth, R.P., 1971. Systemic and regional blood flow changes during halothane anesthesia in the Rhesus monkey. Anesthesiology 35, 81–90.

Antonini, A., Kazumata, K., Feigin, A., Mandel, F., Dhawan, V., Margouleff, C., et al., 1998. Differential diagnosis of parkinsonism with [^{18}F]fluorodeoxyglucose and PET. Mov. Disord. 13, 268–274.

Antonini, A., Moresco, R.M., Gobbo, C., De Notaris, R., Panzacchi, A., Barone, P., et al., 2001. The status of dopamine nerve terminals in Parkinson's disease and essential tremor: a PET study with the tracer [^{11}C]FE-CIT. Neurol. Sci. 22, 47–48.

Antonini, A., Vontobel, P., Psylla, M., Gunther, I., Maguire, P.R., Missimer, J., et al., 1995. Complementary positron emission tomographic studies of the striatal dopaminergic system in Parkinson's disease. Arch. Neurol. 52, 1183–1190.

Berding, G., Odin, P., Brooks, D.J., Nikkhah, G., Matthies, C., Peschel, T., et al., 2001. Resting regional cerebral glucose metabolism in advanced Parkinson's disease studied in the off and on conditions with [^{18}F]FDG-PET. Mov. Disord. 16, 1014–1022.

Bohnen, N., Minoshima, S., Giordani, B., Frey, K.A., Kuhl, D.E., 1999. Motor correlates of occipital glucose hypometabolism in Parkinson's disease without dementia. Neurology 52, 541–546.

Brooks, D., 1997. PET and SPECT studies in Parkinson's disease. Baillieres Clin. Neurol. 6, 69–87.

Brooks, D., 1999. Functional imaging of Parkinson's disease: is it possible to detect brain areas for specific symptoms? J. Neural. Transm. Suppl. 56. 139–153.

Brooks, D.J., 2001. Cerebral blood flow activation studies, in: Calne, D., Calne, S. (Eds.), Parkinson's Disease: Advances in Neurology, Vol. 86. Lippincott Williams & Wilkins, Philadelphia, pp. 225–235.

Brownell, A.-L., Elmaleh, D.E., Meltzer, P.C., Shoup, T.M., Brownell, G.L., Fischman, A.J., et al., 1996. Cocaine congeners as PET imaging probes for dopamine terminals. J. Nucl. Med. 37, 1186–1192.

Brownell, A.-L., Jenkins, B.G., Elmaleh, D.R., Deacon, T.W., Spealman, R.D., Isacson, O., 1998. Combined PET/MRS brain studies show dynamic and long-term physiological changes in a primate model of Parkinson disease. Nature Med. 4, 1308–1312.

Brownell, A.-L., Jenkins, B.G., Isacson, O., 1999. Dopamine imaging markers and predictive mathematical models for progressive degeneration in Parkinson's disease. Biomed. Pharmacother. 53, 131–140.

Brownell, G.L., Burnham, C.A., Stearns, C.W., Chesler, D.A., Brownell, A.-L., Palmer, M., 1989. Development in high-resolution positron emission tomography at MGH. Int. J. Imaging Systems Technol. 1, 207–217.

Carbon, M., Edwards, C., Eidelberg, D., 2003. Functional brain imaging in Parkinson's disease, in: Gordin, A., Kaakkola, S., Teravainen, H. (Eds.), Parkinson's Disease: Advances in Neurology, vol. 91. Lippincott Williams & Wilkins, Philadelphia, pp. 175–181.

Checkoway, H., Nelson, L.M., 1999. Epidemiologic approaches to the study of Parkinson's disease etiology. Epidemiology 10, 327–336.

Chesler, D., 1973. Positron tomography and three-dimensional reconstruction technique, in: Freedman, G.S. (Ed.), Tomographic Imaging in Nuclear Medicine. Soc. Nucl. Med., New York, pp. 176–183.

Chouker, M., Tatsch, K., Linke, R., Pogarell, O., Hahn, K., Schwarz, J., 2001. Striatal dopamine transporter binding in early to moderately advanced Parkinson's disease: monitoring of disease progression over 2 years. Nucl. Med. Commun. 22, 721–725.

Crutcher, M., DeLong, M.R., 1984. Single cell studies of the primate putamen. II. Relations to direction of movement and pattern of muscular activity. Exp. Brain Res. 53, 244–258.

DeLong, M., Wichman, T., 2001. Deep brain stimulation for Parkinson's disease. Ann. Neurol. 49, 142–143.

Doudet, D.J., Holden, J.E., Jivan, S., McGeer, E., Wyatt, R.J., 2000. In vivo PET studies of the dopamine D2 receptors in rhesus monkeys with long term MPTP-induced parkinsonism. Synapse 38, 105–113.

Eberling, J., Richardson, B.C., Reed, B.R., Wolfe, N., Jagust, W.J., 1994. Cortical glucose metabolism in Parkinson's disease without dementia. Neurobiol. Aging 15, 329–335.

Ehrin, E., Farde, L., de Paulis, T., Eriksson, L., Greitz, T., Johnstrom, P., et al., 1985. Preparation of ^{11}C-labelled raclopride, a new potent dopamine receptor antagonist: preliminary PET studies of cerebral dopamine receptors in the monkey. Int. J. Appl. Radiat. Isot. 36, 269–273.

Eidelberg, D., Moeller, J.R., Dhawan, V., Spetsieris, P., Takikawa, S., Ishikawa, T., et al., 1994. The metabolic topography of parkinsonism. J. Cereb. Blood Flow Metab. 14, 783–801.

Eidelberg, D., Moeller, J.R., Ishikawa, T., Dhawan, V., Spetsieres, P., Chaly, T., et al., 1995a. Assessment of disease severity in parkinsonism with fluorine-18-fluorodeoxyglucose and PET. J. Nucl. Med. 36, 378–383.

Eidelberg, D., Moeller, J.R., Ishikawa, T., Dhawan, V., Spetsieres, P., Chaly, T., et al., 1995b. Early differential diagnosis of Parkinson's disease with 18F-fluorodeoxyglucose and positron emission tomography. Neurology 45, 1995–2004.

Eidelberg, D., Moeller, J.R., Ishikawa, T., Dhawan, V., Spetsieres, P., Silbersweig, D., et al., 1996. Regional metabolic correlates of surgical outcome following unilateral pallidotomy for Parkinson's disease. Ann. Neurol. 39, 452–459.

Foster, D., Barrett, P.H.R., Bell, B.M., Beltz, W.F., Cibelli, C., Golde, H.1994. Simulation, analysis and modeling software. BMES Bull., 18.

Frackowiak, R., Lenzi, G.L., Jones, T., Heather, J.D., 1980. Quantitative measurement of regional cerebral blood flow and oxygen metabolism in man using 15O and positron emission tomography: theory, procedure and normal values. J. Comput. Assist. Tomogr. 4, 727–736.

Frey, K.A., 1999. Positron emission tomography, in: Siegel, G.J., Agranoff, B.W., Albers, R.W., Fisher, S.K., Uhler, M.D. (Eds.), Basic neurochemistry. Lippincott-Raven, Philadelphia, pp. 1109–1131.

Fukuda, M., Mentis, M.J., Ma, Y., Dhawan, V., Antonini, A., Lang, A.E., et al., 2001. Networks mediating the clinical effects of pallidal brain stimulation for Parkinson's disease. A PET study of resting-state glucose metabolism. Brain 124, 1601–1609.

Gorrell, J., DiMonte, D., Graham, D., 1996. The role of environment in Parkinson's disease. Environ. Health Perspect. 104, 652–654.

Hantraye, P., Brownell, A.-L., Elmaleh, D.R., Spealman, R.D., Wullner, U., Brownell, G.L., et al., 1992. Dopamine fiber detection by [11C]-CFT and PET in a primate model of parkinsonism. NeuroReport 3, 265–268.

Hoffman, E.J., Huang, S.C., Phelps, M.E., 1979. Quantitation in positron emission tomography. 1 Effect of object size. J. Comput. Assist. Tomogr. 3, 299–308.

Huang, H.S., Lin, C.Z., Lin, J.C., Wey, S.P., Ting, G., Liu, R.S., 2001. Evaluation of early-stage Parkinson's disease with 99mTc-TRODAT-1 imaging. J. Nucl. Med. 42, 1303–1308.

Hwang, W.J., Yao, W.J., Wey, S.P., Shen, L.H., Ting, G., 2002. Down-regulation of striatal dopamine D2 receptors in advanced Parkinson's disease contributes to the development of motor flunctuation. Eur. Neurol. 47, 113–117.

Imon, Y., Matsuda, H., Ogawa, M., Kogure, D., Sunohara, N., 1999. SPECT image analysis using statistical parametric mapping in patients with Parkinson's disease. J. Nucl. Med. 40, 1583–1589.

Isacson, O., van Horne, C., Schumacher, J.M., Brownell, A.-L., 2001. Improved surgical cell therapy in Parkinson's disease—physiological basis and new transplantation methodology, in: Calne, D., Calne, S. (Eds.), Parkinson's Disease: Advances in Neurology, Vol. 86. Lippincott Williams & Wilkins, Philadelphia, pp. 447–454.

Jones, T., Chesler, D.A., Ter-Pogossian, M.M., 1976. The continuous inhalation ofxygen-15 for assessing regional oxygen extraction fraction in the brain of man. Br. J. Radiol. 49, 339–343.

Kaasinen, V., Ruottinen, H.M., Nagren, K., Lehikoinen, P., Oikonen, V., Rinne, J.O., 2000. Upregulation of putaminal D2 receptors in early Parkinson's disease: a comparative PET study with [^{11}C]raclopride and [^{11}C]N-methylspiperoni. J. Nucl. Med. 41, 65–70.

Kaufman, M.J., Madras, B.K., 1992. Distribution of cocaine recognition sites in monkey brain. II.Ex vivo autoradiography with [^{3}H]CFT and [^{125}I]RTI-55. Synapse 12, 99–111.

Kish, S., Shannak, K., Hornykiewicz, O., 1988. Uneven pattern of dopamine loss in the striatum of patients with idiopathic Parkinson's disease. N. Engl. J. Med. 318, 876–880.

Marck, K., Innis, R., van Dyck, C., Fussel, B., Early, M., Eberly, S., et al., 2001. [^{123}I]Beta-CIT SPECT imaging assessment of the rate of Parkinson's disease progression. Neurology 57, 2089–2094.

Markus, H., Lees, A.J., Lennox, G., Marsden, C.D., Costa, D.C., 1995. Patterns of regional cerebral blood flow in corticobasal degeneration studied using HMPAO SPECT; comparison with Parkinson's disease and normal controls. Mov. Disord. 10, 179–187.

Marsden, C.D., 1992. Parkinson disease. Postgrad. Med. J. 68, 538–543.

Mizuno, Y., Shimoda-Matsubayashi, S., Matsumine, H., Morikawa, N., Hattori, N., Kondo, T., 1999. Genetic and environmental factors in the pathogenesis of Parkinson's disease. Adv. Neurol. 80, 171–179.

Moeller, J.R., Eidelberg, D., 1997. Divergent expression of regional metabolic topographies in Parkinson's disease and normal aging. Brain 120, 2197–2206.

Palombo, E., Porrino, L.J., Bankiewicz, K.S., Crane, A.M., Sokoloff, L., Kopin, I.J., 1990. Local cerebral glucose utilization in monkeys with hemiparkinsonism induced by intracarotid infusion of the neurotoxin MPTP. J. Neurosci. 10, 860–869.

Palombo, E., Porrino, L.J., Crane, A.M., Bankiewicz, K.S., Kopin, I.J., Sokoloff, L., 1991. Cerebral metabolic effects of monoamine oxidase in normal and 1-methyl-4-phenyl-1,2,3,6-tetrahydropyridine acutely treated monkeys. J. Neurochem. 56, 1639–1646.

Paxinos, G., Huang, X.-F., Toga, A.W., 2000. The Rhesus Monkey Brain Atlas in Stereotaxic Coordinates. Academic Press, San Diego.

Phelps, M.E., Huang, S.C., Hoffman, E.J., Selin, C., Sokoloff, L., Kuhl, D., 1979. Tomographic measurement of local cerebral glucose metabolic rate in humans with (F-18-2-fluoro-2- deoxy-D-glucose: validation of method. Ann. Neurol. 6, 371–388.

Porrino, L., Burns, R.S., Crane, A.M., Palombo, E., Kopin, I.J., Sokoloff, L., 1987. Changes in local cerebral glucose utilization associated with Parkinson's syndrome induced by 1-methyl-4-phenyl-1,2,3,6-tetrahydropyridine (MPTP) in the primate. Life Sci. 40, 17657–17664.

Puyau, M., Adolph, A.L., Vohra, F.A., Butte, N.F., 2002. Validation and calibration of physical activity monitors in children. Obes. Res. 10, 150–157.

Reivich, M., Alavi, A., Wolf, A., Fowler, J., Russell, J., Arnett, C., et al., 1985. Glucose metabolism rate kinetic model parameter determination in humans: the lumped constants and rate constants for [^{18}F]fluorodeoxy- and [^{11}C]deoxyglucose. J. Cereb. Blood Flow Metab. 5, 179–192.

Sakakibara, R., Shinotoh, H., Yoshiyama, M., Hattori, T., Yamanishi, T., 2001. SPECT imaging of the dopamine transporter with [^{123}I]-beta-CIT reveals marked decline of nigrostriatal dopaminergic function in Parkinson's disease with urinary dysfunction. J. Neurol. Sci. 187, 55–59.

Samuel, M., Ceballos-Baumann, A.O., Turjanski, N., Boecker, H., Gorospe, A., Linazasoro, G., et al., 1997. Pallidotomy in Parkinson's disease increases supplementary motor area and prefrontal activation during performance of volitional movements: an H2(15)O PET study. Brain 120, 1301–1313.

Schapira, A.H.V., 1996. Neurotoxicity and the mechanisms of cell death in Parkinson's disease, in: Battistin, L., Scarlato, G., Carceni, T., Ruggieri, S. (Eds.), Advances in Neurology, Vol. 69. Lippincott-Raven, Philadelphia, pp. 161–165.

Schmidt, N., Ferger, B., 2001. Neurochemical findings in the MPTP model of Parkinson's disease. J. Neural. Transm. 108, 1263–1282.

Sokoloff, L., Reivich, M., Kennedy, C., Des Rosiers, M.H., Patlak, C.S., Pettigrew, K.D., et al., 1977. The (C-14) deoxy glucose method for the measurement of local cerebral glucose utilization: theory, procedure, the normal values in the conscious and anesthetized albino rat. Neurochemistry 28, 897–916.

Stoessl, A.J., de la Fuente-Fernandez, R., 2003. Dopamine receptor in Parkinson's disease: imaging studies, in: Gordin, A., Kaakkola, S., Teravainen, H. (Eds.), Parkinson's Disease: Advances in Neurology, Vol. 91. Lippincott-Raven, Philadelphia, pp. 65–71.

Subramanyam, R., Alpert, N.M., Hoop Jr., B., Brownell, G.L., Taveras, J.M., 1978. A model for regional cerebral oxygen distribution during continuous inhalation of 15O2, C15O, and C15O2. J. Nucl. Med. 19, 43–53.

van Dyck, C., Seibyl, J.P., Malison, R.T., Laruelle, M., Zoghbi, S.S., Baldwin, R.M., et al., 2002. Age-related decline in dopamine transporters: analysis of striatal subregions, nonlinear effects, and hemispheric asymmetries. Am. J. Geriatr. Psychiatry 10, 36–43.

van Nguyen, T., Brownell, A.-L., Chen, Y.I., Livni, E., Coyle, J.T., Rosen, B.R., et al., 2000. Detection of the effects of dopamine receptor supersensitivity using pharmacological MRI and correlation with PET. Synapse 36, 57–65.

Wichman, T., DeLong, M.R., 1996. Functional and pathophysiological models of the basal ganglia [Review]. Curr. Opin. Neurobiol. 6, 751–758.

Wichman, T., DeLong, M.R., 2003. Functional neuroanatomy of the basal ganglia in Parkinson's disease, in: Gordon, A., Kaakkola, S., Teravainen, H. (Eds.), Parkinson's Disease: Advances in Neurology, Vol. 91. Lippincott Williams & Wilkins, Philadelphia, pp. 9–18.

Wullner, U., Pakzaban, P., Brownell, A.-L., Hantraye, P., Burns, L., Shoup, T., et al., 1994. Dopamine terminal loss and onset of motor symptoms in MPTP-treated monkeys: a positron emission tomography study with ^{11}C-CFT. Exp. Neurol. 126, 305–309.

AQ: 2

Synthesis of [^{11}C]Methoxymethyl-MTEP and [^{11}C]Methoxy-PEPy, potent and selective PET radioligands for Metabotropic Glutamate Subtype 5 (mGlu5) receptor

Meixiang Yu[1], Thomas Klaess[2], Alan P. Kozikowski[2], Anna-Liisa Brownell[1]

[1]Department of Radiology, Massachusetts General Hospital, Boston, MA.

[2]Departments of Neurology, Georgetown University Medical Center, Washington, DC

Metabotropic glutamate receptors (mGluRs) are a family of receptors coupled with G-protein in the mammalian nervous system and are activated by L-glutamate. Excessive activation of mGluRs has been implicated in several disease states including pain, anxiety, depression, drug addiction or withdrawal. Research of the mGluRs has been hampered because of the lack of in vivo imaging ligands. We have developed radio-labeling for two antagonists of mGluR5; 2-[(3-methoxy-phenyl) ethynyl]-6-methyl-pyridine (M-MPEP, 2), a novel ligand with high affinity (Kd=2 nM), and 3-methoxy-5-(pyridin-2-ylethynyl)pyridine (M-PEPy, 4) also a mGlu5 antagonist with high affinity (Kd=3.4 nM).

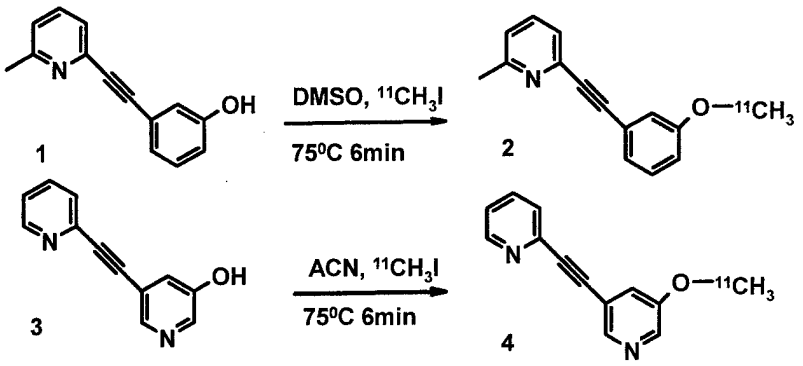

Synthesis of [^{11}C]M-MPEP (2) and [^{11}C]M-PEPy (4)

O.5 mg of precursor 1 dissolved in 400 μL DMSO and 6 mg KOH was used to react with [^{11}C]CH_3I, which was produced by standard method. The reaction mixture was heated at 75^{0}C for 6 min, after which [^{11}C]M-MPEP was purified on a μ-Bondapak® C-18 preparative HPLC column (7.8 × 300 mm, Waters) by washing with methanol and phosphate buffer (pH 7.4) 60/40 at 6 ml/min, with 40% yield. Similarly, O.5 mg of precursor 2 dissolved in 400 μL acetonitrile (CAN) and 6 mg of KOH was used to receive [^{11}C]CH_3I, then the reaction mixture was heated at 75^{0}C for 6 min. [^{11}C]M-PEPy was purified on a above HPLC system, by washing with methanol and phosphate buffer (pH 7.4) 50/50 at 6 ml/min, with 50.5% yield.

The radiolabeled ligands were administered into the normal rats (male Spraque-Dawley, 2 mCi into the tail vein) to evaluate in vivo biodistribution by PET. In 3 min the activity reached the maximum in the brain followed by rapid washout. The abdominal area (liver, spleen and pancreas) had the highest accumulation and the radioactivity did not wash out during the 60 min follow up time. In conclusion, we have successfully labeled M-MPEP and M-PEPy with C-11 in high yield, and in vivo imaging studies have shown that the ligands go through the blood brain barrier. Further analyses will be done to localize possible specific binding sites in the brain.

Dr. Stephen G. Lisberger

3-NITROPROPIONIC ACID INDUCED NEUROTOXICITY – ASSESSED BY ULTRA HIGH RESOLUTION PET WITH COMPARISON TO MRI AND MRS

Anna-Liisa Brownell[1], Y. Iris Chen[1], Meixiang Yu[1], Xukui Wang[1], Kimmo Jokivarsi[1], Aparajita Sarkar[1], Alp Dedeoglu[2], Francesca Cicchetti[3], M. Flint Beal[4], Bruce G. Jenkins[1].

[1]Department of Radiology, Massachusetts General Hospital, Boston, MA 02114, [2]Veterans Administration Medical Center, Bedford, MA 01730, [3]Unite de Neuroscience, CHUL, Quebec, [4]Department of Neurology and Neuroscience, Weill Medical College of Cornell University, New York Presbyterian Hospital, New York, NY 10021

Abbreviated title: PET and MRI/MRS studies of 3-NP neurotoxicity

Number of the text pages: 22

Number of words: Abstract (245); Introduction (489); Discussion (1254)

Acknowledgements: We wish to thank cyclotron operators William Buckelewitz and David Lee and Dr. Steve Dragotakis for synthesis of ^{18}F-FDG and Robert Power for good care of the animals. This work was supported by DOD grant DAMD 17-99-1-9555 to A-LB.

Key words: 3-nitropropionic acid, glucose utilization, PET, MRS, Huntington's disease, neurodegeneration

Correspondence:

Anna-Liisa Brownell, Ph.D.

Associate Professor

Bartlett Hall 504R, Radiology, Massachusetts General Hospital, Boston, MA 02114

tel: 617-726-3807

fax: 617-726-5123

email: abrownell@partners.org

ABSTRACT

Recent development in imaging instrumentation have enabled in vivo imaging studies in small animal models to investigate different physiological processes quantitatively and longitudinally. We used these techniques to explore acute and long-term effects of 3-nitropropionic acid (3-NP) induced neurotoxicity. Longitudinal positron emission tomography (PET) imaging studies of energy metabolism and magnetic resonance spectroscopic (MRS) studies of neurochemicals were conducted in a rat model. The first injection of 3-NP (20 mg/kg i.p.) was followed by MRS study of neurochemicals and PET study of glucose utilization. After that 3-NP administration was done two times a day with a dose of 10 mg/kg i.p. until animals were symptomatic or for a maximum of 5 days. The acute effects were followed during the 3-NP administration with daily PET imaging of glucose utilization using ^{18}F-2-fluorodeoxy-D-glucose (^{18}F-FDG). Long-term effects were investigated 4 weeks and 4 months after cessation of 3-NP. These studies showed a significant inter-animal variation in response of 3-NP toxicity on striatal glucose utilization and neurochemicals. This variation paralleled weight loss and deficits in behavior. Animals, which developed large striatal lesions, had decreased glucose utilization in the striatum and cortex one day after starting 3-NP injections. Similarly succinate and lactate/macromolecule levels were enhanced; these changes being, however, reversible. Progressive degeneration was observed by decreasing striatal glucose utilization and N-acetylaspartate (NAA) and increasing choline. Animals, which did not develop lesions, showed reversible enhancement in cortical glucose utilization and no change in striatal glucose utilization or neurochemicals or locomotor activity.

INTRODUCTION

Neurotoxicity related cell damage is often associated with mitochondrial energy impairment, which originate a chain of different pathophysiological processes finally ending in cell death (Brennan et al., 1985; Beal, 1998). 3-Nitropropionic acid (3-NP), an inhibitor of mitochondrial oxidative metabolism, has been ingested as a component in moldy sugarcane resulting in selective neuronal death and symptoms similar to Huntington's disease (HD) (Ludolph et al., 1991). Subsequently, 3-NP has been widely used as an experimental model of HD as well as a model to study energy metabolism and cell death (Beal, 1992) in vivo (Beal et al., 1993) and in vitro (Fink et al., 1996; Pang and Geddes, 1997). Although HD is associated with a gene mutation (The Huntington's Disease Collaborative Group, 1993), the etiology of the disorder is still unknown. Progression of the disease might be a result of energy impairment induced slow excitotoxic neuronal death (Albin and Greenamyre, 1992; Beal et al., 1993).

3-NP, an inhibitor of succinate dehydrogenase (Alston et al., 1977) creates mitochondrial inhibition and through inhibition of Complex II activity of the electron transport chain causing depletion of intracellular ATP synthesis, leading to striatal degeneration.

3-NP induced pathophysiological changes are time dependent and some are reversible. Lee et al. (2000) showed that after 3-NP toxication, succinate and lactate/macromolecules are increased immediately and remain enhanced for several days; this process is, however, reversible. In addition, Dautry et al (Dautry et al., 2000) showed that the early decrease of N-acetylaspartate (NAA) induced by chronic 3-NP administration, is reversible, consistent with mitochondrial dysfunction since NAA is synthesized within mitochondria. However, when toxicity continues, NAA will decrease again, which indicates the death of neurons.

Since glucose is the major energy source of the brain, changes in glucose utilization can serve as a sensitive indicator of energy requirements in brain (Di Chiro, 1987; Palombo et al., 1990; Eberling et al., 1994; Eidelberg et al., 1996; Antonini et al., 1998; Dethy et al., 1998; Higashi et al., 2000). Glucose utilization can be investigated by PET imaging using fluorine-18 labeled 2-fluorodeoxy-D-glucose (^{18}F-FDG) as a tracer. ^{18}F-FDG is transported from blood stream into brain and to the metabolic cycle by hexokinase enzyme (Sokoloff et al., 1977). ^{18}F-FDG will not go through the whole metabolic cycle but remains in ^{18}F-glucose 6-phosphate in the brain for several hours and enables quantitative imaging studies. Since the hexokinase

enzyme is activated in relation to the energy requirements of the tissue, the accumulation of deoxyglucose reflects the metabolic rate of glucose (Phelps et al., 1979).

To investigate acute and prolonged effects of 3-NP induced neurotoxicity, we conducted in vivo imaging studies in a rat model of striatal energy metabolism using ^{18}F-FDG by PET, neuroanatomy by MRI and neurochemicals by MRS (Jenkins et al., 1996). These in vivo imaging techniques allowed us to perform multimodality longitudinal studies of different pathophysiological processes in the same animals. For PET imaging we used an in house built super-high resolution imaging device.

METHODS

Neurotoxin: 3-nitropropionic acid (3-NP) (Sigma Aldrich Co) solution was prepared by dissolving 3-NP powder in buffered 0.9 % saline and pH was adjusted to 7.4 with concentrated sodium hydroxide.

Experimental procedures in rats: An acute effect of the neurotoxin 3-NP, was investigated in 12 rats (male Spraque-Dawley from Charles River Laboratories, weight of 300 g) using the following daily time schedule: The first injection of 3-NP (20 mg/kg i.p.) was followed by MRS study of neurochemicals and PET study of glucose utilization. After that 3-NP administration was done two times a day with a dose of 10 mg/kg i.p. according the following time schedule: 10 am. PET imaging study; 12 pm. 3-NP administration; and 8 pm. 3-NP administration. This protocol was repeated until symptoms developed (gait observed) or for a maximum of 5 days treatment. During the treatment period, rats were individually housed in metabolic cages, and their diet and excretion were closely monitored. Motor deficits were evaluated using a quantitative neurological coding scale developed by Guyot et al (1997) and Ouary et al (2000). Weight progression was followed by daily measurements (Figure 1).

To investigate long-term degeneration, imaging studies of glucose utilization by PET, neurochemicals by MRS and neuroanatomy by MRI were repeated at 4 weeks and 4 months after the cessation of 3-NP administrations.

For imaging studies rats were anesthetized with halothane (1.0-1.5% with oxygen flow rate of 3 L/min). For PET studies, catheters were introduced into the tail vein for administration of radiolabeled ligands and into the tail artery for drawing of blood samples, which were needed to determine glucose level and blood input function for quantification of glucose metabolic rate.

A heated waterbed was used to maintain body temperature for all imaging sessions (PET, MRI, MRS). Anesthetized animals were mounted onto a stereotactic headholder to allow accurate repositioning of the animal in longitudinal studies.

To verify the information obtained by the imaging studies histological evaluation of brains was performed. Rats were deeply anesthetized by ketamine/xylaxine (100mg/10mg/kg i.m.) and then transcardially perfused with 4% buffered formaldehyde. The brains were removed, post-fixed with the perfusant for 2 hrs, cryoprotected in a graded series of 10% and 20% glycerol in 2% DMSO solution, subsequently serially frozen, sectioned at 50 μm, stored in 6 well tissue collection clusters, and stained for Nissl substance (cresyl violet).

PET imaging techniques with a super-high resolution tomograph: PET imaging studies of glucose metabolism were conducted using a super high resolution in-house built (Correia et al., 1999) PET imaging device (Figure 2). The spatial resolution of the system is at the center of the field 1.16 x 1.16 x 1.3 mm^3. This enables us to investigate metabolic changes in tiny elements (~2μl) inside the rat brain. However, since the signals originate from such tiny elements, high radioactivity levels were required to produce statistically meaningful signals and images.

A computer controlled imaging "table" has been developed for the super high-resolution scanner. The diameter of the bore in the PET system is 6 cm and the imaging "table" moves through it in a "step and shoot" mode (Figure 2). The length of the axial steps can be selected by the acquisition program with the smallest step size of 12.5 μm. The stereotactic headholder with earbars and mouth (teeth) bar can be mounted onto the "table" to ensure the standard positioning of the animals. For the experimental procedure, the animal is secured onto the "table" through the stereotactic headholder, which is equipped with a gas inhalation system. The "table" is then screwed onto a cradle attached to the control motor in the imaging device (Figure 2).

Software was developed to control the movement of the imaging "table" to allow scanning of the whole brain, slice by slice. PET signals were corrected for uniformity and attenuation using a mathematical attenuation correction with an attenuation coefficient of 0.096. Image reconstruction was done using Hanning filtered convolution backprojection with a cut-off value of 1.0. Cross-calibration of the tomograph was done with a gammacounter (Packard Cobra Auto-gamma, Downers, IL, USA) using fluorine-18 labeled water. Cross-calibration is needed to quantify the blood samples drawn during the imaging acquisition.

PET imaging studies of glucose utilization: For imaging studies, 3-4 mCi of ^{18}F-FDG was administered into the tail vein. Ten arterial blood samples (50 μl) were drawn from the tail artery starting 30 s after administration of radioactivity with an increasing time interval for total of 20 min. Glucose level was determined before the administration of radioactivity. Dynamic accumulation of radioactivity into the brain was acquired by PET for 25 min at one brain level (10 mm anterior to the earbar). By that time a steady state level of radioactivity was achieved and sequential imaging of distribution of radioactivity was done by "step and shoot" mode over the whole brain using 1.25 or 2.5 mm steps with slice thickness of 1.3 mm.

After image reconstruction, PET images were overlaid with anatomical MR images for drawing regions of interest from striatum, cingulate, S1/S2 cortex and cerebellum (Figure 3). Glucose utilization was calculated using a Sokoloff model (Sokoloff et al., 1977) extended by Phelps et al (1979) using a value of 0.5 for the lumped constant (Brownell et al., 1991). Data fitting to the model was done using SAAM II software package (Foster, 1994) with convergence criterion of 1.0e-6.

Imaging studies of neurochemicals and anatomy: MRI and MRS studies were conducted with a commercial GE Omega 4.7 T imager using PRESS sequence (TR 2000ms; TE 68, 136 and 272 ms). For single voxel spectra, voxels were located symmetrically over the basal ganglia (6 x 3.5 x 3 mm^3) and the motor cortex (6 x 2 x 3mm^3). Individual spectral peaks were integrated and normalized to the creatine/phosphocreatine peak.

RESULTS

Weight loss and behavior deficit: We found a significant interanimal variation in response of 3-NP toxication on locomotor activity. The motor deficit score (Guyot et al., 1997; Ouary et al., 2000) varied from 0 to 6. Six of the 12 rats showed significant hypokinesia. Three of the six had hindlimb paralyses and the motor score was between 4 and 6. The other 3 rats had motor scores of 2-3. In the remaining group of rats, 3 did not show any observable changes in locomotor activity (scored 0), while the 3 others showed a slight slowness and occasional uncoordinated gait (scored 1). All the animals lost weight after 3-NP administrations. The animals with the strongest response to 3-NP (behavioral score between 2 and 6) lost 24+/-4 % of their weight and the weight loss extended 4 days after the cessation of neurotoxicity. They did not reach the weight level of the weaker response group during the 80 days of follow up (Figure 1).

The maximum weight loss in the other group was 12+/-2 %, and the weight loss stopped the day after the cessation of 3-NP administrations. The observations in motor activity are similar to those published by Borlongan et al (1977) and Guyot et al (1977).

Glucose utilization: The daily ^{18}F-FDG imaging studies during 3-NP administration period showed significant inter-animal variation of glucose utilization in response to the acute toxin; similar to motor activity. The rats, which did not show any motor symptoms, developed enhanced glucose utilization in cortical areas with a maximum enhancement of 19-24% on the third day after starting the 3-NP administration. At the cessation of 3-NP administration, the glucose utilization was still enhanced by 12-16% and 2 days later by 6-8%. No significant changes in striatal glucose utilization were observed during that time (Figure 4). The animals with hindlimb paralyses developed extensive striatal lesions. Table I shows the changes of glucose metabolism in 4 different brain areas (striatum, cingulate, S1/S2 cortex, and cerebellum; Figure 5) during and after 3-NP toxication for the animals whose motor score was between 2 and 6. The striatum is the most affected brain area and the cerebellum is the least affected one. The average decrease of glucose utilization in the striatum at the end of 3-NP injections was 35+/-11 % and the development of the progressive decrease started one day after the first 3-NP injection (Figure 5). On day 3, large lesions were clearly observable in several slices, which cover the whole striatum. Interestingly, glucose utilization continued to decrease until at least 2 days after the cessation of 3-NP, after which a short period of recovery was observed, followed by a long-term degeneration (Figure 6). As an early response to 3-NP toxicity, cingulate and S1/S2 cortical areas showed minimal change or even small increase in glucose utilization while striatal areas showed significant decrease in glucose metabolism. However, these areas also showed decreased glucose utilization with the progression of degeneration. Figure 7 shows the histological validation of the neural loss, which correlates well with the decreased glucose utilization in the striatum 2 days after the cessation of 3-NP.

MRS studies of neurochemicals: In two hours after 3-NP toxicity, MRS showed elevated levels of succinate, lactate and macromolecules (Figures 8 and 9). The increase rate of lactate/macromolecules was 31+/-9%/min; succinate 5.3+/-.5%/min and choline 0.06+/-0.01%/min during the first 5 hours after the administration of 3-NP (Figure 8). These elevated values however, diminished within 4 months (Figure 9) indicating a reversible process. However, elevated striatal choline and decreased N-acetylaspartate levels were observed at this

time point indicating damage and a loss of neurons. These data represent animals with a motor score > 4. In the animals, which did not develop striatal lesions, no succinate or lactate peaks were observed.

DISCUSSION

3-Nitropropionic acid is an irreversible inhibitor of succinate dehydrogenase thereby resulting in cellular ATP depletion and an impairment of energy metabolism (Beal et al., 1993; Guyot et al., 1997; Storgaard et al., 2000; Garcia et al., 2002). 3-NP can induce time dependent 2-way biological processes (Lee et al., 2000; Dautry et al., 2000). Mapping these different components may provide a means to examine the overall regulatory process involved in neurotoxicity. Newly developed high resolution in vivo imaging techniques enable one to investigate multimodality processes simultaneously in the natural biological environment.

Longitudinal imaging studies in the same subjects allowed us to correlate parameters of in vivo physiological functions and the progression of deficits measured by behavioral or weight changes. Basic research in neuroscience typically relies on in vitro experiments. The limitation of in vitro studies is that they provide information at only the end point when biological interactions created by surrounding tissues and elements are no longer present. In vitro studies provide, however, brief analyses of the isolated biological processes with large amounts of data and high statistical accuracy (Fink et al., 1996).

Based on the responses to 3-NP induced neurotoxicity in our experiments, we divided animals into two groups depending on their behavioral responses, weight loss and the glucose utilization, investigated by PET. The animals with the strongest response to 3-NP (behavioral score between 2 and 6) lost about 24 % of their weight and the weight loss extended 4 days after the cessation of neurotoxicity. The maximum weight loss in the other group was about 12 %, and the weight loss stopped the day after the cessation of 3-NP administrations. The observations on motor activity were scored according to the method developed by Guyot et al (1997) and Ouary et al (2000) and the observations are similar to those published by Borlongan et al (1997) and Guyot et al (1997).

We and others (Guyot et al., 1997; Brouillet et al., 1998; Ouary et al., 2000; El Massioui et al., 2001) have observed significant inter-animal variation in 3-NP induced changes in motor

activity (Borlongan et al., 1997; Guyot et al., 1997), energy metabolism as well as in the severity of lesions (Beal, 1992; Beal et al., 1993; Beal, 1998).

A recent study by Guo et al (2000) showed that dietary restriction can inhibit the effect of 3-NP neurotoxicity. However, a low glucose level alone, which could inhibit 3-NP neurotoxicity, is not enough to explain the inter-animal variation observed in these studies. During 3-NP administration, our animals were housed separately in metabolic cages, fed in the same way and fasted from the night till the following morning for imaging studies of glucose metabolism, which were conducted 2 hours before 3-NP administration. Every other 3-NP administration was done in a fasted condition while the 3-NP administration in the evening was done after feeding. This should minimize the possible inter-animal difference induced by dietary patterns. It has been also proposed that strain dependent genetic aspects might be part of these inter-animal variations of 3-NP induced neurotoxicity (Ouary et al., 2000). Interestingly, rotenone toxicity shows similar inter-animal variation (Betarbet et al., 2000).

Based on in vivo imaging studies, we propose that the variation of 3-NP induced pathophysiological changes might depend on the metabolic status of the mitochondrion and the tolerance level of the neuron for neurotoxicity. The rats, which did not develop any behavioral symptoms or striatal lesions, may have a high tolerance level for 3-NP neurotoxicity. Interestingly, these animals developed enhanced cortical glucose utilization as an early response to 3-NP and this change was reversible.

In vitro studies have demonstrated that 3-NP induced cell killing may have two different mechanisms: toxicity induced necrosis and apoptosis (Pang and Geddes, 1997). The relationship of these two mechanisms is dependent on the level of toxicity and ATP depletion (Pang and Geddes, 1997). These biological degenerative processes are different: necrosis is characterized as the rapid swelling of cells and cell lyses (Wyllie et al., 1980; Cepeda et al., 1998) while in apoptosis, cells are shrunken and cytoplasm and nucleus are fragmented in a slow long lasting process requiring ATP (Wyllie et al., 1984; Kim and Chan, 2001). In addition to intracellular energy metabolism, 3-NP induced neurotoxicity is also dependent on glutamate (Fink et al., 1996) and dopamine concentration (Cepeda et al., 1998; Reynolds et al., 1998).

Our studies show that 3-NP launched development of neurotoxicity is a rapid process and happens in hours. It is possible to record this in real time with MRS of neurochemicals (Figure 8) and PET imaging studies of glucose utilization (Figure 5). We observed a 31+/-

9%/min increase rate of lactate/macromolecule level during 150 min follow up time 2 hours after injection of the first dose of 3-NP. Similarly we observed a 5.3+/0.5%/min increase rate in succinate level. Thus our results agree with the data reported by Lee et al (2000) that succinate was rapidly observable in MRS, minutes after the injection of 3-NP. In addition, the early increases of succinate and lactate/macro- molecule levels were indicative for the development of large striatal lesions. On the third day of 3-NP injections a significant decrease in striatal glucose utilization was observable with similar decrease in cortical areas. Already in the first day after 3-NP administration it is possible to separate animals, which will develop lesions based on changes in glucose utilization. The animals, which will develop lesions have decreased levels of glucose utilization in striatum (9.8+/-6.1%) and cortex (6.7+/-4.0) and the animals, which do not develop lesions have enhanced cortical values with no change in striatal values. After this period of neurotoxicity induced necrosis and fast cell killing, we observed a period of partial recovery followed by slowly progressive degeneration detected by decreases in glucose utilization and NAA and increases of choline.

Based on our results, we hypothesize that in addition to rapidly induced necrosis, 3-NP may have induced a slower form of cell death in less severely affected cells. These cells start to degenerate gradually and the cell death may be caused by an apoptotic processes over a long period of time. This slow progression may be more important in studying HD-type neurodegeneration. Vis et al (Vis et al., 1999) published that a mild response to 3-NP most closely resembles the characteristics HD neuropathology and similar observations were initially made by Beal et al (Beal et al., 1993). The striatum is the most vulnerable brain region to systemic intoxication of 3-NP (Brouillet et al., 1998). This may be due to the cumulative impairment in energy metabolism caused partially by 3-NP and dopamine toxicity (Reynolds et al., 1998; Johnson et al., 2000).

MRS studies of striatal neurochemicals correlate well with those of glucose utilization. MRS studies showed reversible changes in succinate and lactate/ macromolecules in affected animals and progressively increasing choline and decreasing NAA indicating progressive degeneration. These animals developed large lesions and progressively decreasing glucose utilization. The animals, which did not develop lesions, did not show succinate or lactate peaks.

To enhance the accuracy in the data analyses, the regions of interest were drawn based on the anatomical MR images overlaid with PET images and the same areas of interest were used in

longitudinal studies to partially eliminate the effects of partial volume. In addition the size of the selected regions of interest are larger than 2.3 mm, which significantly minimize partial volume effects, since the size of the object should we at least two times the resolution element (Brownell et al., 1991), which in our instrument is1.16 mm.

These multimodality longitudinal imaging techniques provide a powerful tool to investigate the progression of pathophysiological processes and assess therapeutic approaches in small animal models.

BIBLIOGRAPHY

Albin L, Greenamyre JT (1992) Alternative excitotoxic hypothesis. Neurology 42: 733-738.

Alston TA, Mela L, Bright HJ (1977) 3-Nitropropionate, the toxic substance of Indiofera, is a suicide inactivator of succinate dehydrogenase. Proc Natl Acad Sci USA 74: 3767-3771.

Antonini A, Kazumata K, Feigin A, Mandel F, Dhawan V, Margouleff C, Eidelberg D (1998) Differential diagnosis of parkinsonism with [18F]fluorodeoxyglucose and PET. Mov Disord 13(2): 268-274.

Beal MF (1992) Does impairment of energy metabolism result in exitotoxic neural death in neurodegenerative illness. Ann Neurol 31: 119-130.

Beal MF, Brouillet E, Jenkins BG, Ferrante RJ, Kowall NW, Miller J.M, Storey E, Srivastava R, Rosen BR, Hyman BT (1993) Neurochemical and histologic characterization of striatal excitotoxic lesions produced by the mitochondrial toxin 3-nitropropionic acid. J Neurochem 13: 4181-4192.

Beal MF (1998) Mitochondrial dysfunction in neurodegenerative diseases. Biochim Biophys Acta 1366: 211-223.

Beal M.F, Brouillet E, Jenkins BG, Ferrante RJ, Kowall NW, Miller JM, Storey E, Srivastava R, Rosen BR, Hyman BT (1993) Neurochemical and histologic characterization of striatal excitotoxic lesions produced by the mitochondrial toxin 3-nitropropionic acid. J Neurochem 13: 4181-4192.

Betarbet R, Sherer T.B, MacKenzie G, Garcia-Osuna M, Panov AV, Greenamyre JT (2000) Chronic systemic pesticide exposure reproduces features of Parkinson's disease. Nat Neurosci 3: 1301-1306.

Borlongan C, Koutouzis TK, Freeman TB, Hauser RA, Cahill DW, Sanberg PR (1997) Hyperactivity and hypoactivity in a rat model of Huntington's disease: the systemic 3-nitropropionic acid model. Brain Res Protoc 1(3): 253-257.

Brennan WAJ, Bird ED, Aprille JR (1985) Regional mitochondrial respiratory activity in Huntington's disease brain. J Neurochem 44: 1948-1950.

Brouillet E, Guyot MC, Mittoux V, Altaire S, Conde F, Palfi S, Hantraye P (1998) Partial inhibition of brain succinate dehydrogenase by 3-nitropropionic acid is sufficient to initiate striatal degeneration in rat. J Neurochem 70(2): 794-805.

Brownell A-L, Kano M, McKinstry RC, Moskowitz MA, Rosen BR, Brownell GL (1991) PET and MR studies of experimental focal stroke. J Comput Assist Tomogr :376-380.

Cepeda C, Colwell CS, Itri JN., Gruen E, Levine MS (1998) Dopaminergic modulation of early signs of excitotoxicity in visualized rat neostriatal neurons. Eur J Neurosci 10(11): 4391-4397.

Correia J, Burnham C, Kaufman D, Fischman A (1999) Development of a small animal PET imaging device with resolution approaching 1mm. IEEE Trans Nucl Sci 46(3): 631-635.

Dautry C, Vaufrey F, Brouillet E, Bizat N, Henry PG, Conde F, Bloch G, Hantraye P (2000) Early N-acetylaspartate depletion is a marker of neuronal dysfunction in rats and primates chronically treated with the mitochondrial toxin 3-nitropropionic acid. J Cereb Blood Flow Metab 20(5): 789-799.

Dethy S, van Blercom N, Damhaut P, Wikler D, Hildebrand J, Goldman S (1998) Asymmetry of basal ganglia glucose metabolism and dopa responsiveness in parkinsonism. Mov Disord 13(2): 275-280.

Di Chiro G (1987) Positron emission tomography using [18F]fluorodeoxyglucose in brain tumors. A powerful diagnostic and prognostic tool. Invest Radiol 22(5): 360-371.

Eberling J, Richardson BC, Reed BR, Wolfe N, Jagust WJ (1994) Cortical glucose metabolism in Parkinson's disease without dementia. Neurobiol Aging 15(3): 329-335.

Eidelberg D, Moeller JR, Ishikawa T, Dhawan V, Spetsieres P, Silbersweig D, Strean E, Woods RP, Fazzini E, Dogali M, Beric A (1996) Regional metabolic correlates of surgical outcome following unilateral pallidotomy for Parkinson's disease. Ann Neurol 39: 452-459.

El Massioui N, Ouary S, Cheruel F, Hantraye P, Brouillet E (2001) Perseverative behavior underlying attentional set-shifting deficit in rats chronically treated with the neurotoxin 3-nitropropionic acid. Exp Neurol 172(1): 172-181.

Fink SL, Ho DY, Sapolsky RM (1996) Energy and glutamate dependency of 3-nitropropionic acid neurotoxicity in culture. Exp Neurol 138: 298-304.

Foster DM (1994) SAAM II: simulation, analysis and modeling software. BMES Bull 18: 19-21.

Garcia M, Vanhoutte P, Pages C, Besson MJ, Brouillet E, Caboche J (2002) The mitochondrial toxin 3-nitropropionic acid induces striatal neurodegeneration via a c-Jun N-terminal kinase/c-Jun module. J Neurosci 22(6): 2174-2184.

Guo Z, Ersoz A, Butterfield DA, Mattson MP (2000) Beneficial effects of dietary restriction on cerebral cortical synaptic terminals: preservation of glucose and glutamate transport and mitochondrial function after exposure to amyloid beta-peptide, iron, and 3-nitropropionic acid. J Neurochem 75(1): 314-320.

Guyot M-C, Hantraye P, Dolan R, Palfi S, Maziere M, Brouillet E (1997) Quantifiable bradykinesia, gait abnormalities and Huntington's disease-like striatal lesions in rats chronically treated with 3-nitropropionic acid. Neurosci 79: 45-56.

Higashi K, Ueda Y, Yagishita M, Arisaka Y, Sakurai A, Ogushi M, Seki H, Nambu Y, Tonami H., Yamamoto I. (2000) FDG PET measurement of the proliferative potential of non-small cell lung cancer. J Nucl Med 41(1): 85-92.

Jenkins BG, Brouillet E, Chen YC, Storey E, Schultz JB, Kirschner P, Beal MF, Rosen BR (1996) Non-invasive neurochemical analysis of focal excitotoxic lesions in models of neurodegenerative ilness using spectroscopic imaging. J Cereb Blood Flow Metab 16(3): 450-461.

Johnson J, Robinson BL, Ali SF, Binienda Z (2000) Dopamine toxicity following long term exposure to low doses of 3-nitropropionic acid (3-NP) in rats. Toxicol Lett 116(1-2): 113-8.

Kim GW, Chan PH (2001) Oxidative stress and neuronal DNA fragmentation mediate age-dependent vulnerability to the mitochondrial toxin, 3-nitropropionic acid, in the mouse striatum. Neurobiol Dis 8(1 Pt B): 114-126.

Lee W-T, Lee C-S, Pan Y-L, Chang C (2000) Temporal changes of cerebral metabolites and straital lesions in acute 3-nitropropionic acid intoxication in the rat. Magn Res Med 44: 29-34.

Ludolph AC, He F, Spencer PS, Hammerstad J, Sabri M (1991) 3-nitropropionic acid - Exogenous animal neurotoxin and possible human striatal toxin. Can J Neurol Sci 18: 492-498.

Ouary S, Bizat N, Altairac S, Menetrat H, Mittoux V, Conde F, Hantraye P, Brouillet E (2000) Major strain differences in response to chronic systemic administration of the mitochondrial toxin 3-nitropropionic acid in rats: implications for neuroprotection studies. Neurosci 97: 521-530.

Palombo E, Porrino LJ, Bankiewicz KS, Crane AM, Sokoloff L, Kopin IJ (1990) Local cerebral glucose utilization in monkeys with hemiparkinsonism induced by intracarotid infusion of the neurotoxin MPTP. J Neurosci 10(3): 860-869.

Pang Z, Geddes JW (1997) Mechanisms of cell death induced by the mitochondrial toxin 3-nitropropionic acid: acute excitotoxic necrosis and delayed apoptosis. J Neurosci 17(9): 3064-3073.

Phelps ME, Huang SC, Hoffman EJ, Selin C, Sokoloff L, Kuhl D (1979) Tomographic measurement of local cerebral glucose metabolic rate in humans with (F-18-2-fluoro-2-deoxy-D-glucose: Validation of method. Ann Neurol 6: 371-388.

Reynolds DS, Carter RJ, Morton J (1998) Dopamine modulates the susceptibility of striatal neurons to 3-nitropropionic acid in the rat model of Huntington's disease. J Neurosci 18(23): 10116-10127.

Sokoloff L, Reivich M, Kennedy C, Des Rosiers MH, Patlak CS, Pettigrew KD, Sakurada D, Shinohara M (1977) The (C-14) deoxy glucose method for the measurement of local cerebral glucose utilization: Theory, procedure, the normal values in the conscious and anesthetized albino rat. Neurochem 28: 897-916.

Storgaard J, Kornblit BT, Zimmer J, Bert J, Gramsbergen P (2000) 3-nitropropionic acid in organotypic striatal and corticostriatal slice cultures is dependent on glucose and glutamate. Exp Neurol 164(1): 227-235.

The Huntington's Disease Collaborative Group (1993) A novel gene containing a trinucleotide repeat is expanded and unstable on Huntington's disease chromosomes. Cell 72:971-983.

Vis JC, Verbeek MM, De Waal RM, Ten Donkelaar HJ, Kremer HP (1999) 3-nitropropionic acid induces a spectrum of Huntington's disease-like neuropathology in rat striatum. Neuropathol Appl Neurobiol 25(6): 513-521.

Wyllie AH, Kerr JF, Currie A.R (1980) Cell death: the significance of apoptosis. Int Rev Cytol 68: 251-306.

Wyllie AH, Morris RG, Smith AL, Dunlop D (1984) Chromatin cleavage in apoptosis: association with condensed chromatin morphology and dependence on macromolecular synthesis. J Pathol 142: 67-77.

Table I. Percentage change of glucose utilization from the pre 3-NP values in 4 brain regions during and after 3-NP neurotoxicity in rats with motor scores between 2 and 6 (Guyot et al., 1997; Ouary et al., 2000). Glucose metabolic rate was calculated using Sokoloff (Sokoloff et al., 1977) model based on in vivo PET imaging studies using ^{18}F-fluorodeoxyglucose as tracer. Value of 0.5 was used for the lump constant. The values of glucose metabolic rate before 3-NP were 8.0+/-2.2 mg/100g min in the striatum, 8.6 +/-2.8 mg/100g min in the cingulate, 9.5+/-1.8 mg/100g min in the S1/S2 cortex and 8.8+/0 1.4 mg/100g min in the cerebellum, correspondingly. * = $p<0.05$.

	N	Striatum	Cingulate	S1/S2 cortex	Cerebellum
During 3-NP administrations:					
After starting 1.day	6	- 9.8 +/- 6.1	-11.9 +/- 6.4	-6.7 +/- 4.0	- 0.1 +/- 0.1
2.day	6	-14.5 +/- 3.3	+ 3.8 +/- 0.6	+0.6 +/- 0.2	- 2.9 +/- 0.3
3.day	6	-26.8 +/- 2.9*	-11.3 +/- 1.2	-21.2 +/- 2.0	- 2.2 +/- 0.2
4.day	4	-35.1 +/- 11.2*	-44.1 +/- 24.3*	-23.6 +/- 6.6	-23.5 +/- 13.1
After cessation of 3-NP:					
2 days	3	-52.5 +/- 21.0*	-45.3 +/- 25.8*	-46.0 +/- 18.4*	-18.1 +/- 7.2
4 weeks	3	-26.7 +/- 8.5	-36.6 +/- 12.1*	-28.2 +/- 10.2	- 7.2 +/- 2.0
16 weeks	2	-46.8 +/-10.1*	-41.6 +/- 14.0*	-42.6 +/- 15.2*	-17.4 +/- 9.4

FIGURE LEGENDS

1. Rat experiment in a super high resolution PET scanner. Side view shows a rat secured into the stereotactic headholder in the imaging "table" sliding into the tomograph. Front view shows the head inside the collimator ring and some electronics of the tomograph.

2. Weight progression during and after 3-NP administrations. The curves represent maximum (highly symptomatic, behavioral score 2-6) and minimum (no symptoms, behavioral score 0-1) changes of twelve animals investigated.

3. Regions of the interest were drawn on the coronal MR images (striatum is1; cingulate is 2; S1/S2 cortex is 3) and then overlaid with PET images. The PET data used for quantification was averaged from the areas on the left and right side.

4. Coronal PET images of glucose utilization in a rat brain before 3-NP; 2^{nd}, 3^{rd}, and 4^{th} day during 3-NP administration; and 2 days after the cessation of 3-NP.
   The images show enhanced cortical accumulation of ^{18}F-FDG during the 3-NP administration and this rat did not develop striatal lesions or motor symptoms. The slice thickness is 1.3 mm and slice to slice distance 3.75 mm.

5. Follow-up studies of an acute response of 3-NP toxicity in a rat, which developed striatal lesions. Coronal slices of ^{18}F-FDG accumulation before 3-NP and 2^{nd}, 3^{rd} and 4^{th} day during 3-NP administrations show time scale of the development of lesions. This rat had significant behavioral deficit (score 5).

6. Long-term follow up studies of glucose utilization showed some striatal recovery, 4 weeks after 3-NP toxicity, as enhanced ^{18}F-FDG accumulation. After this, progressive degeneration continued during the 4 month follow-up period.

7. Verification of a striatal lesion 2 days after the cessation of 3-NP detected by decreased glucose utilization using PET with postmortem histology. Nissl stained

whole brain coronal section through the striatum at the level of the anterior commisure shows extension of the neuronal damage. The magnification (x200) shows the level of damage.

8. Acute changes of neurochemicals in the striatum observed immediately after the first injection of 3-NP (20mg/kg i.p.). Increased lactate and succinate can be observed two hours after 3-NP injection accompanied with a slow increase in choline. The fast increased succinate (5.3+/-0.5%/min) and lactate/macromolecule (31+/-9%/min) levels might be an indication of 3-NP induced necrosis in the striatum. These fast processes were reversible, as shown in Figure 9.

9. Comparison of glucose utilization using PET, single voxel MRS and T2 weighted MR and NAA-MRS images. One day after 3-NP PET studies showed decreased glucose utilization as large striatal lesions and MRS showed enhanced succinate and lactate/macromolecules peaks in striatum. At this time there were no changes observable in NAA or choline peaks. However, 4 weeks later succinate and lactate/macromolecyle peaks disappeared, indicating that these peaks are related to acute neurotoxicity and reversible processes. At this time, decreased NAA and increased choline peaks were observed and T2 weighted MR image showed similar lesions and enlarged ventricles, observed by PET study of glucose utilization. Decreased NAA can also been observed as a lesion in NAA-MRS image.

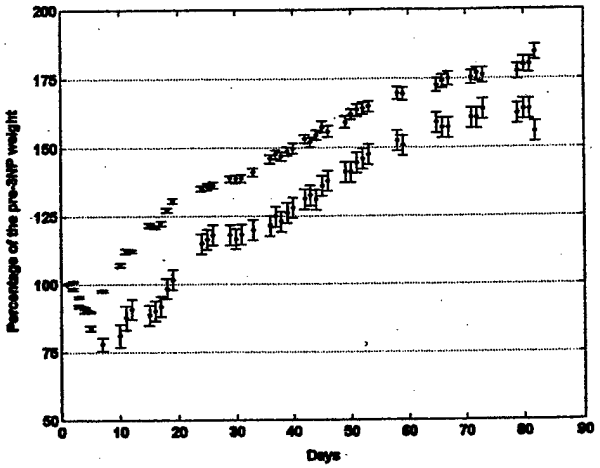

Figure 1.

Figure 2.

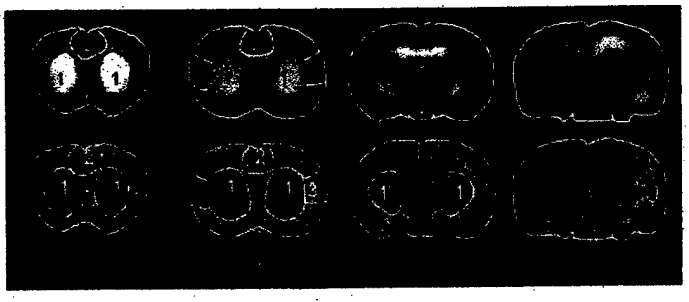

Figure 3.

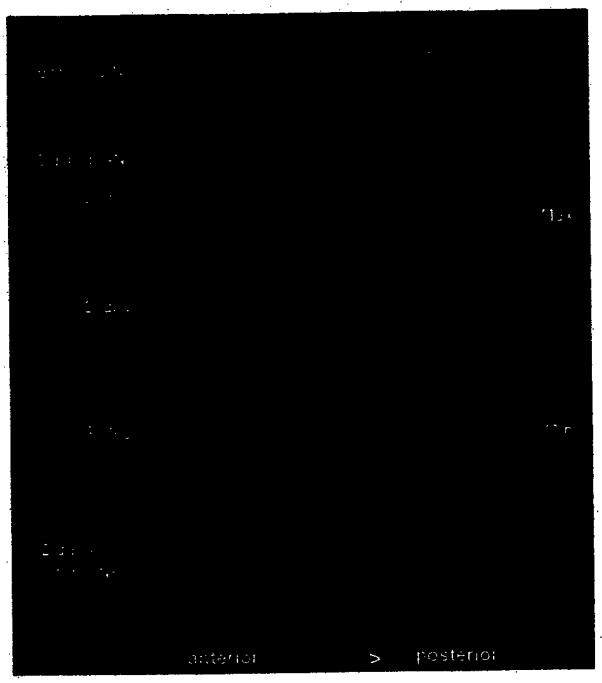

Figure 4.

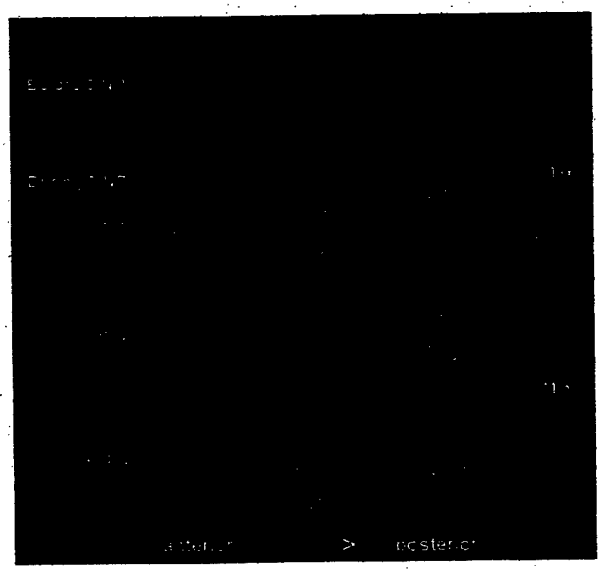

Figure 5.

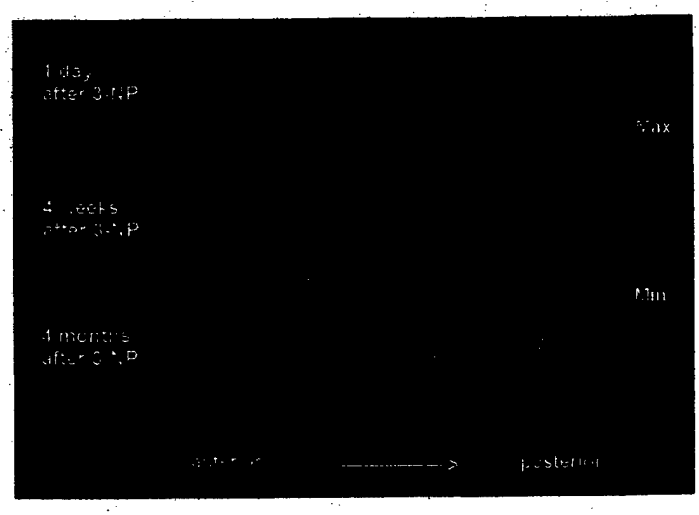

Figure 6.

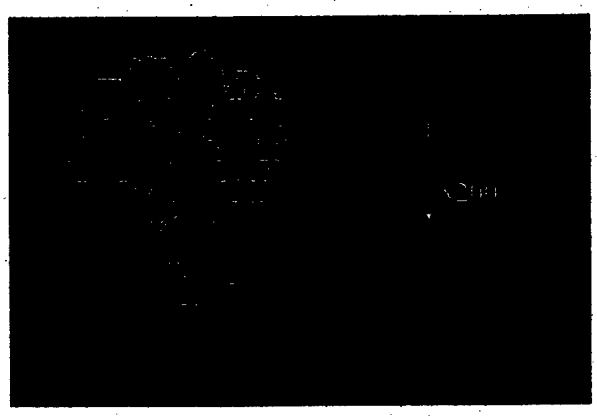

Figure 7.

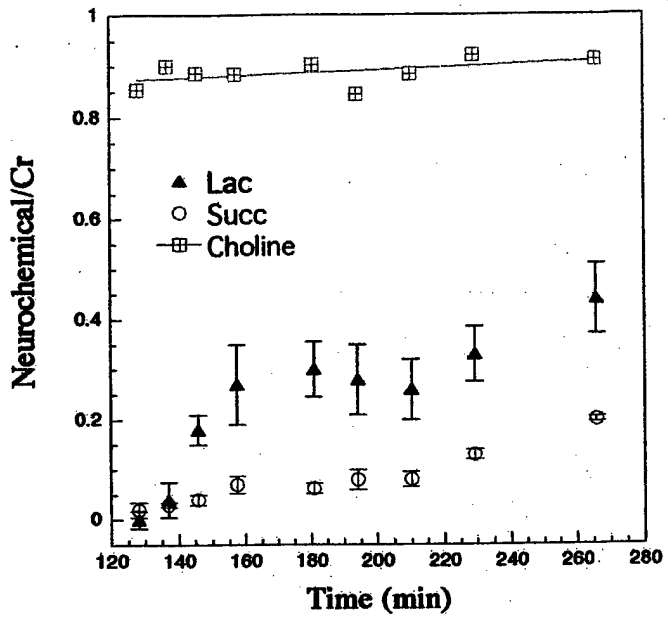

Figure 8.

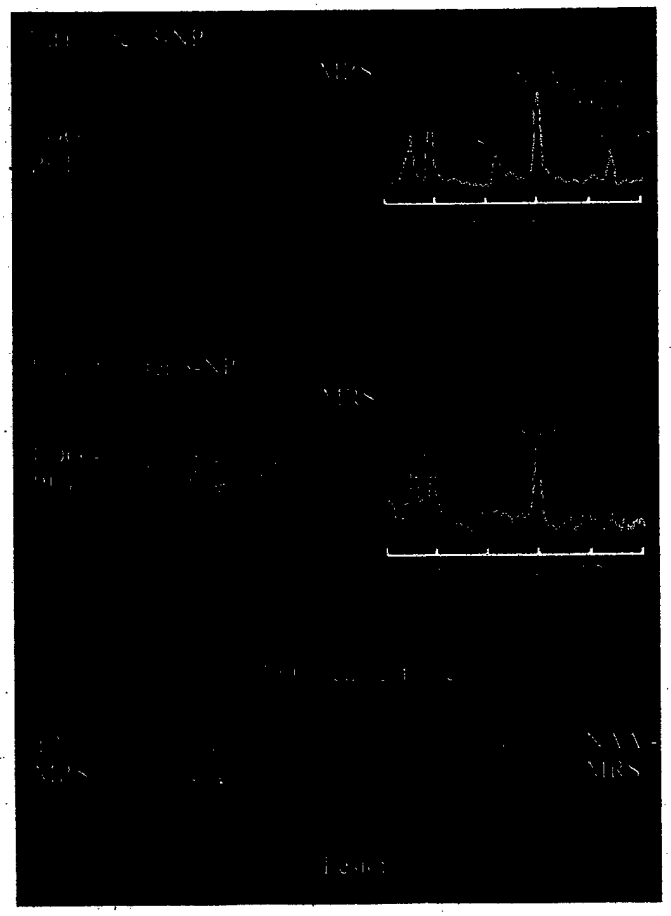

Figure 9.

Abstract ID: 238

Synthesis of C-11 CPCCOMe, a Potential PET Ligand for Imaging mGluR1 In Vivo

Meixiang Yu and Anna-Liisa Brownell
Radiology, Massachusetts General Hospital

Chemistry and Probes

Objectives: Metabotropic glutamate receptors (mGluRs) have been identified as a family of excitatory amino acid receptors coupled to intracellular signal transduction via G-proteins. However, the lack of specific imaging ligands has limited the precise characterization of the role of individual mGluRs and has thus hampered the progress in identifying the physiological and pathological roles of mGluRs.

Methods: A new potential mGluR1 antagonist CPCCOMe, (methyl-7-(hydroxyimino)-7,7-dihydrocyclopropachromene-1(1*H*)-carboxylate), an analog of CPCCOEt was synthesized and was labeled with C-11 for PET study. 0.2 mg precursor was dissolved in 300 μL acetonitrile (ACN) with 6 μL 0.8 M tetrabutylammonium hydroxide, after trapping the C-11 methyl triflate in room temperature, the reaction vessel was heated at 60° for 1.5 min. After purification by HPLC, the collected fraction was evaporated and dissolved in saline, followed by sterile filtration.

Result and Conclusion: The new compound CPCCOMe could be labeled with C-11 in 40 min with a yield of 60%, and this compound may be a good candidate for the in vivo imaging of mGluR1.